Turbulent mixing due to high pressure safety injection during a small-break loss-of-coolant accident

by

Felicia A. Plesic

A Thesis Submitted to the
Graduate Faculty in Partial Fulfillment of the
Requirements for the Degree of
MASTER OF SCIENCE

Major: Nuclear Engineering

Iowa State University
Ames, Iowa

1984

TABLE OF CONTENTS

LIST OF FIGURES

LIST OF TABLES

LIST OF NOTATION

C_j - Characteristic curve

C_p - Heat capacity

D - Diameter

E - Entrainment coefficient

Eff - Effectiveness factor

f - Dummy variable

Fr - Froude number

g - Gravitational constant

h - Heat transfer coefficient

i - Directional vector

j - Directional vector

k - Directional vector

k - Thermal conductivity

k - Turbulent kinetic energy

l_m - Mixing length

L - Length scale

L - Length

$\dot{m}$ - Mass flow rate

M_j - Node in Method of Characteristics

P - Fluid pressure

P_j - Position in Method of Characteristics

P_r - Prandtl number

$\mathring{q}$ - Heat flux

r - Radius

Re - Reynolds number

Ri - Richardson number

t - Time

T - Temperature

u - Fluid velocity

u - Internal energy

v - Fluid velocity - y direction

V - Bulk fluid velocity

x - Directional quantity

y - Directional quantity

z - Directional quantity

β - Dilatation coefficient

Γ - Eddy diffusivity

Δ - Delta

∂ - Partial

δ - Kronecker delta

ε - Viscous dissipation

Θ - Dimensionless temperature

λ - Thermal diffusivity

μ - Viscosity

ν - Kinematic viscosity

ρ - Fluid density

τ_{ij} - Stress tensor

τ - Characteristic mixing coefficient

ϕ - Dimensionless time

ψ - Stream function

ω - Vorticity

∇ - $i\,\partial/\partial x + j\,\partial/\partial y + k\,\partial/\partial z$

∇^2 - $\partial^2/\partial x^2 + \partial^2/\partial y^2 + \partial^2/\partial z^2$

List of Subscripts

e - Effective

H - HPSI

i - Directional vector

I - Interface

j - Directional vector

k - Directional vector

L - Loop

m - Mixed

(m, n) - Node points

o - Initial

p - Pipe

ref - Reference

t - Turbulent

trans - Transit

x - Directional quantities

y - Directional quantities

z - Directional quantities

List of Superscripts

' - Fluctuating component

- - Averaged quantity

aux - Auxiliary

N, N+1 - Time step

. - Vector quantity

.. - Tensor quantity

List of Abbreviations

^{o}C - Degrees Centigrade

CPU - Central Processing Unit

^{o}F - Degrees Fahrenheit

HPSI - High Pressure Safety Injection

LOCA - Loss of Coolant Accident

m - Meters

NDT - Nil Ductility Transition

PTS - Pressurized Thermal Shock

sec - Seconds

1. INTRODUCTION

One of the many design considerations in a nuclear power plant is pressurized thermal shock (PTS). In order to prevent brittle (i.e. sudden) failure of the pressure vessel as a result of thermal and mechanical stresses within the wall, the Nil Ductility Transition (NDT) temperature of the steel is designed to be below the lowest temperature the vessel will ever experience. However, as the vessel is irradiated by fast neutrons, the ductility of the steel is decreased and the NDT temperature (which represents the temperature at which the metal changes from ductile to brittle behavior) is increased markedly. This increase in NDT temperature leads to the possibility that when the reactor is being shut down, the vessel temperature could fall below the NDT value. If this occurs while the internal pressure remains high, brittle fracture may result [25].

While PTS always has been of concern, the Three Mile Island incident showed the industry that contrary to what was believed previously, the large break loss-of-coolant accident (LOCA) is not always the limiting transient. In particular, in the case of PTS, the limiting transient can be a small break in one of the hot legs of the primary coolant circuit. This could result in sustained high-pressure safety injection (HPSI) into the cold leg with no natural circulation in the breached primary coolant loop (see Figure 1.1) [26]. Two parameters which strongly influence the degree of thermal shock

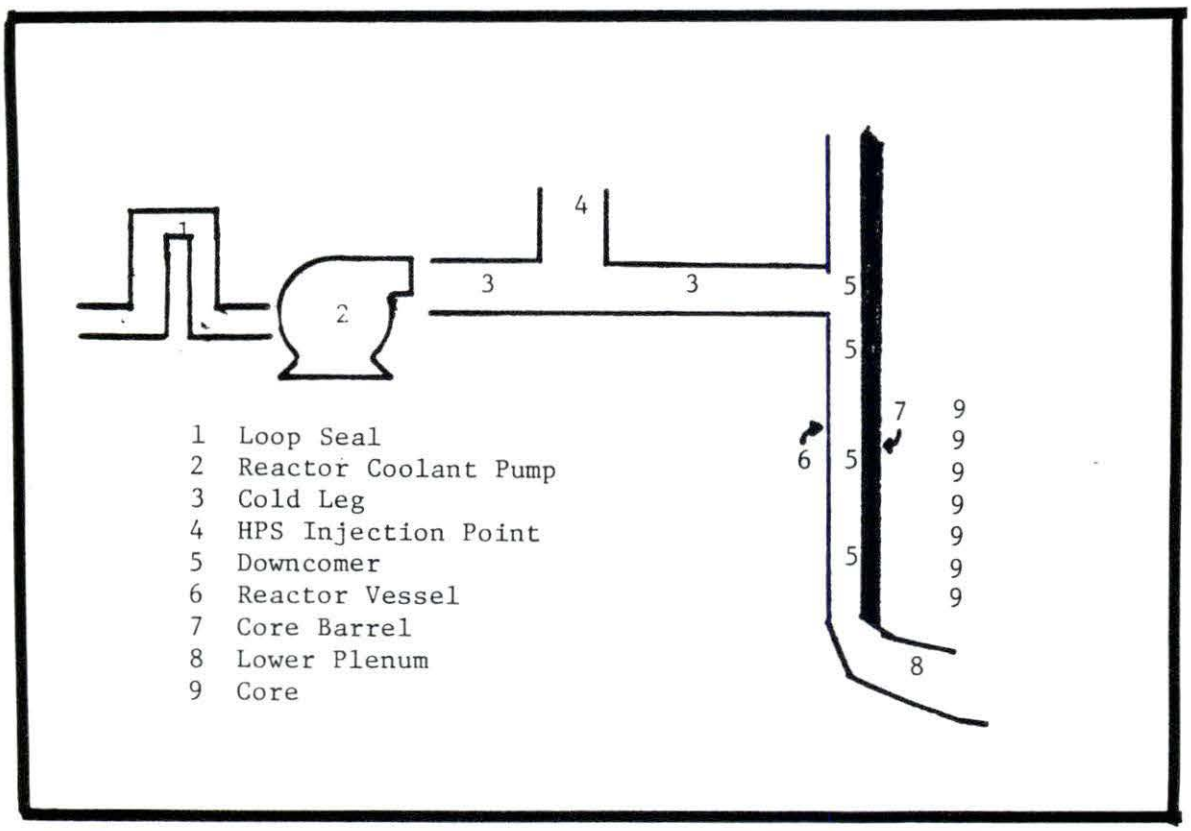

Figure 1.1 Schematic for HPSI problem

are the temperature and flow rate of the water adjacent to the vessel. These depend on the degree of mixing between the cold HPSI flow and the warm, stagnant fluid in the cold leg and downcomer.

Due to the significance of this problem, three aspects of the mixing phenomena are being investigated concurrently by the industry. These include:

- an experimental phase to provide both a qualitative understanding of flow and temperature distributions and quantitative empirical correlations.
- the use of nodal solutions to the Navier-Stokes equations to provide a theoretical prediction for fluid and thermal mixing.
- the development of a simpler, semi-empirical model to predict mixing.

The ultimate goal of any of these three approaches is to be able to generate accurate temperature and velocity profiles in the cold leg and downcomer. These profiles would be used along with plant-specific neutron-fluence and materials properties to predict the number of years a plant could withstand specified PTS conditions without danger of brittle fracture.

Only one aspect of this large PTS problem was investigated in this work. That aspect was the theoretical prediction of the temperature profiles in the cold leg by using a computer code to solve the time-averaged Navier-Stokes equations.

2. A DESCRIPTION OF THE PROBLEM

Because the thermal stresses due to the rapid cooling of the reactor vessel wall combined with the mechanical stresses due to repressurization may initiate or propagate cracks in the vessel if the vessel materials properties have been sufficiently degraded by long-term irradiation [6], experiments were performed by Creare Inc. of Hanover, NH under contract to EPRI [7,8,9] to visualize the flow patterns. A schematic of their results is presented in Fig. 2.1. It shows the following phenomena due to the mixing of cold HPSI fluid with the warmer stagnant fluid in the cold leg of the primary coolant loop:

- Buoyancy-induced flow and fluid stratification
- Shear fluid entrainment and growth of the HPSI jet
- Counter-current flow of warm water into the cold leg

The phenomena of stratification have been investigated both experimentally and theoretically [19,21,22,27]. Reference 22 describes stratification as:

> "a change of density along the vertical, the direction of gravity force. In a stratified fluid, vertical displacements of fluid particles from their equilibrium positions produce buoyancy forces $(\rho_1-\rho)g$ where ρ_1 is the density of the fluid particle, ρ is the density of the surrounding medium and g is the acceleration due to gravity."

The buoyant force generates an exchange between the potential energy of the stratified fluid in the gravity field and the kinetic energy

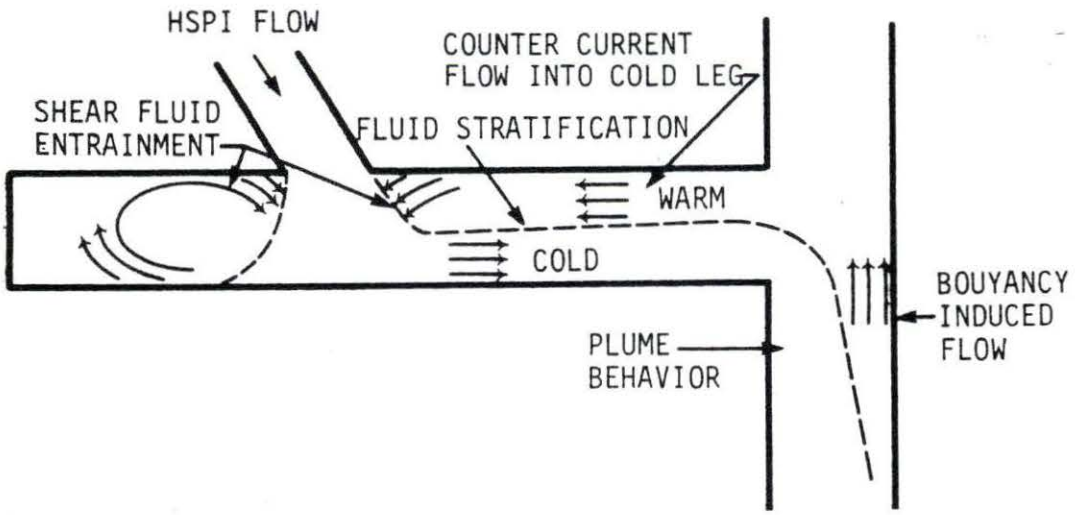

Figure 2.1 Experimentally observed mixing phenomena

of fluid motion. A stratified fluid is either stably or unstably stratified. In a stably stratified fluid, $\partial\rho/\partial z$ is positive and the work of the buoyancy forces transforms the kinetic energy into potential energy. An unstably stratified fluid has a negative value for $\partial\rho/\partial z$. In that case, the work of the buoyancy forces transforms a part of the potential energy into kinetic energy of motion; thereby, generating convection. This leads to an increase in turbulence intensity which, in turn leads to an increase in mixing because the lack of density uniformity is a source of shear in the fluid. Referring again to Figure 2.1, it is obvious that the injection point

is an area of unstable stratification because the higher density fluid enters at the top causing the density to increase with increasing height.

The mechanism of entrainment is the process by which the turbulence of the HPSI jet spreads into the initially quiescent fluid in the cold leg. The area of fluid entrainment by jets has been extensively studied [1,2,10,13,17,23,33] but usually in the context of the jet flowing into an infinite reservoir. Reference 13 describes entrainment as "the apparent unilateral transport of mass across a density interface which is brought about by the turbulent velocity fluctuations of the turbulent fluid."

In principle, the calculation of these complex flow phenomena involves the solution of the time-dependent Navier-Stokes equations. In turbulent flow, these equations can not be solved without numerical methods. Because it was only recently that progress in numerical methods and the increasing calculational speed of computers allowed the analytical solutions to be economically feasible, much of the earlier work prior to 1970 focused on the experimental determination of entrainment coefficient. Such studies are described in references 1, 2, 10, 13, 17, 23, 29, and 33. These studies concern either channel flow or jet discharge into an infinite reservoir. These are of interest in the area of thermal discharge from power plants. While these experiments are of importance in understanding the fundamental behavior of entrainment and statification, they are not directly applicable to the problem considered here, because of the differences

in geometry and flow conditions. No previous experimental studies performed for a cylindrical pipe geometry were found and few studies in any geometry were found which included the counter-current flow depicted in Figure 2.1.

One concept which was clearly established by all experiments was the densimetric Froude number as the governing dimensionless parameter. This is discussed further in Chapter 5.

The progress in both computational speed and size of computers has made it possible to get accurate solutions to complex flow situations. This work investigated the use of a nodal solution to the time averaged Navier-Stokes equations as a means of predicting thermal mixing between the HPSI fluid and the stagnant fluid in the cold leg. The computational scheme used was a code entitled ULYSSE developed by Electricite de France. It is described in reference 12 and was verified experimentally as described in references 3, 30, 31 and 32. It is based on statistically averaged Navier-Stokes equations which are, in themselves, an approximation since as is described in reference 11, "the averaging process itself may mask some characteristic patterns in the flow field." This averaging process leads to correlations between fluctuating quantities such as Reynold's stress, $\rho \overline{u_i' u_j'}$ and the turbulent heat flux, $\rho \overline{u_i' T'}$ where u is velocity and T is the temperature. The overbar indicates the averaging process while the prime indicates the fluctuations in mean quantities due to turbulence. The subscripts indicate the direction of the component.

These quantities must be modeled. A detailed discussion of the evolution of turbulence modeling is found in reference 23 and is summarized briefly in Section 3.4. The computational model used in this work closes the turbulence model with the k-ε equations proposed by reference 23.

The numerical methods include the Gauss-Seidel technique to solve the diffusion portion of the Navier-Stokes equations and the method of characteristics to solve the non-linear advection terms. The method of characteristics is used because it is believed to minimize numerical diffusion. These methods are described in more detail in Chapter 4.

The objectives of the present work can be summarized as:

- to solve the time averaged Navier-Stokes equations using the k-ε turbulence model for the HPSI scenario.
- to compare the trends generated by the computational model with the results generated by the Creare experiments in an effort to determine the adequacy of the computational model.

3. THE EQUATIONS TO BE SOLVED

3.1. Development of the Equations of Change

The derivation of the equations of change has been presented in great detail by several authors [4,16]. A summary of the derivation of these equations in Cartesian coordinates follows based primarily on reference 4.

The equation of continuity is developed by writing a mass balance over a stationary volume element of dimensions $\Delta x \Delta y \Delta z$ through which the fluid is flowing (see Figure 3.1). The equation is merely a statement of the conservation of mass and is of the form:

$$\left[\begin{array}{c}\text{rate of}\\ \text{mass}\\ \text{accumulation}\end{array}\right] = \left[\begin{array}{c}\text{rate of}\\ \text{mass in}\end{array}\right] - \left[\begin{array}{c}\text{rate of}\\ \text{mass out}\end{array}\right] \qquad (3.1)$$

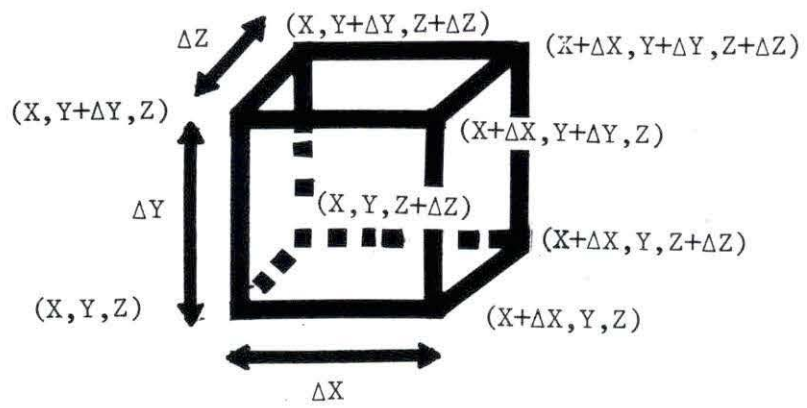

Figure 3.1 Volume element for mass, momentum and energy balance

The rate of mass accumulation within the volume is $(\partial\rho/\partial t)(\Delta x\ \Delta y\ \Delta z)$ where ρ is fluid density and t is time. Assuming the flow is in the positive x, y, and z directions, then the rate of mass in is equal to the sum of the rates at which mass enters through the yz face at x, the xz face at y and the xy face at z. Similarly, the rate of mass out is equal to the sum of the rates at which mass exits through the yz face at $x + \Delta x$, the xz face at $y + \Delta y$ and the xy face at $z + \Delta z$. This yields:

$$\Delta x\Delta y\Delta z\ \frac{\partial \rho}{\partial t} = \Delta y\Delta z[(\rho u_x)\Big|_x - (\rho u_x)\Big|_{x+\Delta x}] + \Delta x\Delta z[\rho u_y\Big|_y - \rho u_y\Big|_{y+\Delta y}] + \Delta x\Delta y[\rho u_z\Big|_z - u_z\Big|_{z+\Delta z}] \tag{3.2}$$

where u_x, u_y and u_z are the instantaneous values of the fluid velocity in the x, y, and z directions, respectively. When this equation is divided by $\Delta x\Delta y\Delta z$ and the limit is taken as the volume of the cube approaches zero, the equation of continuity results.

$$\frac{\partial \rho}{\partial t} = -\frac{\partial}{\partial x}(\rho u_x) - \frac{\partial}{\partial y}(\rho u_y) - \frac{\partial}{\partial z}(\rho u_z))$$

which can be written in vector notation as:

$$\frac{\partial \rho}{\partial t} = -(\nabla \bullet \rho \overset{\bullet}{u}) \tag{3.3}$$

where the superscript indicates a vecter quantity.

The second of the equations of change is the equation of motion and is developed from a momentum balance on the volume element of the form:

$$\left[\begin{array}{c}\text{rate of}\\ \text{momentum}\\ \text{accumulation}\end{array}\right] = \left[\begin{array}{c}\text{rate of}\\ \text{momentum}\\ \text{in}\end{array}\right] - \left[\begin{array}{c}\text{rate of}\\ \text{momentum}\\ \text{out}\end{array}\right] + \left[\begin{array}{c}\text{sum of the}\\ \text{forces acting}\\ \text{on the system}\end{array}\right] \qquad (3.4)$$

The equation of motion is basically a statement of Newton's second law: mass times acceleration equals the sum of the forces.

Working first with the x - component of momentum, the accumulation term is $(\Delta x\ \Delta y\ \Delta z)(\partial \rho u_x / \partial t)$. Momentum enters the volume by both bulk fluid flow (convection) and by molecular transfer. Convective terms for the x-component of momentum are of the form $\rho u_x\ u_j\big|_x\ \Delta y\ \Delta z$ (entering) or $\rho\ u_x\ u_j\big|_{x+\Delta x}\ \Delta y\ \Delta z$ (exiting). There are six of these convective terms, one for each face. There are also six molecular transport terms (again for the x-component only) of the form $\tau_{jx}\big|_x$ $\Delta y \Delta z$ (entering) and $\tau_{jx}\big|_{x+\Delta x}\ \Delta y\ \Delta z$ (exiting) where j equals x, y and z. The body forces on the system are usually only those arising from fluid pressure and/or gravity. These forces are written $\Delta y \Delta z$ $(P_x - P_{x+\Delta x}) + \rho g\ \Delta x \Delta y \Delta z$. When these expressions are substituted into equation 3.4, and the expression is divided by $\Delta x \Delta y \Delta z$ and the limit is taken as the volume approaches zero, then the x component of the equation of motion results:

$$\frac{\partial}{\partial t}(\rho u_x) = -\left(\frac{\partial}{\partial x}\rho\, u_x u_x + \frac{\partial}{\partial y}\rho\, u_x u_y + \frac{\partial}{\partial z}\rho\, u_z u_x\right)$$

$$-\left(\frac{\partial}{\partial x}\tau_{xx} + \frac{\partial}{\partial y}\tau_{yx} + \frac{\partial}{\partial z}\tau_{zx}\right) - \frac{\partial P}{\partial x} + \rho g_x \qquad (3.5)$$

τ_{xx} in equation 3.5 represents the normal stress on the x-face and is defined for a Newtonion fluid as:

$$\tau_{xx} = -2\mu\frac{\partial u_x}{\partial x} + 2/3\ \mu(\nabla\bullet\overset{\bullet}{u})$$

where ∇ is the gradient of u and μ is the bulk fluid viscosity. τ_{yx} and τ_{zx} represent the x-directed tangential (or shear) stress on the y and z faces respectively. These stresses are:

$$\tau_{yx} = \tau_{xy} = -\mu(\frac{\partial u_x}{\partial y} + \frac{\partial u_y}{\partial x})$$

and

$$\tau_{zx} = \tau_{xz} = -\mu(\frac{\partial u_z}{\partial x} + \frac{\partial u_x}{\partial z})$$

Exactly similar equations can be written for the y and z components of momentum. For simplicity, the three equations can be combined and rewritten:

$$\frac{\partial}{\partial t}\rho\ \overset{\bullet}{u} = -[\nabla\rho\bullet\overset{\bullet\bullet}{uu}] - \nabla\ \overset{\bullet}{P} \qquad (3.6)$$

[Rate of increase of momentum per unit volume] [rate of momentum gain by convection per unit volume] [pressure force on element per unit volume]

$$- [\nabla\bullet\overset{\bullet\bullet}{\tau}] + \rho\ \overset{\bullet}{g}$$

[rate of momentum gain by viscous transfer per unit volume] [gravitational force on element per unit volume]

These two equations, 3.3 and 3.6, completely describe an isothermal system. For a non-isothermal system a third equation, the equation of energy, must be developed. As before, an energy balance reflecting the law of the conservation of energy is written in the following form:

$$\left[\begin{array}{l}\text{rate of accumulation of internal and kinetic energy}\end{array}\right] = \left[\begin{array}{l}\text{rate of internal and kinetic energy in by convection}\end{array}\right] - \left[\begin{array}{l}\text{rate of internal and kinetic energy out by convection}\end{array}\right] \quad (3.7)$$

$$+ \left[\begin{array}{l}\text{net rate of heat addition by conduction}\end{array}\right] - \left[\begin{array}{l}\text{net rate of work done by system on surroundings}\end{array}\right]$$

Kinetic energy is the energy associated with observable fluid motion ($1/2\rho\bar{u}^2$) while internal energy is that associated with random translational and internal motions of the molecules plus the energy of interaction between the molecules ($\hat{U}$). The rate of internal and kinetic energy in by convection is the sum of the rates of energy influx through the x, y and z faces of the form:

$$\Delta i \Delta k \; (u_j (\rho\hat{U} + 1/2\rho\bar{u}^2)\big|_j) \quad \Big| \begin{array}{l} j=x,y,z \\ i\neq k\neq j \end{array}$$

The rate of energy efflux due to convection out the $x+\Delta x$, $y+\Delta y$ and $z+\Delta z$ faces is of the same form; i.e.

$$\Delta i \Delta k (u_j (\rho\hat{U}+1/2\rho\bar{u}^2)\big|_{j+\Delta j}) \quad \Big| \begin{array}{l} j=x,y,z \\ i\neq k\neq j \end{array}$$

The net rate of energy input by conduction is:

$$\Delta y\Delta z(q_x\big|_x - q_x\big|_{x+\Delta x}) + \Delta x\Delta z(q_y\big|_y - q_y\big|_{y+\Delta y}) +$$

$$\Delta x\Delta y(q_z\big|_z - q_z\big|_{z+\Delta z}).$$

where q_x, q_y, q_z are the x, y and z components of the heat flux vector q. The rate at which work is done consists of two parts: gravity, which is a volume force and pressure and viscosity, which are surface forces. The rate at which work is done against gravity is:

$$-\rho\Delta x\Delta y\Delta z\ (u_x g_x + u_y g_y + u_z g_z)$$

The rate at which work is done against static pressure is:

$$\Delta y\Delta z\ ((Pu_x)\big|_{x+\Delta x} - (Pu_x)\big|_x) + \Delta x\Delta y\ ((Pu_y)\big|_{y+\Delta y} - (Pu_y)\big|_y)$$

$$+ \Delta x\Delta y\ ((Pu_z)\big|_{z+\Delta z} - (Pu_z)\big|_z)$$

The rate of doing work against viscious forces is the sum of three terms of the following form:

$$\Delta y\Delta z((\tau_{xx}u_x + \tau_{xy}u_y + \tau_{xz}u_z)\big|_{x+\Delta x} - (\tau_{xx}u_x + \tau_{xy}u_y + \tau_{xz}u_z)\big|_x)$$

As before, these expressions are substituted into equation 3.7. The equation is divided by $\Delta x\Delta y\Delta z$ and the limit is taken as the volume approaches zero. The resulting equation written in vector-tensor notation is:

$$\frac{\partial}{\partial t}\ \rho(\hat{U}+1/2\overset{\bullet}{u}^{2}) \;=\; -\ (\nabla\cdot\rho\overset{\bullet}{u}(\hat{U}+1/2\overset{\bullet}{u}^{2}))\ -\ \nabla\cdot\overset{\bullet}{q} \qquad (3.8)$$

[rate of gain of energy per unit volume]	[rate of energy input per unit volume by convection]	[rate of energy input per unit volume by conduction]
$+\ \rho(\overset{\bullet}{u}\cdot\overset{\bullet}{g})$	$-\ (\nabla\cdot\overset{\bullet\bullet}{P}\overset{\bullet}{u})$	$-\ (\nabla\cdot[\overset{\bullet\bullet}{\tau}\cdot\overset{\bullet}{u}])$
[rate of work done on fluid per unit volume by gravitational forces]	[rate of work done on fluid per unit volume by pressure forces]	[rate of work done on fluid by viscous forces]

These three equations completely describe any non-isothermal Neutonian system since no assumptions have yet been made. The following section will deal with the simplification of these equations.

3.2. Simplification of the Equations of Change - The Navier-Stokes Equations

The following approximations will now be made in order to simplify the problem. First, the fluid is assumed to be incompressible but with small variations in density due to changes in temperature. Following the Boussinesq approximation, it is assumed that the only effect of density variation is in the gravitational body force term in the momentum equation. This approximation also assumes that the equation of state can be written $\rho_r - \rho = \rho\beta(T-T_r)$ where β is the dilatation constant [16]. Since the density is assumed to be constant in the equation of continuity, equation 3.3 simplifies to:

$$\nabla \cdot \dot{u} = 0 \tag{3.9}$$

If the additional assumption of constant viscosity is made and equation 3.9 is used, equation 3.6 simplifies to:

$$\rho \frac{Du_i}{Dt} = \nabla P_i + \mu \nabla^2 u_i + g_i \left(\frac{\rho - \rho_r}{\rho}\right) \tag{3.10}$$

where $\frac{Du_i}{Dt}$ is the substantial time derivative:

$$\text{e.g.} \quad \frac{Du_x}{Dt} = \frac{\partial u_x}{\partial t} + u_x \frac{\partial u_x}{\partial x} + u_y \frac{\partial u_x}{\partial y} + u_z \frac{\partial u_x}{\partial z}$$

and ∇^2 is the Laplacian operator:

$$\nabla^2 = \frac{\partial^2}{\partial x^2} + \frac{\partial^2}{\partial y^2} + \frac{\partial^2}{\partial z^2}$$

This form of the momentum equation is the Navier-Stokes equation. By making use of these two simplified equations, 3.8 and 3.10, equation 3.8 can be reduced to:

$$\rho \frac{DU}{Dt} = - (\nabla \cdot \dot{q}) - (\ddot{\tau} : \nabla \dot{u})$$

[rate of gain of internal energy per unit volume] [rate of internal energy input by conduction per unit volume] [irreversible rate of internal energy increase per unit volume by viscous dissipation]

The next assumption involves neglecting the viscous dissipation term which is generally only important for high Prandtl number fluids. If

the Prandtl number, Pr, is of the order of one, the velocity must approach Mach 1 before the viscous dissipation term becomes important [16]. If q is expressed in terms of temperature gradients and a constant thermal conductivity, k, if U is expressed in terms of a constant heat capacity, C_p, and internal temperature, T; and if viscous dissipation effects are ignored then (3.11) can be rewritten as:

$$\frac{DT}{Dt} = \lambda \nabla^2 T$$

where λ is the thermal diffusivity and equals $\frac{k}{\rho C}$.

Obviously, the turbulence problem to be solved is a three dimensional problem (see Sketch A, Figure 3.2). Initially, all flow is in the -y direction. Where the HPSI pipe intersects the cold leg, an x-component of velocity develops. Furthermore, because of the stratification which takes place in the cold leg due to temperature differences, the flow is not axisymmetric. However, since solving the problem in three dimensions is not tractable, some method of reducing it to a two-dimensional problem must be chosen. If one works in r,z cylindrical coordinates, a restraint of axisymmetry is implied, whereas working with the x,y cartesian coordinates merely states that the z direction is infinite and does not affect what happens in the x,y plane (see Sketch B, Figure 3.2). Because of the strong asymmetry caused by the stratification, one must work in the x,y plane. The basic assumption is that given a certain density difference, the level

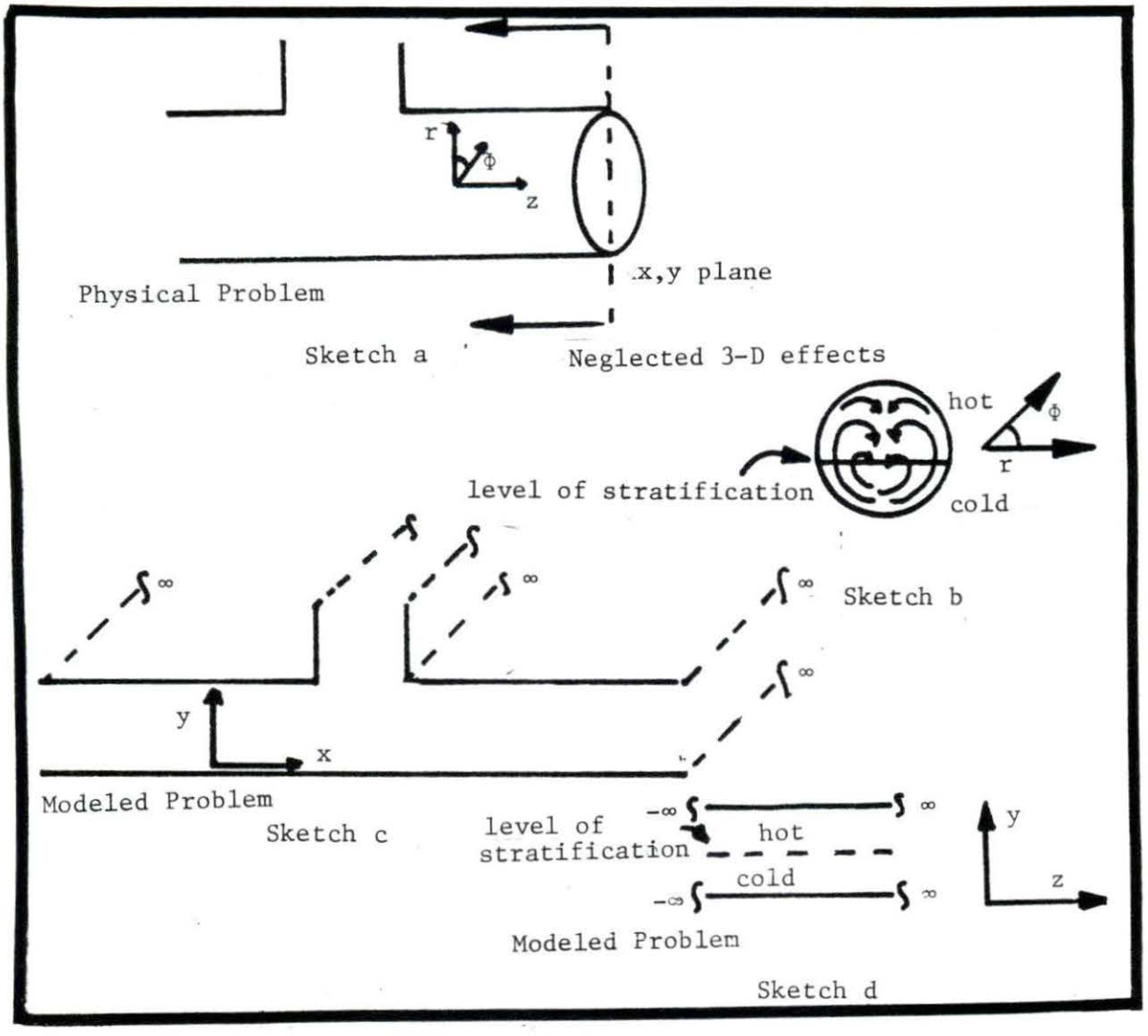

Figure 3.2 Two dimensional modeling of three dimensional problem

of stratification is the same, regardless of whether the geometry is a pipe or a closed channel. While at first glance this may not seem to be an adequate assumption, good results have been obtained using this approximation [3,30,32,33].

Working only in the x,y plane, the three equations to be solved become:

Continuity:

$$\frac{\partial u_x}{\partial x} + \frac{\partial u_y}{\partial y} = 0 \tag{3.11}$$

Momentum:

$$\frac{\partial u_x}{\partial t} + u_x \frac{\partial u_x}{\partial x} + u_y \frac{\partial u_x}{\partial y} = -\frac{1}{\rho}\frac{\partial P}{\partial x} + \nu\left(\frac{\partial^2 u_x}{\partial x^2} + \frac{\partial^2 u_x}{\partial y^2}\right) + g_x\left(\frac{\rho-\rho_r}{\rho}\right) \tag{3.12}$$

and

$$\frac{\partial u_y}{\partial t} + u_x \frac{\partial u_y}{\partial x} + u_y \frac{\partial u_y}{\partial y} = -\frac{1}{\rho}\frac{\partial P}{\partial y} + \nu\left(\frac{\partial^2 u_y}{\partial x^2} + \frac{\partial^2 u_y}{\partial y^2}\right) \tag{3.13}$$

where ν is the kinematic viscosity (μ/ρ)

Thermal Energy:

$$\frac{\partial T}{\partial t} + u_x \frac{\partial T}{\partial x} + u_y \frac{\partial T}{\partial y} = \lambda\left(\frac{\partial^2 T}{\partial x^2} + \frac{\partial^2 T}{\partial y^2}\right) \tag{3.14}$$

Given that the above described assumptions are adequate, these four equations are an exact and complete solution for turbulent flow provided that instantaneous values for velocity, density, temperature and pressure are known. Unfortunately, this is not possible since, in turbulent flow, the velocity fluctuates in an irregular manner around a steady time-independent velocity as does the density, pressure and temperature. Because these fluctuating components are random and tend to be very small relative to the respective mean values, it is possible to treat them statistically, an approach first suggested by Osbourne Reynolds.

3.3. The Time-Averaged Navier-Stokes Equations

The instantaneous values of velocity, pressure, density and temperature can be written:

$$u_i = \bar{u}_i + u_i' \quad , \quad \rho = \bar{\rho} + \rho' \quad , \quad P = \bar{P} + P', \; T = \bar{T} + T'.$$

The overbar represents time-averaged quantities:

$$\text{e.g.} \quad \bar{u}_i = \frac{1}{t_2 - t_1} \int_{t_1}^{t_2} u_i \, dt$$

where $t_2 - t_1$ is long compared to the time scale of turbulent motion and for transient problems, short compared to the time scale of the mean flow. The prime represents the randomly fluctuating component. It is assumed that the turbulent flow is stationary and homogeneous and, therefore, ergodic. This implies that the time average, space average and ensemble average will all lead to the same result [14]. In order to develop the time-averaged Navier-Stokes equations, the following rules of averaging are used [14]:

If $A = \bar{A} + a$ and $B = \bar{B} + b$, then

$$\bar{A} = \overline{\bar{A}+a} = \bar{A} + \bar{a} = \bar{A} \qquad \bar{a} = 0 \tag{3.15a}$$

$$\overline{AB} = \bar{A}\bar{B} + \overline{ab} \tag{3.15b}$$

$$\overline{Ab} = \bar{A}\bar{b} + \overline{ab} = 0 \quad \text{since } \bar{b} = 0 \tag{3.15c}$$

and

$$\overline{AB} = \overline{(\bar{A}+a)(\bar{B}+b)} = \bar{A}\bar{B} + \overline{Ab} + \overline{Ba} + \overline{ab} = \bar{A}\bar{B} + \overline{ab} \tag{3.15d}$$

By using these rules, substituting the sum of the time-independent plus the fluctuating quantity for the instantaneous values in equations 3.11, 3.12, 3.13 and 3.14 and taking the mean value, the time-averaged Navier-Stokes equations are obtained [28]. The implicit assumption in this process is that the mean values of the instantaneous quantities will obey the Navier-Stokes equations in the same way that instantaneous values do. One cannot, however, substitute the mean value everywhere one encounters the instantaneous value. One must go through the averaging process to properly account for extra terms which occur.

e.g. $\frac{\partial u_x}{\partial x} + \frac{\partial u_y}{\partial y} = 0$ Navier-Stokes equation with instantaneous values

$$0 = \frac{\partial(\bar{u}_x + u_x')}{\partial x} + \frac{\partial(\bar{u}_y + u_y')}{\partial y}$$ Substitution of the sum of the time independent plus the fluctuating component for the instantaneous quantity

$$0 = \frac{\partial(\overline{\bar{u}_x + u_x'})}{\partial x} + \frac{\partial(\overline{\bar{u}_y + u_y'})}{\partial y}$$ Taking the average of instantaneous quantities

$$0 = \frac{\partial \bar{u}_x}{\partial x} + \frac{\partial \bar{u}_x'}{\partial x} + \frac{\partial \bar{u}_y}{\partial y} + \frac{\partial \bar{u}_y'}{\partial y}$$ Applying averaging rules

$$\frac{\partial \bar{u}_x}{\partial x} + \frac{\partial \bar{u}_y}{\partial y} = 0 \qquad (3.16)$$

Using the same procedure detailed in the example results in the following time-averaged momentum equation:

$$\frac{\partial \bar{u}_i}{\partial t} + \bar{u}_i \frac{\partial \bar{u}_i}{\partial i} + \bar{u}_j \frac{\partial \bar{u}_i}{\partial j} = -\frac{1}{\rho}\frac{\partial \bar{P}}{\partial i} + \mu\left(\frac{\partial^2 \bar{u}_i}{\partial i^2} + \frac{\partial^2 \bar{u}_i}{\partial j^2}\right) - \frac{\partial \overline{u_i' u_i'}}{\partial i} \quad (3.17)$$

$$- \frac{\partial \overline{u_i' u_j'}}{\partial j} + g_i\left(\frac{\rho - \rho_{ref}}{\rho}\right) \qquad \text{where } i = x \text{ and } y,\ j = x \text{ and } y, \text{ and } i \neq j$$

Similarly the resulting energy equation is:

$$\frac{\partial T}{\partial t} + u_x \frac{\partial T}{\partial x} + u_y \frac{\partial T}{\partial y} = \lambda\frac{\partial^2 T}{\partial x^2} + \frac{\partial^2 T}{\partial y^2} - \frac{\partial \overline{u_x' T'}}{\partial x} - \frac{\partial \overline{u_y' T'}}{\partial y} \quad (3.18)$$

The extra terms in the momentum equation are of the form $-\overline{\rho u_i' u_j'}$. For example, $-\overline{\rho u_x' u_j'}$ represents the transport of x momentum in the y direction and is called the turbulent or Reynolds stress. Similarly, the extra term in the thermal energy equation is $-\rho\overline{u_i' T'}$. It represents the transport of temperature due to turbulent fluctuations in the x or y direction and is called turbulent heat flux.

These equations no longer form a closed set, since there are 4 equations and 7 unknowns, $\bar{u}_x$, $\bar{u}_y$, $\bar{T}$, $\bar{P}$, u_x', u_y', and T'. Exact transport equations can be derived for $\overline{u_i' u_i'}$, $\overline{u_i' u_j'}$, $\overline{u_i' T'}$ and $\overline{u_j' T'}$ but these will contain turbulence correlations of the next higher order such as $\overline{u_k' u_i' u_j'}$ [11,20]. It is the introduction of models for turbulent stress and heat flux which leads to the approximate nature of the solution for turbulent flow.

3.4. Closing the Turbulence Model

The turbulence model must simulate the averaged character of real turbulence. The oldest and most widely used turbulence models (including the model used to perform this analysis) are based on the eddy viscosity/eddy diffusivity concept introduced by Boussinesq in 1877 [24]. The concept was originally conceived by presuming an analogy between molecular motion and turbulent motion. Since molecular motion is proportional to the average velocity and the mean free path of the molecules, turbulent motion was assumed to be proportional to a velocity characterizing the fluctuating motion and a typical length which Prandtl called a "mixing length." The concept of eddy viscosity/eddy diffusivity has been found to work well in practice.

The eddy viscosity ν_t is defined from:

$$-\overline{u_i' u_j'} = \nu_t \left(\frac{\partial u_i}{\partial x_i} + \frac{\partial u_j}{\partial x_i}\right) - 2/3\ k\ \delta_{ij} \tag{3.19}$$

where δ_{ij} is the Kronecker delta which equals 0 where $i \neq j$ and where for convenience the overbar has been dropped from the non-fluctuating component. Introduction of the $-2/3k\ \delta_{ij}$ term makes the equation applicable to normal stresses. Equation 3.19 assumes that in analogy to the viscous stresses in laminar flows the turbulent stresses are proportional to the mean velocity gradients. However, the eddy viscosity, unlike molecular viscosity, is not a fluid property; rather it depends strongly on the nature of the turbulence. Similarly, the eddy diffusivity is defined from:

$$- \overline{u_i'T'} = \Gamma \, \partial T/\partial x_i$$

which is a relationship directly analogous to turbulent momentum transport (i.e. turbulent heat transport is assumed to be related to the gradient of the mean temperature). Γ, like ν_t, is not a fluid property but also depends on the degree of turbulence. Γ and ν_t can be related by the Reynold's analogy, which is based on the fact that the phenomena of heat and momentum transport are of the same form [16]:

$$\text{i.e.} \quad \tau = \rho(\nu + \nu_t) \frac{du}{dy}$$

and

$$Q = C_p\left(\frac{k}{C_p} + \Gamma\right) \frac{dT}{dy}$$

Reynolds postulated that since these phenomena were so closely related then the coefficients must also be closely related. They can be combined into a dimensionless number, the turbulent Prandtl number

$$Pr_t = \frac{\nu_t}{\Gamma}$$

which is analogous to the usual Prandtl number $C_p\mu/k$. That is since the usual Prandtl number represents ν/λ or the ratio of the diffusion of molecular momentum to the thermal diffusivity in main flow, the turbulent Prandtl number is the ratio of the diffusion of molecular momentum due to turbulent fluctuations to the diffusion of thermal energy due to turbulent flucuations. The turbulence models based on

the eddy viscosity/eddy diffusivity concept have been divided by Rodi [23,24] into 3 categories:

1) 0-equation model

2) 1-equation model

3) 2-equation model

The model used in this work is a 2-equation model but the others will be discussed briefly.

The 0-equation models do not involve additional transport equations for the turbulent quantities. Eddy viscosity is specified directly from experiments or empirical formulae. An example of this type of model is the well-known Prandtl mixing length model. Prandtl assumed [16] that

$$\nu_t \alpha u_i' l_m$$

where u_i' is the mean magnitude of the fluctuating velocity and l_m is a "mixing length."

Furthermore, u_i' is equal to the mean velocity gradient times the mixing length yielding

$$\nu_t = l_m^2 \partial u/\partial y.$$

To account for heat transfer, the relationship $\Gamma = \nu_t/Pr_t$ is used. l_m^2 and Pr_t are empirically determined and are far from universal constants. While this model can be successfully applied in simple flows, it is not generally applicable because ν_t and therefore

Γ equal zero whenever the velocity gradient equals zero. In a case such as the problem discussed in this work where there is recirculating flow, this would imply that heat is not transferred from the hot to the cold fluid.

One-equation models give up the direct link between the fluctuating velocity scale and the mean velocity gradients. The magnitude of the fluctuating velocity is determined by writing an additional transport equation. Physically, the most meaningful scale is the $\sqrt{k}$ where k is the kinetic energy of the turbulent motion. k is defined by (for a two-dimensional problem)

$$k = 1/2(\overline{u_x'^2} + \overline{u_y'^2})$$

The $\sqrt{k}$ is a velocity scale for large-scale turbulent motion since $\nu_t \alpha u_i' L$ and $\sqrt{k} \alpha u_i'$ then

$$\nu_t = C_\mu' \sqrt{k}\, L \tag{3.20}$$

which is known as the Kolmogorov-Prandtl expression. The distribution of k can be found by writing a transport equation for k as follows:

$$\frac{\partial k}{\partial t} + u_i \frac{\partial k}{\partial x_j} = \frac{\partial}{\partial x_i}\left(u_i' \frac{\overline{u_j' u_j'}}{2} - \frac{P}{\rho}\right)\Big) - \overline{u_i' u_j'} \frac{\partial u_i}{\partial x_j}$$

[rate of change] [convective transport] [diffusive transport] [production by shear]

$$\underbrace{-\beta g_i \overline{u_i' T'}}_{\text{Buoyant production/ destruction}} \qquad \underbrace{-\nu \overline{\frac{\partial u_i'}{\partial x_j} \frac{\partial u_i'}{\partial x_j}}}_{\text{viscous dissipation}}$$

Unfortunately, the exact k equation is of no use because new unknown correlations appear in the diffusion and dissipation terms.

$$\text{(i.e. } \overline{u_i' \left(\frac{u_i' u_j'}{2} + \frac{P'}{\rho}\right)} \text{ and } \overline{\frac{\partial u_i'}{\partial x_j'} \frac{\partial u_i'}{\partial x_h'}}\text{)}$$

Therefore, model assumptions must be introduced for these terms. For the diffusive transport term, the diffusive flux of k is often assumed proportional to the gradient of k:

$$\overline{u_i' \left(\frac{u_j' u_j'}{2} + \frac{P'}{\rho}\right)} = \frac{\nu_t}{\sigma_k} \frac{\partial k}{\partial x_i}$$

where σ_k is an empirical diffusion constant. The entire dissipation term is modeled as:

$$\varepsilon = -\nu \overline{\frac{\partial u_i'}{\partial x_j} \frac{\partial u_i'}{\partial x_i}} = C_D \frac{k^{3/2}}{L}$$

where C_D is another empirical constant. The k-equation then reads

$$\frac{\partial k}{\partial t} + u_i \frac{\partial k}{\partial x_i} = \frac{\partial}{\partial x_i} \left(\frac{\nu_t}{\sigma_k} \frac{\partial k}{\partial x_i}\right) + \nu_t \left(\frac{\partial u_i}{\partial x_j} + \frac{\partial u_j}{\partial x_i}\right) \frac{\partial u_i}{\partial x_j} + \beta g_i \frac{\nu_t}{Pr_t} \frac{\partial T}{\partial x_i} - \frac{C_D k^{3/2}}{L} \tag{3.21}$$

This equation still contains a length-scale L which needs to be specified usually from simple empirical relationships like those used for l_m, the mixing length in the Prandtl model.

The two-equation models attempt to write a transport equation for the length scale in addition to turbulent kinetic energy. This transport equation need not have L as a dependent variable. Many authors have proposed using ε, the dissipation rate, as the dependent variable.

Since $\varepsilon \alpha k^{3/2}/L$ and k is known from the solution of the k equation, solving for ε specifies L. While an exact ε-equation can be derived from the Navier-Stokes equations, the resulting equation contains complex correlations whose behavior is little known. The modeled form of the ε equation is

$$\underbrace{\frac{\partial \varepsilon}{\partial r}}_{\left[\begin{array}{c}\text{rate of}\\ \text{change}\end{array}\right]} + \underbrace{u_i \frac{\partial \varepsilon}{\partial x_i}}_{\left[\text{convection}\right]} = \underbrace{\frac{\partial}{\partial x_i}\left(\frac{\nu_t}{\sigma_\varepsilon} \frac{\partial \varepsilon}{\partial x_i}\right)}_{\left[\text{diffusion}\right]}$$

$$+ \underbrace{C_{1\varepsilon} \frac{\varepsilon}{k}(P+G)(1+C_{3\varepsilon}R_f) - C_{2\varepsilon}\left(\frac{\varepsilon^2}{k}\right)}_{\left[\text{generation - destruction}\right]} \qquad (3.22)$$

where σ_ε, $C_{1\varepsilon}$, $C_{2\varepsilon}$ and $C_{3\varepsilon}$ are empirical constants and R_f is the flux Richarson number, a dimensionless number which indicates the magnitude of buoyancy effects.

The k-equation (3.21) and the ε equation (3.22) form the basis of the k-ε turbulence model used in this study. A discussion of how

the empirical constants were determined can be found in Rodi [24]. Suffice it to say that in the model used, the empirical constants had the following values [30].

Table 3.1. Constants used in k-ε model

C_μ	$C_{1\varepsilon}$	$C_{2\varepsilon}$	σ_k	σ_ε	$C_{3\varepsilon}$	Pr_t
.09	1.44	1.92	1	1.3	1	1

Bouyancy effects are accounted for at two levels in the k-ε model: the β term in the k equation and the flux Richardson number term in the ε equation. In both references 11 and 27, suggestions can be found as to how to improve results by having the constants "vary" with parameters such as Richardson number (a dimensionless measure of stratification) or the deceleration of centerline velocity.

In summary, the equations to be solved are:

Continuity

$$\nabla \cdot \vec{u} = 0 \tag{3.23}$$

Momentum

$$\frac{Du_i}{Dt} = -\nabla \frac{P_i}{o} - \nabla \cdot (\nu_t \nabla u_i) - \beta(T-T_o)\, g_i \tag{3.24}$$

Energy

$$\frac{dT}{dt} = \nabla\cdot(k_\varepsilon \nabla T) \tag{3.25}$$

where

$$\nu_\varepsilon = \nu + \nu_t$$

$$k_\varepsilon = K + \Gamma$$

$$Pr_t = \frac{\nu_t}{\lambda}$$

Kolmogorov-Prandtl

$$\nu_t = C_\mu' \quad k\, L \tag{3.26}$$

k equation

$$\frac{\partial k}{\partial t} + u_i \frac{\partial k}{\partial x_i} = \frac{\partial}{\partial x_i}\left(\frac{\nu_t}{\sigma_k} \frac{\partial k}{\partial x_i}\right) + \nu_t\left(\frac{\partial u_i}{\partial x_j} + \frac{\partial u_j}{\partial x_i}\right) \frac{\partial u_i}{\partial x_j} + \beta g_i \frac{\nu_t}{Pr_t} \frac{\partial T}{\partial x_i}$$

$$- \frac{C_D\, k^{3/2}}{L} \tag{3.27}$$

ε equation

$$\frac{\partial \varepsilon}{\partial t} + u_i \frac{\partial \varepsilon}{\partial x_i} = \frac{\partial}{\partial x_i}\left(\frac{\nu_t}{\sigma_\varepsilon} \frac{\partial \varepsilon}{\partial x_i}\right) \tag{3.28}$$

$$+ C_{1\varepsilon} \frac{\varepsilon}{k} (P+G)(1+C_{3\varepsilon} R_f) - C_{2\varepsilon} \frac{\varepsilon^2}{k}$$

Pr_t, C_μ', C_D, $C_{1\varepsilon}$, $C_{2\varepsilon}$, $C_{3\varepsilon}$, σ_k and σ_ε are empirically defined constants. β, ν, k and R_f are fluid properties, while g, T_o and P should be defined by the problem leaving seven unknowns (u_x, u_y, T, ν_t, Γ, k and ε) and seven equations. The method of solution for these equations is discussed in the next chapter.

4. THE METHOD OF SOLUTION

In order to solve the differential equations developed in the previous chapter, approximate finite difference equations must be derived. There are a number of ways that finite difference equations can be written which greatly influence both the magnitude of the error introduced by the approximation and the stability of the solution. The numberical scheme presented in this chapter was developed by the Laboratorie National de Hydraulique of Electricite de France. It is described in references 3, 30, 31 and 32 and is the scheme used to analytically solve the problem of the turbulent mixing of the HPSI jet.

The primitive variables involved in the equations to be solved are u, v and P. (In the previous section, the subscripts x and y or i and j were used to denote the directional component of velocity. In the following sections, for convenience, the subscripts are dropped and v indicates the velocity component in the y direction.) The solution can be found directly in terms of these variables or it can be found in terms of the vorticitiy, ω, and the stream function, ψ. The algorithms which use the pressure variable have more complicated boundary conditions because the equations require knowledge of the pressure gradient. In cases where a solution for the pressure field is not a desired result of the calculation it is easier to work in terms of the vorticity and stream function because of the simpler form of the boundary condition. The stream/function/vorticity method assumes that the main flow outside the viscous sublayer is ideal (i.e. inviscid and irrotational). The outer edge of the viscous sublayer is then connected to the known "no-slip"

boundary condition at the wall by means of an empirical relationship such as the "universal law of the wall" [16]. Because detailed knowledge of the pressure field is not of interest in this problem, the stream function/vorticity method was used.

For simplicity, only the discretization of the equations of continuity, momentum and internal energy will be discussed in detail. The kinetic energy and viscous dissipation equations are similar and treated analogously. The equations to be solved are:

x-component of momentum:

$$\frac{\partial u}{\partial t} + u \frac{\partial u}{\partial x} + v \frac{\partial u}{\partial y} = - \frac{1}{\rho_o} \frac{\partial P}{\partial x} + \text{div } (\nu_e \text{ grad } u) \tag{4.1}$$

y-component of momentum:

$$\frac{\partial v}{\partial t} + u \frac{\partial v}{\partial x} + v \frac{\partial v}{\partial y} = - \frac{1}{\rho_o} \frac{\partial P}{\partial y} + \text{div } (\nu_e \text{ grad } v) + \beta g(T-T_o) \tag{4.2}$$

continuity:

$$\frac{\partial u}{\partial x} + \frac{\partial v}{\partial y} = 0 \tag{4.3}$$

internal energy:

$$\frac{\partial T}{\partial t} + u \frac{\partial T}{\partial x} + v \frac{\partial T}{\partial y} = \text{div } (K_e \text{ grad } T) \tag{4.4}$$

where u, v, T, and P now represent the mean flow values of velocity in the x component, y component, temperature and pressure. As before, β is the dilatation coefficient defined from:

$$\rho_{\text{reference}} - \rho = \rho\beta(t-t_{\text{reference}}).$$

T_o is the initial temperature, and K_e and ν_e are effective thermal conductivity and kinematic viscosity which include turbulent effects. The orientation is assumed such that gravity acts only in the upward, vertical direction (which eliminates the bouyancy term from equation 4.1).

4.1. Discretization in Time

Assume that all values are known at time step N and that it is desired to solve for the values at time step n+1. The method described is based on Chorin [5]. First, the auxiliary variable u^{aux} and v^{aux} are defined such that:

$$\frac{u^{aux} - u^N}{\delta t} + u^N \frac{\delta u^N}{\delta x} + v^N \frac{\delta u^N}{\delta y} = \text{div}(\nu_e \text{ grad } u^{aux}) \tag{4.5}$$

and

$$\frac{v^{aux} - v^N}{\delta t} + u^N \frac{\delta v^N}{\delta x} + v^N \frac{\delta v^N}{\delta y} = \text{div}(\nu_e \text{ grad } v^{aux}) \tag{4.6}$$

where the superscript N represents the time step at which the values of these variables are to be used. Since u^N and v^N are known, u^{aux} and v^{aux} are given by solving the two equations 4.5 and 4.6. By subtracting equation 4.5 from 4.1 and equation 4.6 from 4.2, it is found that the auxiliary variables are related to the desired variable, u^{N+1} and v^{N+1}, in the following way:

$$\frac{u^{N+1} - u^{aux}}{t} = - \frac{1}{\rho_o} \frac{\partial P^{N+1}}{\partial x} \tag{4.7}$$

$$\frac{v^{N+1} - v^{aux}}{\delta t} = - \frac{1}{\rho_o} \frac{\partial P^{N+1}}{\partial y} \tag{4.8}$$

To eliminate the need for knowledge of the pressure function, the curl of the vector $\dot{V}$ is taken. When this is done, all terms involving the pressure, P, cancel.

$$\dot{V}^{N+1} = u_i^{N+1} + v_j^{N+1} = - \frac{1}{\rho_o} \frac{\partial P^{N+1}}{\partial x} \delta t + u^{aux} - \frac{1}{\rho_o} \frac{\partial P^{N+1}}{\partial y} \delta t$$

$$+ v^{aux} + \beta g (T^{N+1} - T_o) \delta t$$

$$\text{curl } \dot{V}^{N+1} = \begin{vmatrix} i & j & k \\ \partial/\partial x & \partial/\partial y & \partial/\partial z \\ u & v & w \end{vmatrix}$$

$$= \frac{\partial v^{aux}}{\partial x} - \frac{\partial u^{aux}}{\partial y} - \beta g \frac{\partial T^{N+1}}{\partial x} \delta t$$

or

$$\text{curl } (u^{N+1}, v^{N+1}) = \text{curl } (u^{aux}, v^{aux}) - \beta g \frac{\partial T^{N+1}}{\partial x} \delta t \tag{4.9}$$

By definition, the curl of the velocity vector is the vorticity, ω. This vorticity is related to the stream function as:

$$\nabla \psi = - \omega \tag{4.10}$$

and the stream function is related to the final velocities as:

$$u^{N+1} = -\frac{\partial \psi}{\partial y} \tag{4.11}$$

$$v^{N+1} = \frac{\partial \psi}{\partial x} \tag{4.12}$$

Equation 4.9 involves the temperature at time step N+1 which can be found from the discretization of equation 4.4:

$$\text{i.e. } \frac{T^{N+1} - T^{N}}{\delta t} + u^{N} \frac{\delta T^{N}}{\delta x} + v^{N} \frac{\delta T^{N}}{\delta y} = \text{div}(K_e \text{ grad } T^{N+1}) \tag{4.13}$$

Since all variables are known at time step N, T^{N+1} can be found directly from the solution of equation 4.13.

In summary, the procedure is as follows:

- solve equations 4.5 and 4.6 for u^{aux} and v^{aux}
- solve equation 4.13 for T^{N+1}
- solve equation 4.9 for the vorticity
- solve equation 4.10 for the stream function
- solve equations 4.11 and 4.12 for the final velocities u^{N+1} and v^{N+1}.

Thus, the computation of time step N+1 is completed and the computation of time step N+2 may be begun if desired.

4.2. Discretization in Space

The above discussion focused on the discretization of the differential equations with time. In order to utilize the outlined procedure, there must also be a discretization with space. This is done by dividing equations 4.5, 4.6, and 4.13 into two parts and solving them separately. The equations are of the general form:

$$\frac{\partial f}{\partial t} + u \frac{\partial f}{\partial x} + v \frac{\partial f}{\partial y} = C\left(\frac{\partial^2 f}{\partial x^2} + \frac{\partial^2 f}{\partial y^2}\right) \tag{4.14}$$

where f is either u^{aux}, v^{aux} or T^{N+1}. The left-hand side of equation 4.14 represents the transport term while the right-hand side represents the diffusion term. In solving such transport equations, the advection and diffusion steps are separated and solved successively.

4.2.1. Diffusion term

To solve the diffusion component of equation 4.14, the following equation must be discretized and solved:

$$\frac{\partial^2 f}{\partial x^2} + \frac{\partial^2 f}{\partial y^2} = 0 \tag{4.15}$$

Referring to Figure 4.1, it can be seen that

$$\left.\frac{\partial^2 f}{\partial x^2}\right|_{m,n} = \left.\frac{\partial f}{\partial x}\right|_{m+1/2,n} - \left.\frac{\partial f}{\partial x}\right|_{m-1/2,n}$$

where

$$\left.\frac{\partial f}{\partial x}\right|_{m+1/2,n} \cong \frac{f_{m+1,n} - f_{m,n}}{\Delta x}$$

and

$$\left.\frac{\partial f}{\partial x}\right|_{m-1/2,n} \cong \frac{f_{m,n} - f_{m-1,n}}{\Delta x}$$

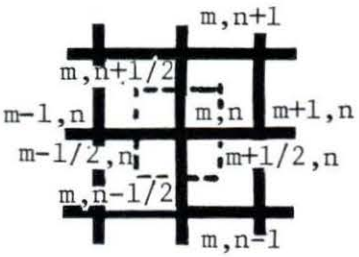

Figure 4.1 Node locations for Finite Difference equations

When similar equations are written for $\partial^2 f/\partial y^2$ and these are substituted into equation 4.15 the following equation results:

$$f_{mn}(2\Delta x + 2\Delta y) = (f_{m+1,n} + f_{m-1,n})\Delta y + (f_{m,n+1} + f_{m,n-1})\Delta x$$

This equation was solved with the Gauss-Seidel method. This method of discretization is called a central difference approximation. The order of a discretization approximation is usually determined from a Taylor's series expansion:

$$\text{i.e.} \quad f_{m+1,n} = f_{m+1/2,n} - \frac{\Delta x}{2}\frac{\partial f}{\partial x}\bigg|_{m+1/2,n} + \frac{\Delta x^2}{8}\left(\frac{\partial^2 f}{\partial x^2}\right)\bigg|_{m+1/2,N}$$

$$+ O(\Delta x^3)$$

and

$$f_{m,n} = f_{m+1/2,n} + \frac{\Delta x}{2}\frac{\partial f}{\partial x}\bigg|_{m+1/2,n} + \frac{\Delta x^2}{8}\frac{\partial^2 f}{\partial x^2}\bigg|_{m+1/2,n} + 0(\Delta x^3)$$

The central difference approximation used above is obtained by subtracting these 2 equations. Since all terms up to Δx^2 are retained (or cancelled), the approximation is third order accurate.

4.2.2. Transport term

The transport term of equation 4.14 is of the form:

$$\frac{\partial f}{\partial t} + u\frac{\partial f}{2x} + v\frac{\partial f}{2y} \qquad (4.16)$$

The unknown f is defined by its value at each node. The field f is known at time step N as is the boundary condition f_o at the area where the flow enters the domain. For the transport term, rather than considering convection fluxes through central surfaces (as in the diffusion term), it is more natural to follow a quantity as it is convected along a stream line. Consider Figure 4.2 which illustrates the method used called the Characteristic Method. Given a particle which is at node M_j at time $t_N + \delta t$, the position P_j where it was at time t_N can be calculated by solving for the pathline [3].

Along the characteristic curve C_j (defined by $\frac{dx}{dt} = u_i$), equation 4.16 can be written as $\frac{df}{dt} = 0$. Therefore, to compute f^{N+1} (which is in this case, either T^{N+1}, u^{aux} or v^{aux}) for any node M_j, the following is done:

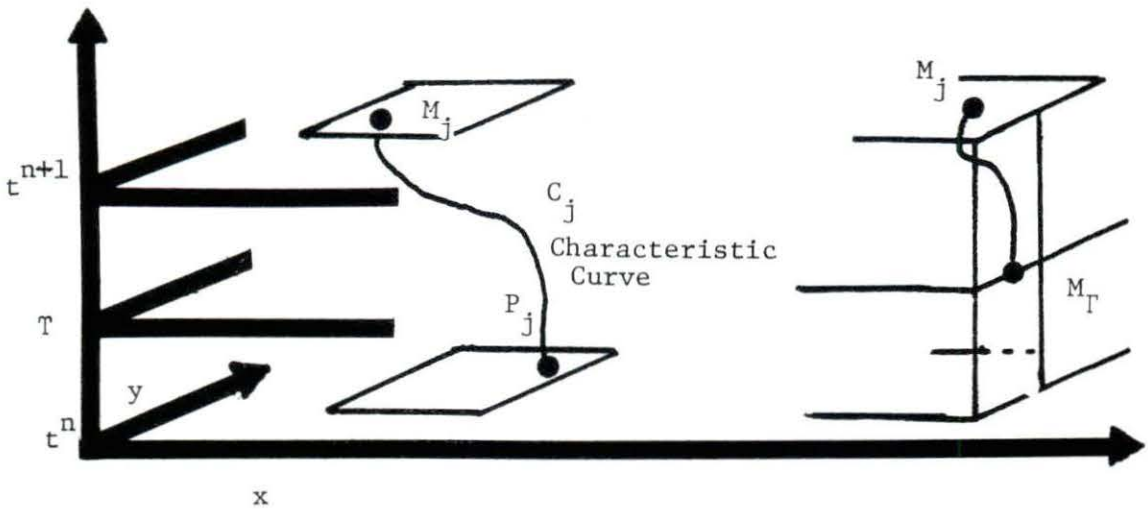

Figure 4.2 Illustration of the Method of Characteristics

- compute the characteristic line C_j leading to M_j at time t^{N+1} from

$$\frac{dx_i}{dt} = u_i \,, \quad x(t^{N+1}) = M_j \tag{4.17}$$

- compute $f_j^N = f^N(P_j)$ where P_j is the foot of the pathline (i.e. $x(t^N)$).

The expected result is $f^{N+1}(M_j) = f^N(P_j)$ because P_j and M_j belong to the same characteristic. Equation 4.17 is an ordinary differential equation. Its solution was carried out by a Runge Kutta Method.

In most cases P_j is not a discretized node, so the value $f^N(P_j)$ must be interpolated from the following Hermetical polynomial:

$$f^N(P_j) = \sum_{i=1}^{4} \left(C_i f_i + C_{x,i} \left.\frac{\partial f}{\partial x}\right|_i + C_{y,i} \left.\frac{\partial f}{\partial y}\right|_i + C_{xy,i} \left.\frac{\partial^2 f}{\partial x \partial y}\right|_i \right)$$

where $f^N(P_j)$ is the interpolated scalar at point P, $\partial f/\partial x|_i$, $\partial f/\partial y|_i$ and $\partial^2 f/\partial x \partial y|_i$ are the derivatives of the scalar field at the nodes forming the corner of the cell (i=1,4). C_i, $C_{x,i}$, $C_{y,i}$ and $C_{xy,i}$ are cubic polynomials in x and y which relate the location of P to the grid. The spatial discretization is, therefore, fourth order accurate.

Boundary conditions are taken into account when, between t^N and t^{N+1}, the pathline crosses a boundary. In such a case, the integration of equation 4.17 stops at time τ and gives the intersection M_Γ between the characteristic and the boundary. At this point, $f^{N+1}(M_j)$ is set equal to the boundary value $f_o(\tau, M_\Gamma)$.

This method of calculation of the advection terms is very stable. Usually the Courant number:

$$Co = \frac{\Delta t \; u_x}{\Delta x}$$

must be less than unity. With this scheme, the Courant number may be greater than 1 and the time step is dictated by the time variation of the velocity field.

The solution to the two separated terms of the equation (advection and diffusion) are repeated until the solution for f converges.

4.2.3. The vorticity and stream function

The above is a description of how equations 4.5, 4.6 and 4.13 are solved. Once they are solved for a certain time step, the u^{aux}, v^{aux}

and T^{N+1} fields are known and equation 4.9, the solution for vorticity can be found directly from:

$$\omega = \frac{v^{aux}_{m+1,n} + v^{aux}_{m-1,n} - 2v^{aux}_{m,n}}{\Delta x} - \frac{u^{aux}_{m+1,n} + u^{aux}_{m-1,n} - 2u^{aux}_{m,n}}{\Delta y}$$

$$\beta - \frac{g\Delta t\ (T^{N+1}_{m+1,n} + T^{N+1}_{m-1,n} - 2T^{N+1}_{m,n}}{\Delta x}$$

Equation 4.10 is discretized using nine points. Additionally the grid for ψ and ω is offset from the grid for u, v, and T (see Figure 4.3). This is for convenience because velocity is obtained from a simple derivative of ψ.

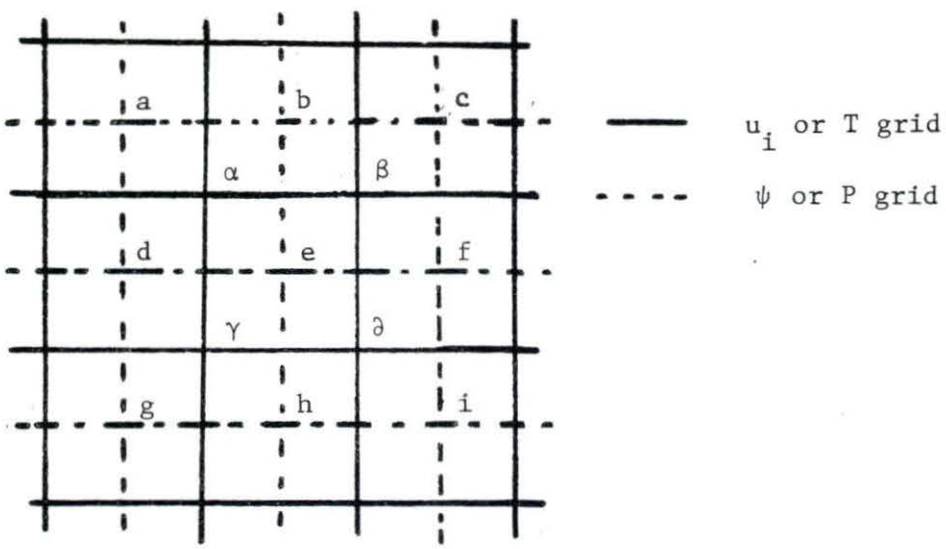

Figure 4.3 Staggered P,ψ grid

The nine point discretization is:

$$\Delta\psi = C_1\psi_a + C_2\psi_b + C_1\psi_c - C_2\psi_d - C_2\psi_f + C_1\psi_g + C_2\psi_h$$

$$+ C_1\psi_i - 4C_1\psi_e = \omega$$

where

$$C_1 = \frac{1}{4\Delta x^2} + \frac{1}{4\Delta y^2}$$

and

$$C_2 = \frac{1}{2\Delta y^2} - \frac{1}{2\Delta x^2} .$$

Equations 4.11 and 4.12 are similarly discretized and the final velocities are found. This system of equations (the discretized approximations to 4.10, 4.11, and 4.12) are solved together using a successive over-relaxation techique. (They are solved together because boundary conditions are known for u^{N+1} and v^{N+1} rather than ψ.) The numerical solutions to the k and ε equations are of the same form and are done analogously.

4.3. The Computer Code

This solution scheme is programmed as ULYSSE, a proprietary code of the Laboratorie National de Hydraulique de Electricite de France. The use of the code is described in reference 12.

4.3.1. Boundary conditions

The boundary conditions and initial conditions which are necessary to solve the described system of equations are introduced either as input to the code or within the code itself. Turbulent flow can be bounded by either a free-surface (e.g. ocean-air interface), non-turbulent flow (e.g. a jet injected into a large stagnant body) or by solid walls, as in this problem. In the case of solid walls, the boundary condition which is known for the velocity is the "no-slip" condition; i.e. $\partial u_i/\partial x_i = 0$ at the wall. Unfortunately, the equations derived in Chapter 3 (specifically the k and ε equations) assume that the large-scale interactions predominantly responsible for scalar transport are unaffected by the fluid's viscosity. Therefore, they are not applicable to the viscous sub-layer next to the wall. Even if they were applicable, there are very steep gradients near the wall and many grid points would have to be placed there for adequate resolution. These problems can be avoided by using an empirical law which connects the wall conditions to the variables outside the viscous sublayer. In this work, the "universal law of the wall" [16] is used where:

$$\frac{u_o}{u_*} = \frac{1}{\kappa} \ln \frac{u_* \delta_n}{\nu} + 5$$

u_o is the velocity parallel to the wall, u_* is the frictional velocity ($u_* = \tau/\rho$), κ is the von Karmen constant (.41) and δ_N is the boundary

layer thickness. For the temperature boundary condition, the walls were assumed to be adiabatic; i.e. $\partial T/\partial y = 0$. Boundary conditions for k and ε were

$$k = \frac{u_*^2}{C\mu} \quad \text{and} \quad \varepsilon = \frac{10\ u_*^3}{\alpha\ \delta N}$$

which result from the fact that in the boundary layer region, Reynolds stresses are nearly constant. In this region, convection and diffusion of $\overline{u_i\ u_j}$ are negligible so that local equilibrium prevails.

Initial conditions are T_o, the fluid temperature at time 0, u_{io} the velocity of the fluid at time 0, and k_o and ε_o the initial value of turbulent kinetic energy and dissipation, respectively. k_o and ε_o were calculated from empirical equations of the form:

$$k_o = .003u_o^2$$
$$\varepsilon_o = .000675u_o^3$$

With these boundary and initial conditions, the equations form a closed set which can be solved.

4.3.2. Grid spacing

The choice of Δx, Δy and Δt is left to the user of the code. The x,y grid used to solve the problem considered in this thesis is shown in Figure 4.4. The overall dimensions of the problem are based on a personal letter[1]. The modeled length of the cold leg (6.86 m) is

[1] D. A. Peck, Combustion Engineering Power Systems, Windsor, Connecticut, personal letter to K.H. Sun (October 19, 1981).

represented by 84 grid points in the x direction and 16 in the y direction. The HPSI piping is modeled by 5 grid points in the x direction and 8 in the y direction. The grid is non-regular but it is rectilinear. The points on the left-hand side are .1524 m apart in the x direction; the points in the area of intersection of the two pipes are .0508 m apart in the x direction; the points on the right hand side of the cold leg were .0762 m apart. The irregular spacing results from a desire to minimize computing time and a belief that in the stagnant end of the cold leg (left-hand side, Figure 4.4) only the gross characteristics of the fluid flow were necessary. Spacing in the y direction is regular throughout the cold leg at .0508 m, while in the HPSI pipe it is .0762 m. Again these are based on the belief that the detail in the HPSI pipe is less important than the detail in the mixing region. The length of HPSI piping modeled was arbitrary but intended to be long enough so that a parabolic velocity profile could develop. In general, the grid spacing and dimensions for this problem were based on the spacing and dimensions of grids successfully used in other problems.

As input to the code, each point P (i,j) is designated either:

1) outside the boundary of the problem
2) a wall
3) in the flow field
4) an entering or exiting point of the fluid.

For example, points P(i,j) where i = 1 through 85 and j=1 are all outside the boundary of the problem. Points P(i,j) where i=2 and j=2

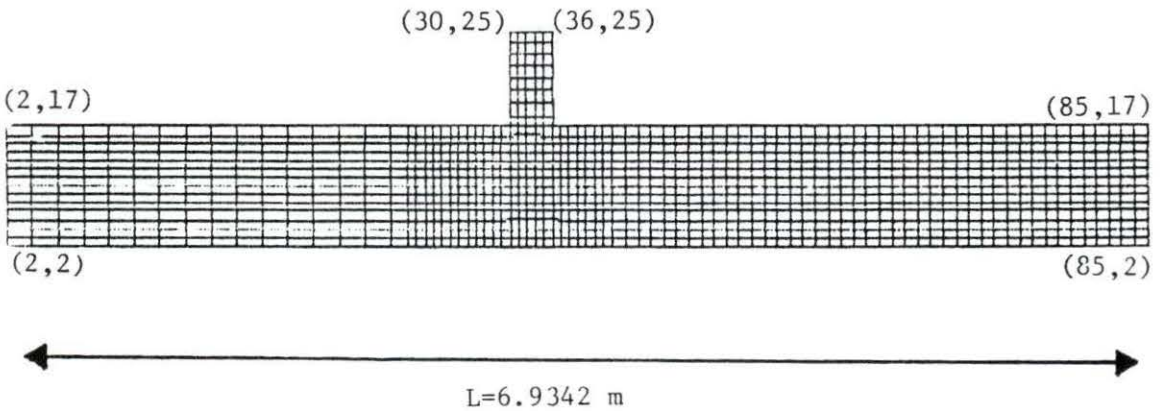

Figure 4.4 Grid used for analysis of HPSI problem

through 17 are solid wall while points P(i,j) where i=31 through 35 and j=25 are entering points. Initial conditions are prescribed for the velocity and temperature of the entering points and the temperature of the flow field. These are discussed further in the next chapter.

5. THE RESULTS

The problem which was investigated using the ULYSSE code described in Chapter 4 is one which arises due to the injection of High-Pressure Safety Injection (HPSI) fluid into the cold leg of the reactor (see Figure 1.1). The cold HPSI fluid does not mix completely with the warmer stagnant fluid found in the cold leg. Instead, the fluid stratifies with a colder, more dense layer settling at the bottom of the pipe and a warmer, less dense layer rising to the top. The goal of this work was to account for stratification in order to predict the temperature of the fluid at the reactor vessel wall as a function of time. The results presented herein represent an attempt to accurately model these buoyancy effects.

The region which was modeled is shown in Figure 5.1. In the interest of saving computation time, only the cold leg and injection point are modeled. The addition of the downcomer would have increased computation time and costs by approximately a factor of four. The transients in the cold leg are the most severe since the fluid has had little time to entrain warmer fluid. The further the fluid is from the point of injection, the longer the fluid has had to mix with the warmer fluid; therefore, it is conservative to assume that any transient the reactor vessel wall might experience would be bound by the transient experienced in the lower half of the cold leg piping.

The fluid enters the modeled volume at point 1 with a volumetric flow rate of 0.0174 m^3/sec and a flat velocity profile of 0.3434 m/sec. The fluid exits the volume at point 2 with the same volumetric flow rate, but with the velocity profile unspecified. The temperature of the HPSI fluid is approximately room temperature, 26.7°C, while the initial temperature of the stagnant fluid in the cold leg is 282°C. Point 3, a solid boundary, represents the loop seal which occurs in the reactor coolant piping prior to the reactor coolant pump (backflow through the pump will occur).

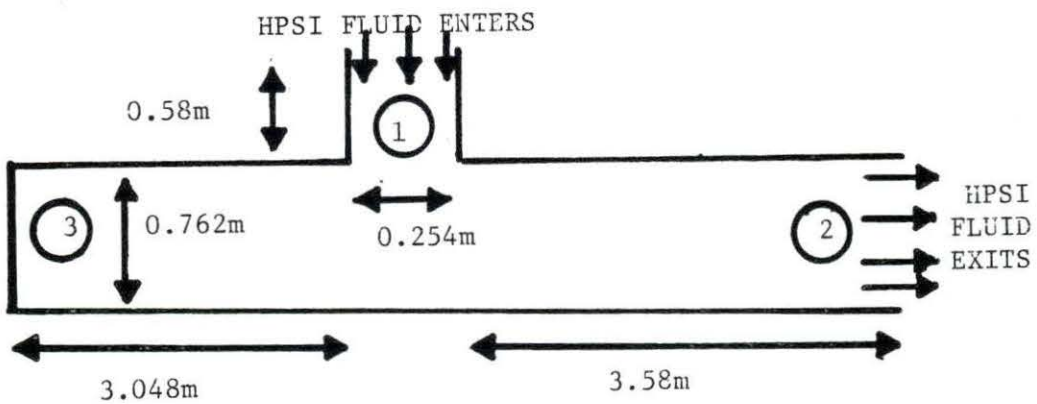

Figure 5.1 Region modeled for HPSI analysis

Important dimensionless parameters which characterize this flow are Reynolds number, densimetric Froude number, and Richardson number

[29]. The Reynold's number, $DV\rho/\mu$, is a standard dimensionless number indicating turbulence where:

D - pipe diameter

V - mean fluid velocity

ρ - fluid density

μ - fluid viscosity

Based on the HPSI fluid, Re equals 102,000 - indicative of turbulent flow. The densimetric Froude number is defined [29]:

$$Fr = \frac{V}{\left(gD \frac{\rho_m - \rho_o}{\rho_m}\right)^{1/2}}$$

where g is gravity (9.8 m/sec^2) and the subscripts m and o refer to fully mixed and initial (ambient) densities respectively. In this case, the mean fluid velocity is 0.3434 m/sec and D is the diameter of the cold leg. The ambient density prior to buoyant flow is the density of the cold leg fluid while the fully mixed density (due to the stagnation of the coolant flow in the loop) will eventually be the HPSI fluid density. The Froude number for this case is 0.032.

The pipe Richardson number is defined by [29]:

$$Ri_\rho = \frac{\rho_m - \rho_o}{\rho_o} \quad g \frac{d \cos \theta}{V^2}$$

where all the variables have the meanings as previously defined. Because of the horizontal orientation, cos θ is equal to 1. The

pipe Richardson number can be interpreted as a measure of buoyancy flux per unit width and indicates the degree of stratification. Ri_ρ equals 1114 for this problem. Except for the fact that $\Delta\rho/\rho$ is defined as $\rho_m-\rho_o/\rho_o$ in the Richardson number while it is defined as $\rho_m-\rho_o/\rho_o$ in the Froude number, the Froude number is equal to the inverse of the square root of the Richardson number.

5.1. A Qualitative Discussion of the Results

The results from the computer analysis are presented in Figures 5.2 through 5.18. At each time, isotherms and velocity profiles are shown. The magnitude of the directional arrows indicate the relative magnitude of the velocity vector at that point. The isotherms are plotted every 30^oC beginning at 30^oC with the largest isotherm equal to 270^oC. Examining Figure 5.3 shows that the recirculation patterns set up by the entrainment of warm fluid by the colder HPSI jet are apparent at only 3.3 seconds. The times reported here are real time, not computation time. For example, because time steps of 0.05 seconds were used, 3.3 seconds represents the 66th time step. Since each time step required approximately 3 seconds of C.P.U. time to complete the calculations, 3.3 seconds represents 1.6 minutes of computation time. Figure 5.4 demonstrates that the stratification of the cold fluid is readily apparent by only 6.3 seconds. It also demonstrates how the HPSI flow separates into two components - one which flows back towards the closed end and one which flows forward

to the open end. In Figure 5.5, the development of counter-current flow into the open end of the cold leg is predicted even though the velocity profile at this point was unspecified. Following the temperature and velocity profiles chronologically, both the growth of the cold HPSI layer along the bottom of the cold leg and the growth of the recirculation pattern is observable. Isolated pockets of cold or hot fluid are also seen; these grow and dissipate with increasing time. Throughout the transient, the HPSI jet remains intact as it falls to the bottom of the cold leg.

In order to gain confidence in the results of the computer model for such a complex flow situation, a comparison of the analytical results with experimental results was undertaken. The experimental results are from 1/5 scale tests performed by Creare, Inc. of Hanover, New Hampshire. The results are published in references 7 through 9. In performing these experiments, prototypical Froude numbers were preserved. Both quantitative and qualitative data were recorded. The qualitative data result from dye being injected with the HPSI fluid and the diffusion of the dye being recorded with photography.

The following are some of the reported observations [7]:

"Extensive still and motion picture photography reveal the following key phenomena within the range of the study:

- buoyancy induced flow stratification
- turbulent mixing and entrainment
- counter current flow into the cold leg."

Other qualitative experimental findings include those in reference 9:

> "... the jet remains relatively intact as it falls. When the injected jet strikes the bottom of the cold leg pipe, the HPI flow spreads along the pipe wall as a thin film.... The HPI flow splits roughly equally with about half being directed toward the vessel and the remainder, in backflow, toward the pump.... After a time [...] a stratified layer of cold water forms, thickens and eventually fills the pipe."

Certainly qualitatively the analytical results match the experimental findings well. A quantitative discussion of the results follows.

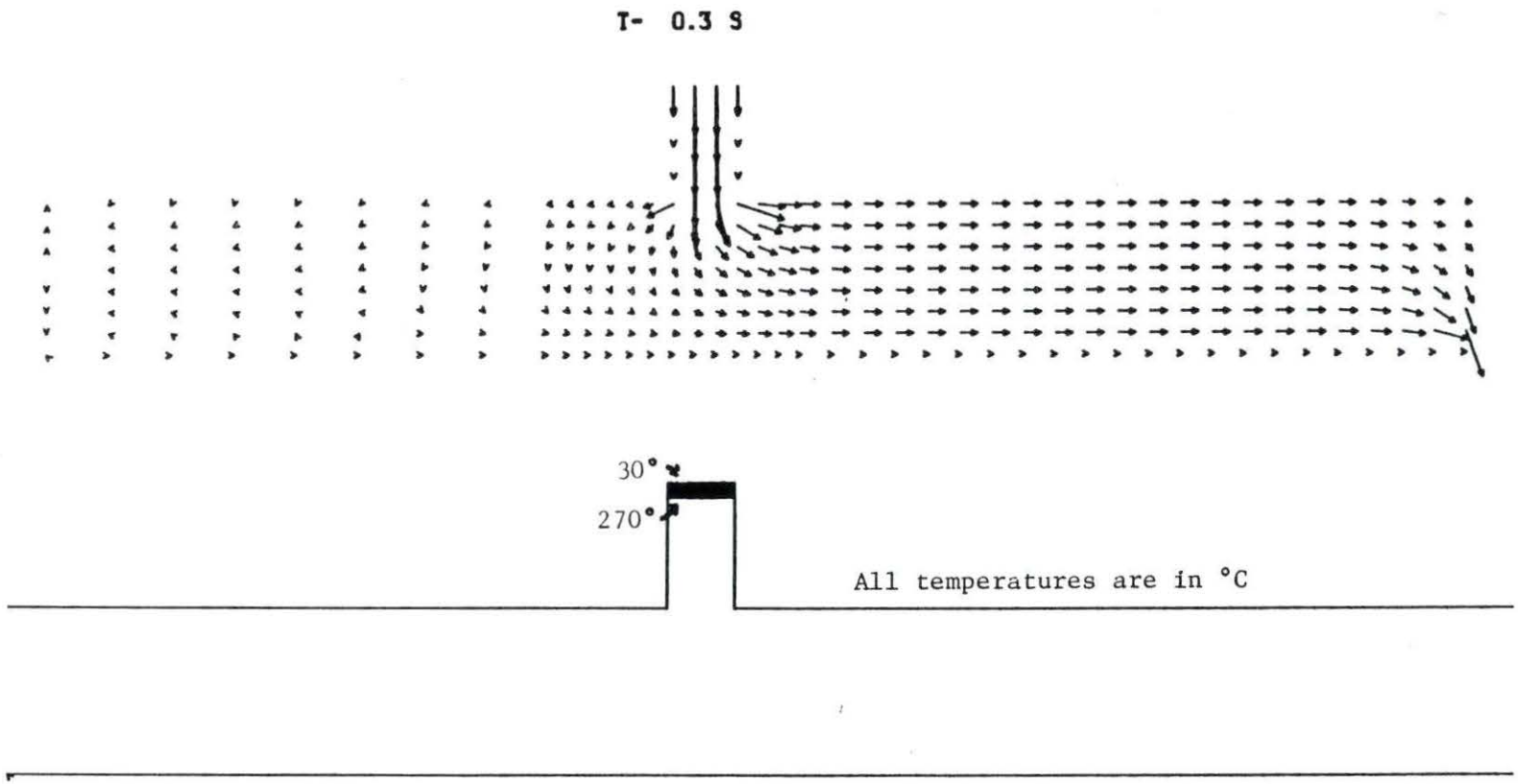

Figure 5.2 Temperature and velocity profiles at 0.3 seconds

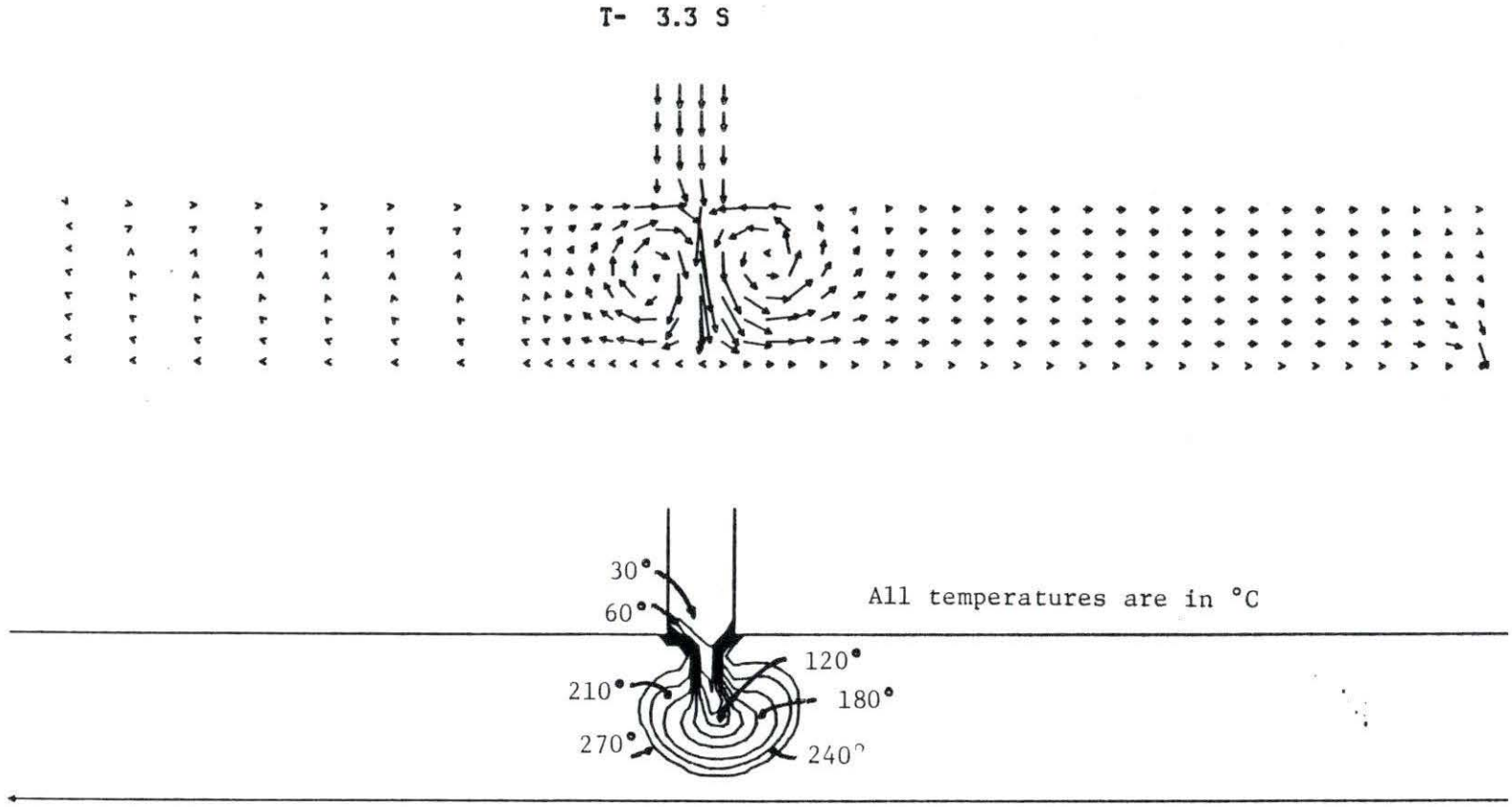

Figure 5.3 Temperature and velocity profiles at 3.3 seconds

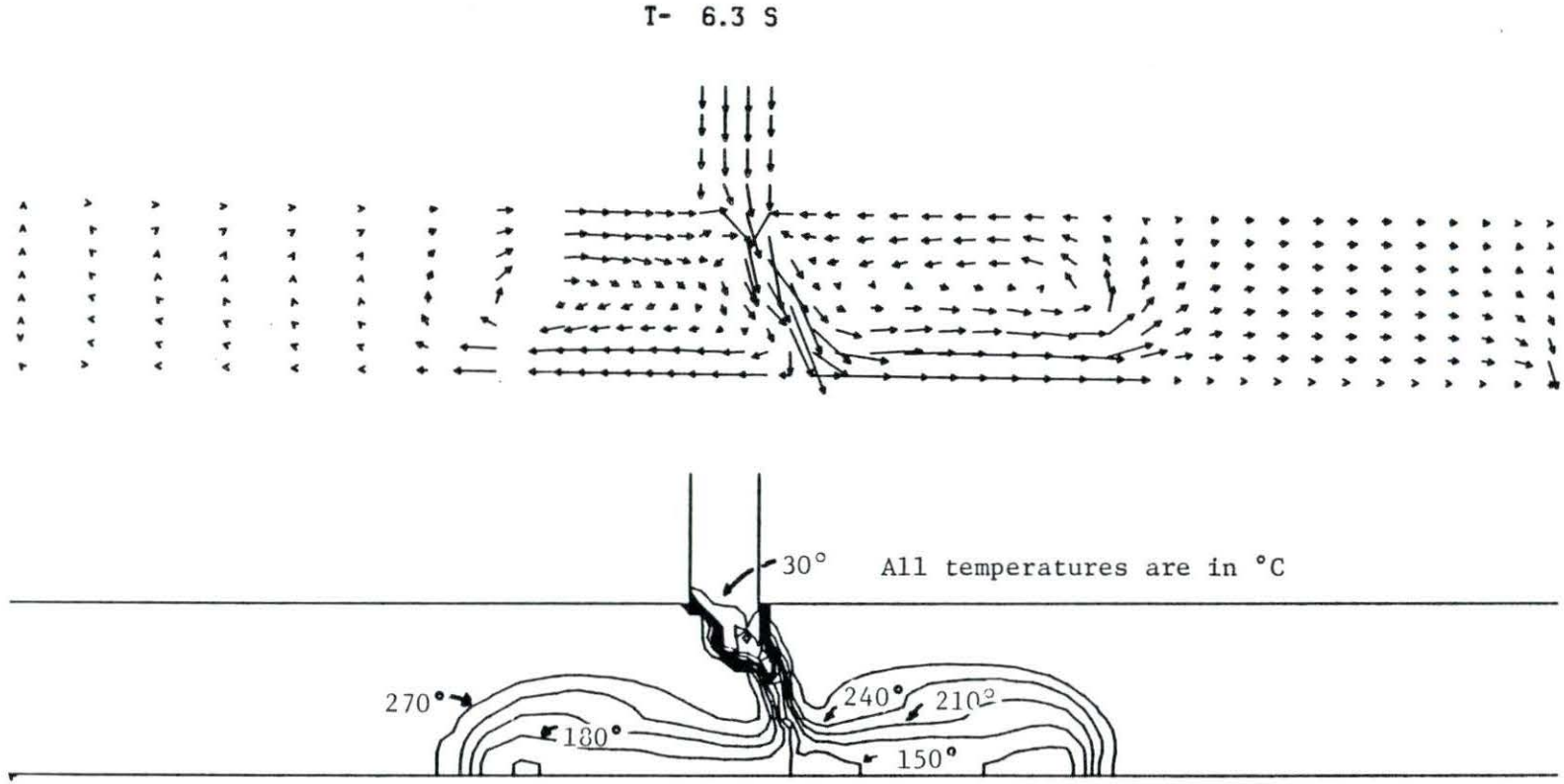

Figure 5.4 Temperature and velocity profiles at 6.3 seconds

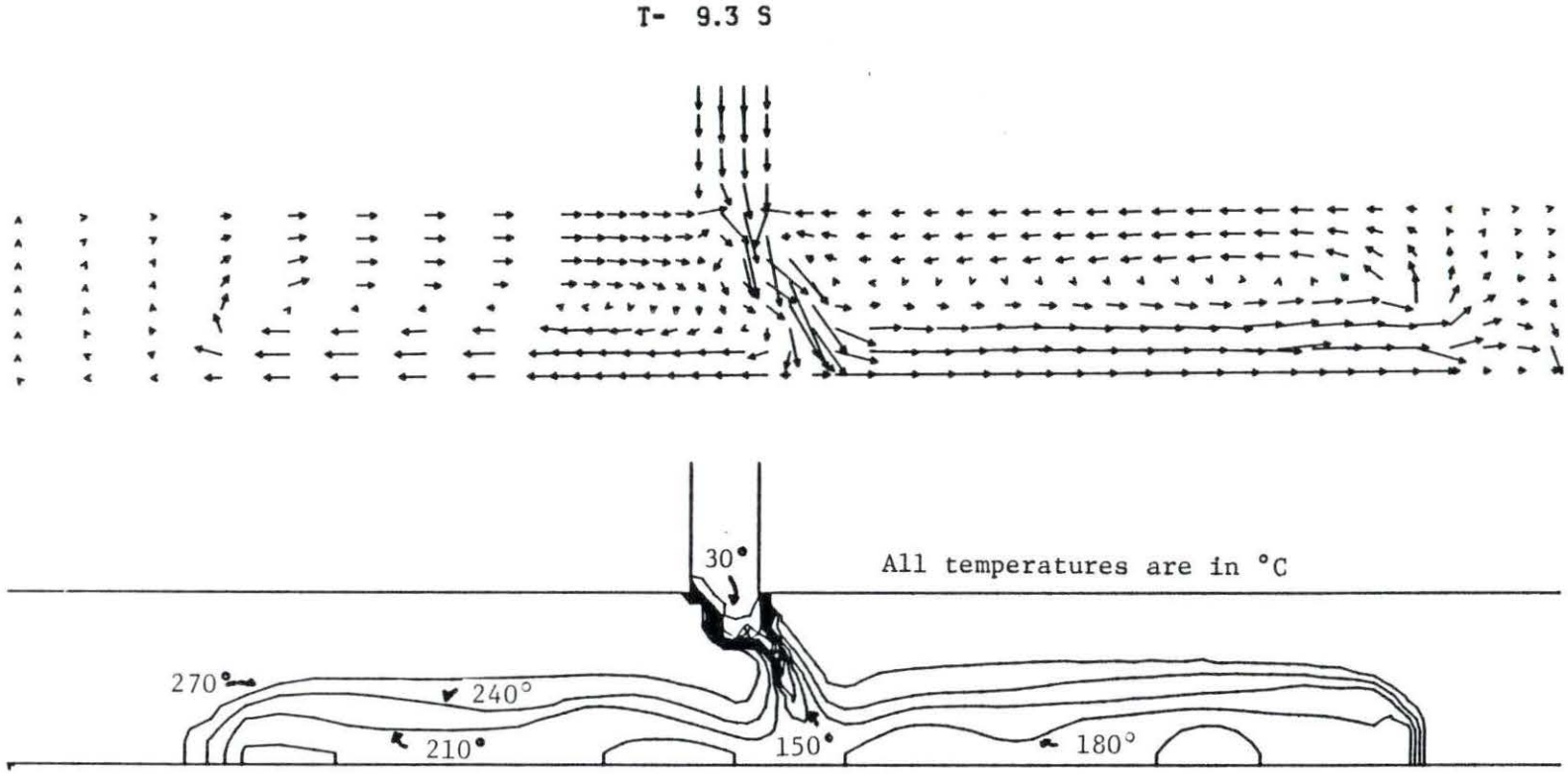

Figure 5.5 Temperature and velocity profiles at 9.3 seconds

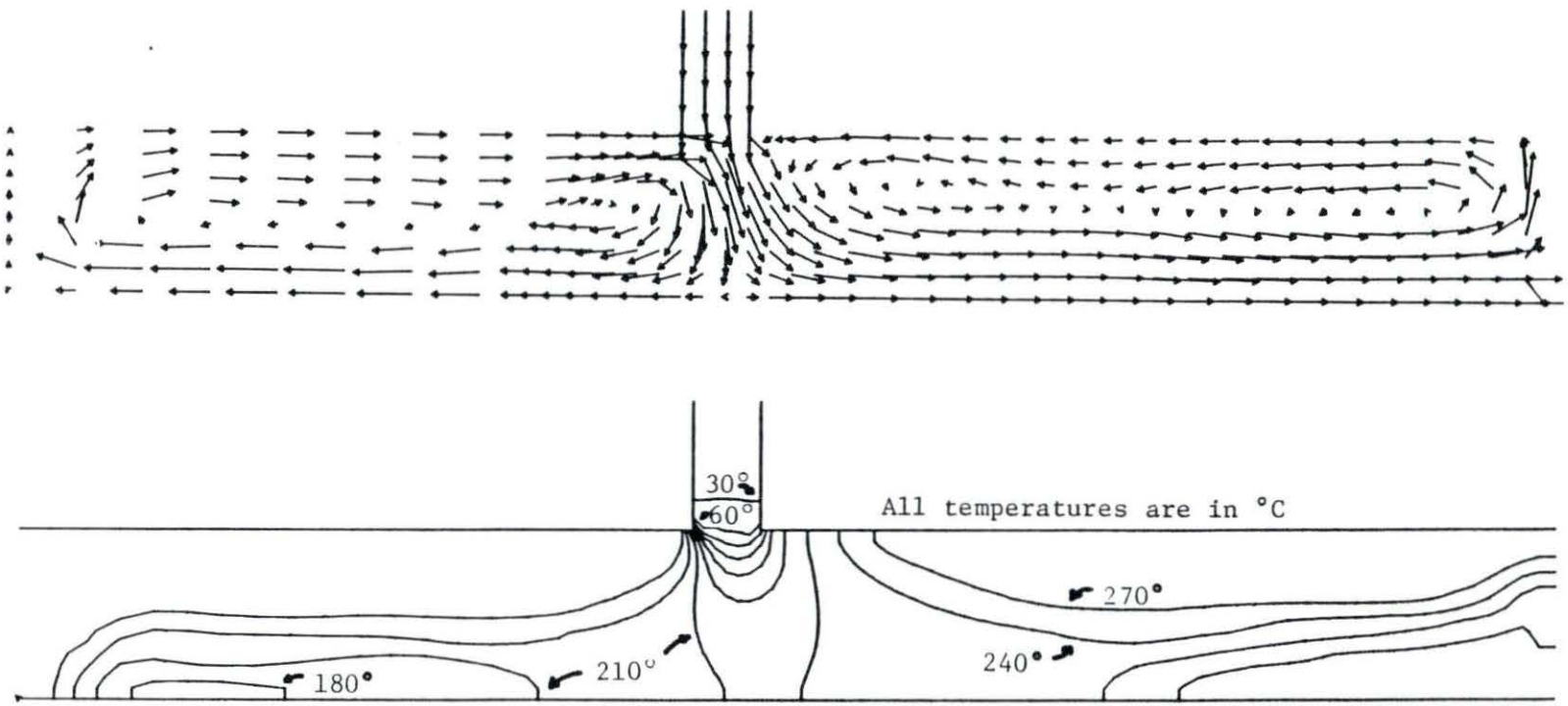

Figure 5.6 Temperature and velocity profiles at 11.4 seconds

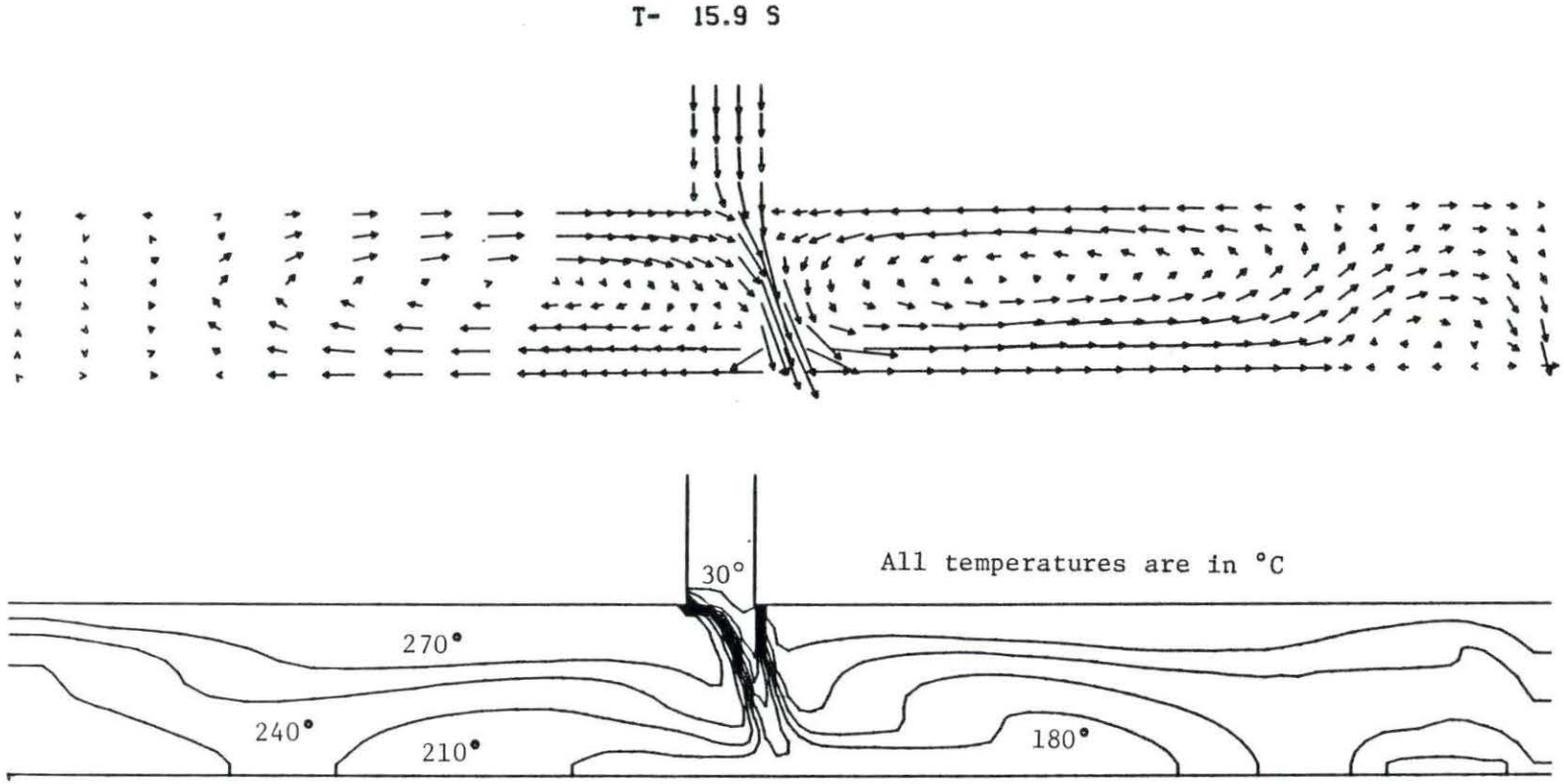

Figure 5.7 Temperature and velocity profiles at 15.9 seconds

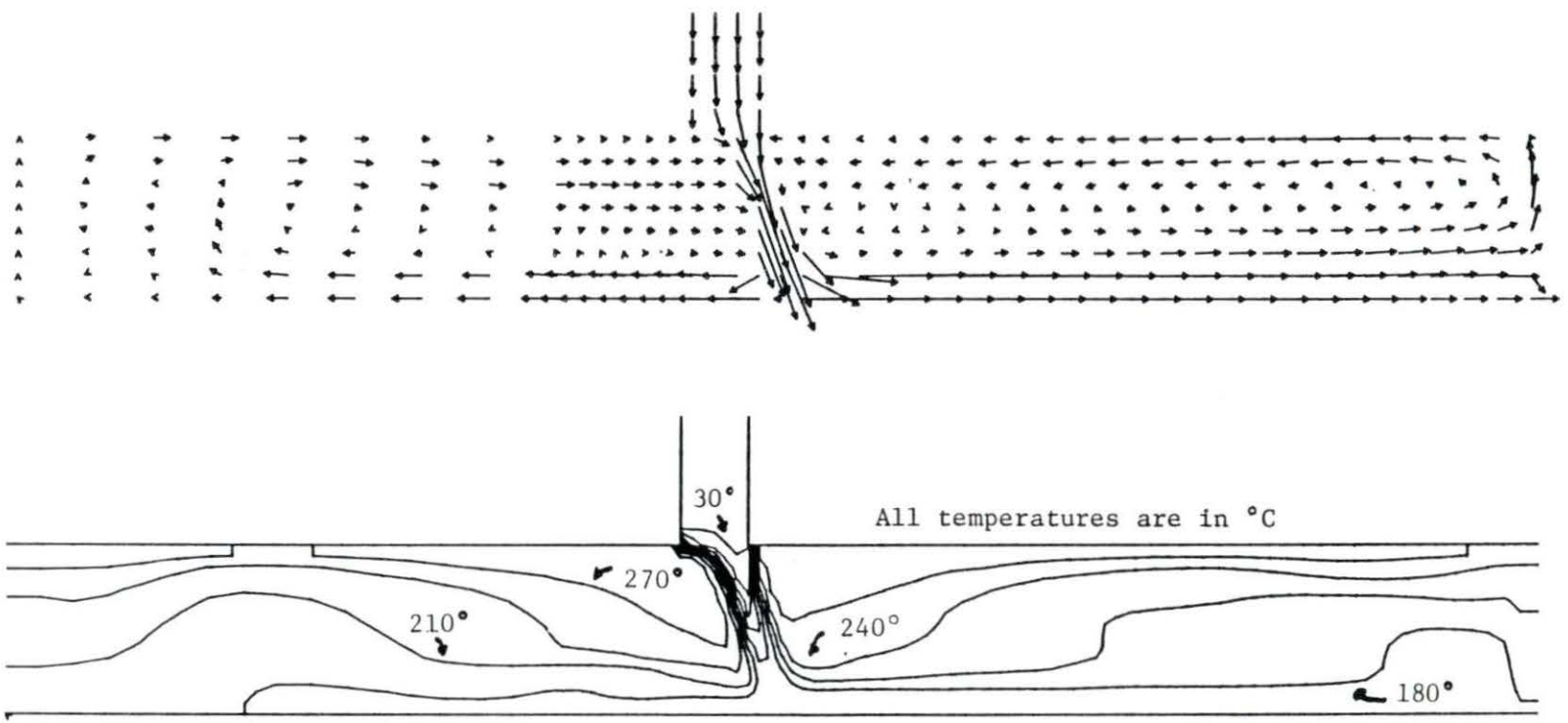

Figure 5.8 Temperature and velocity profiles at 20.4 seconds

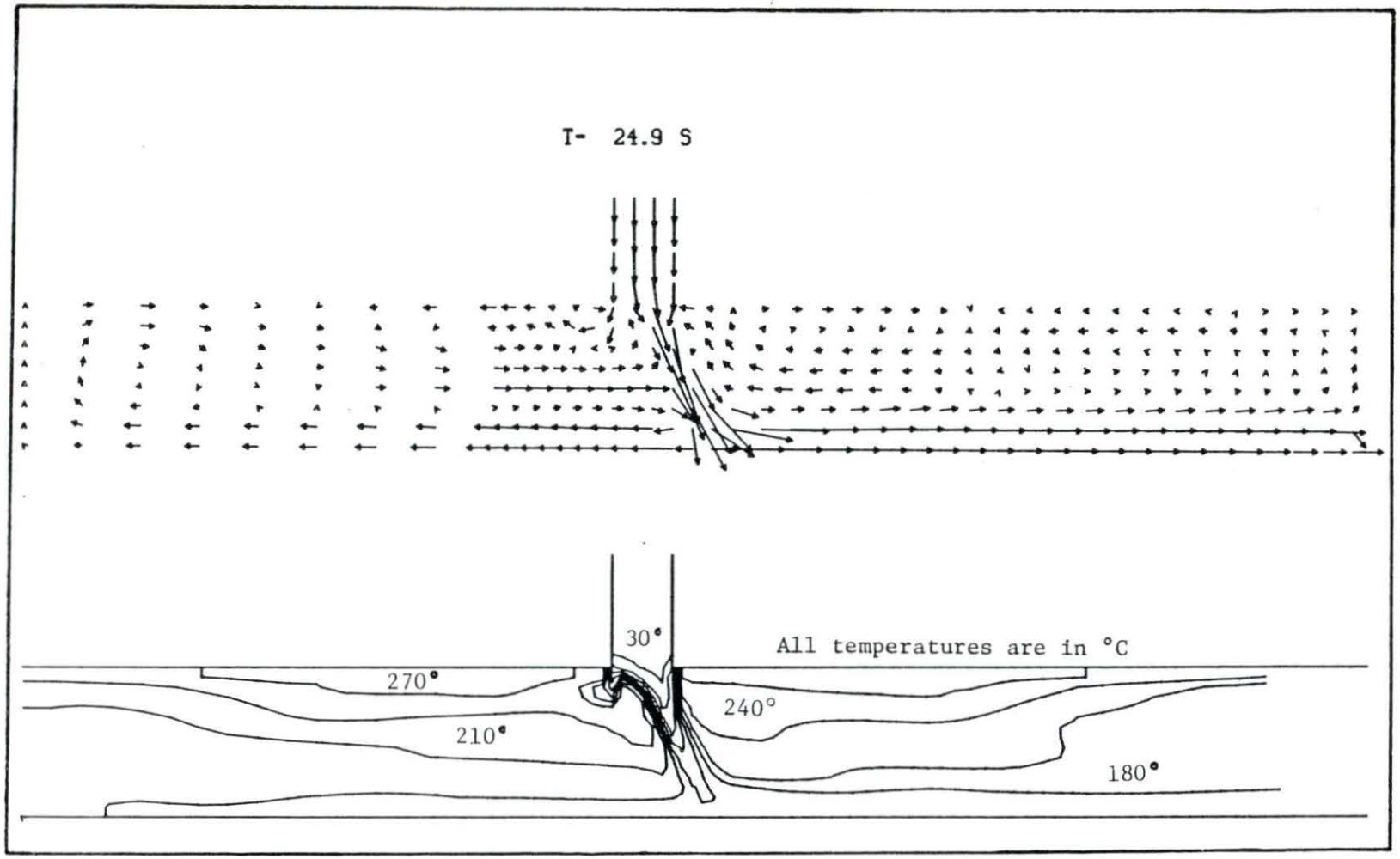

Figure 5.9 Temperature and velocity profiles at 24.9 seconds

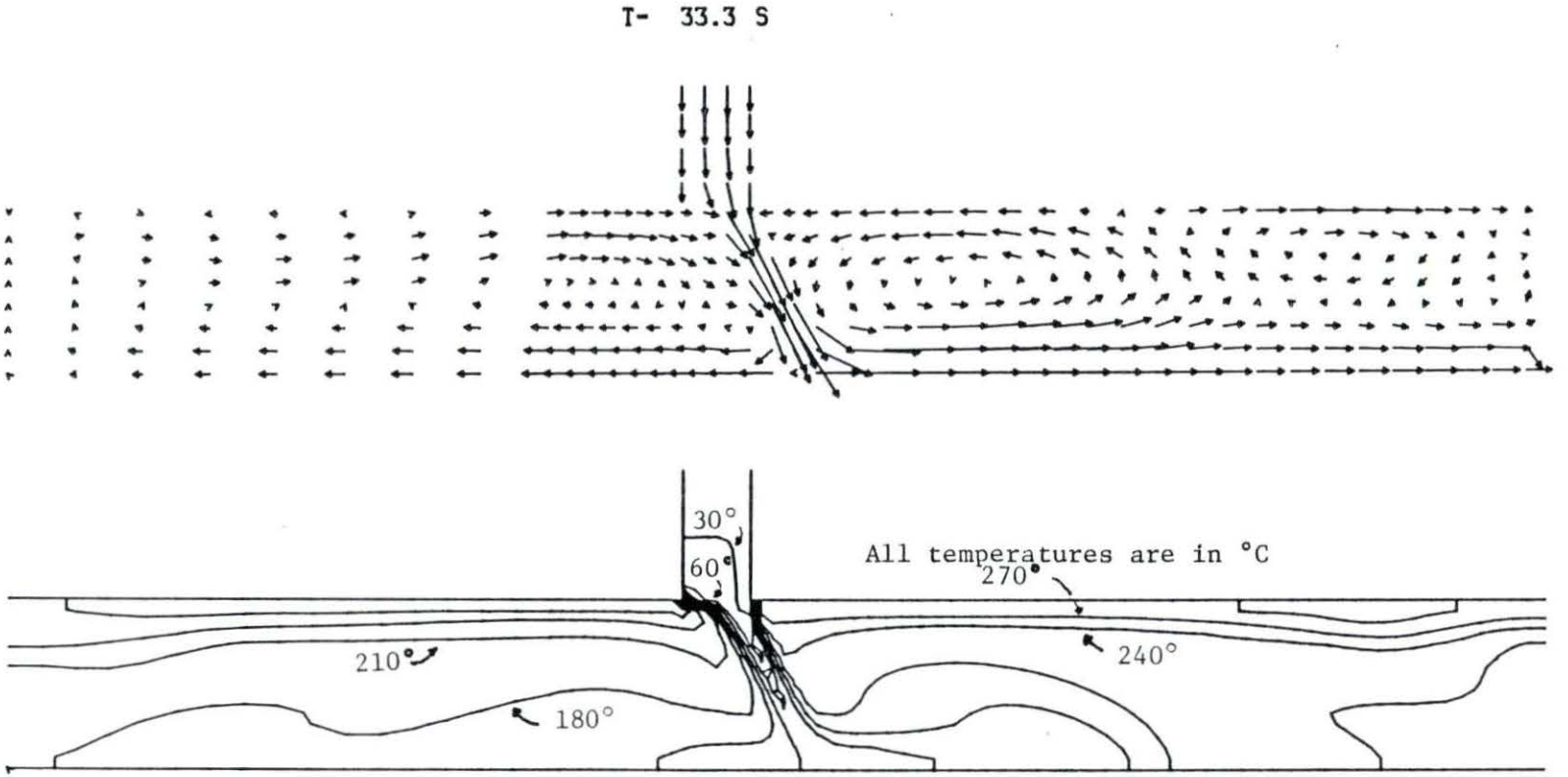

Figure 5.10 Temperature and velocity profiles at 33.3 seconds

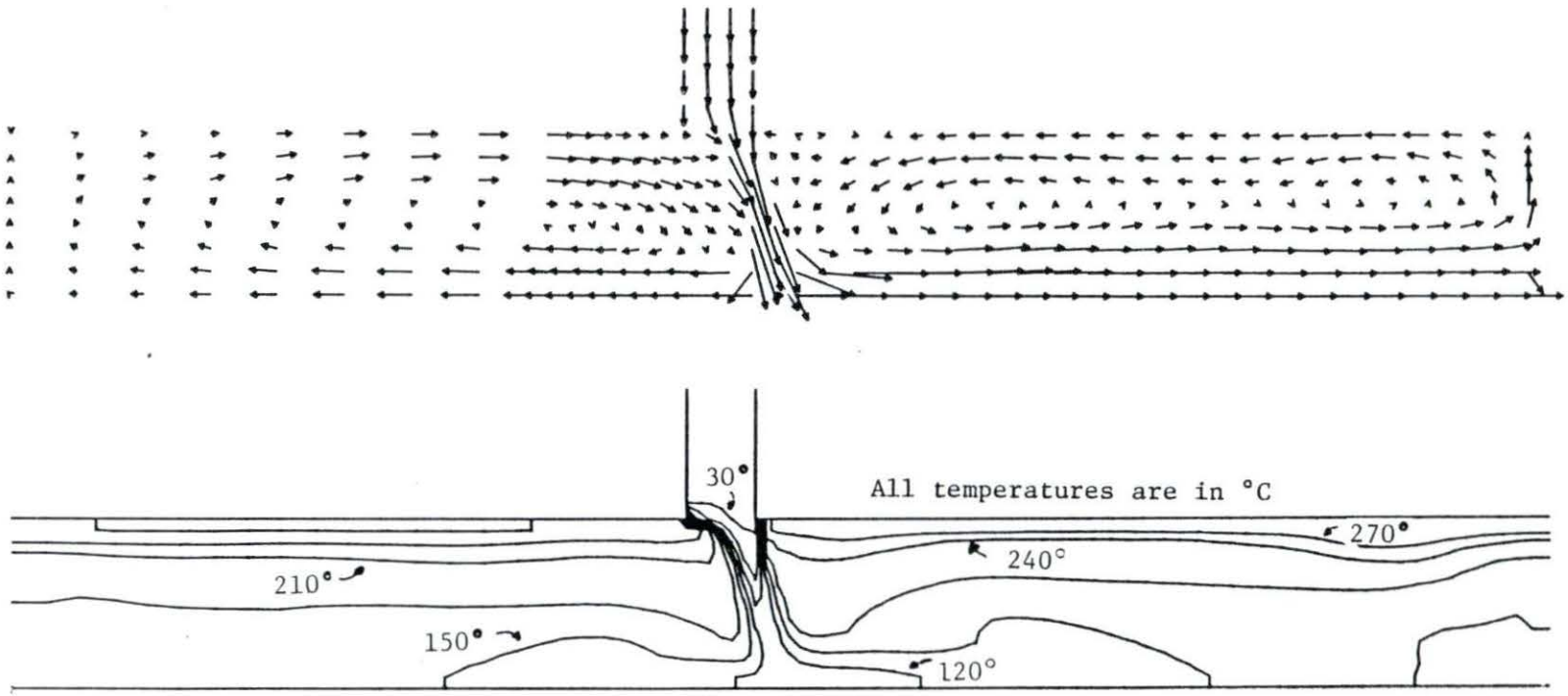

Figure 5.11 Temperature and velocity profiles at 38.2 seconds

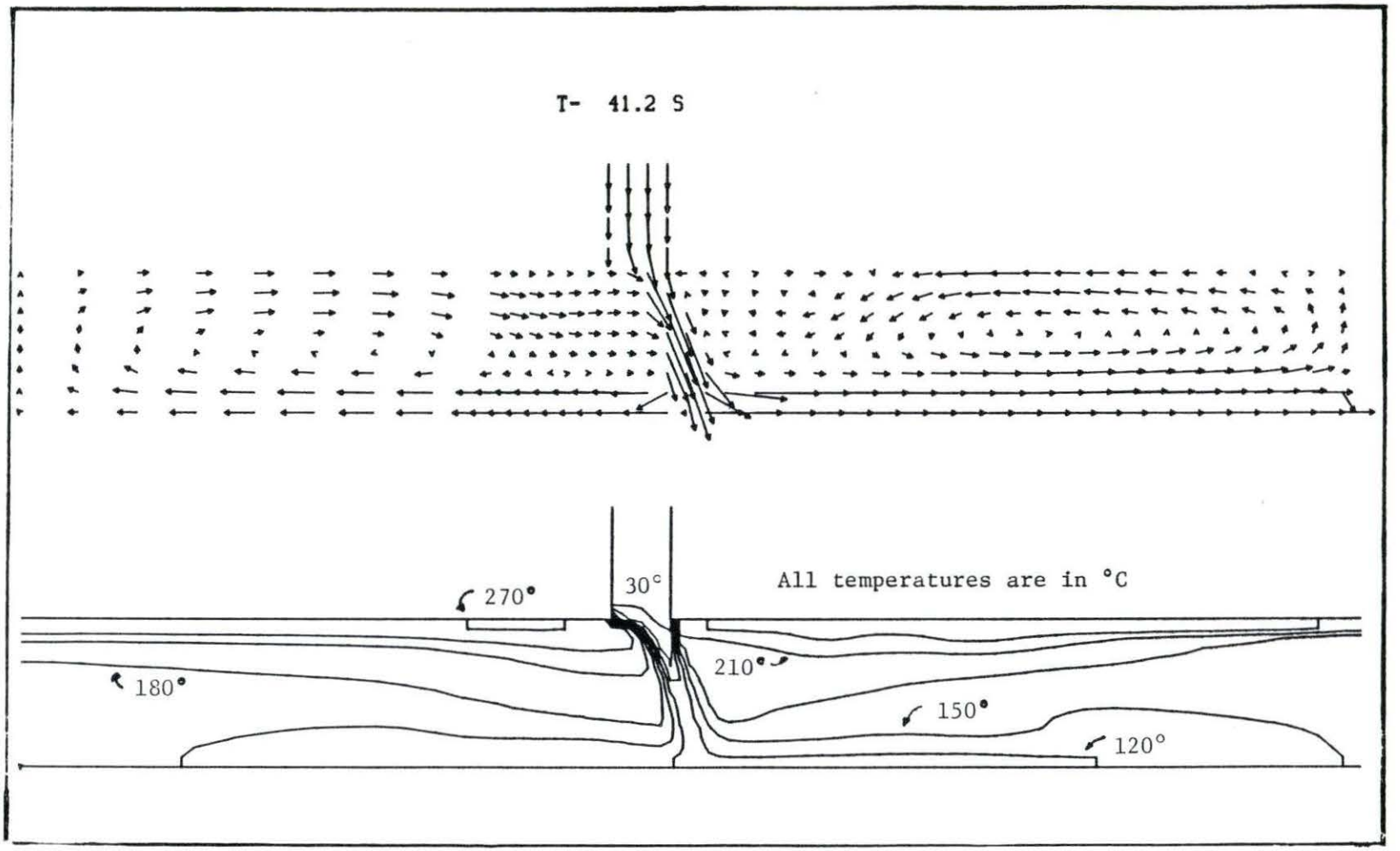

Figure 5.12 Temperature and velocity profiles at 41.2 seconds

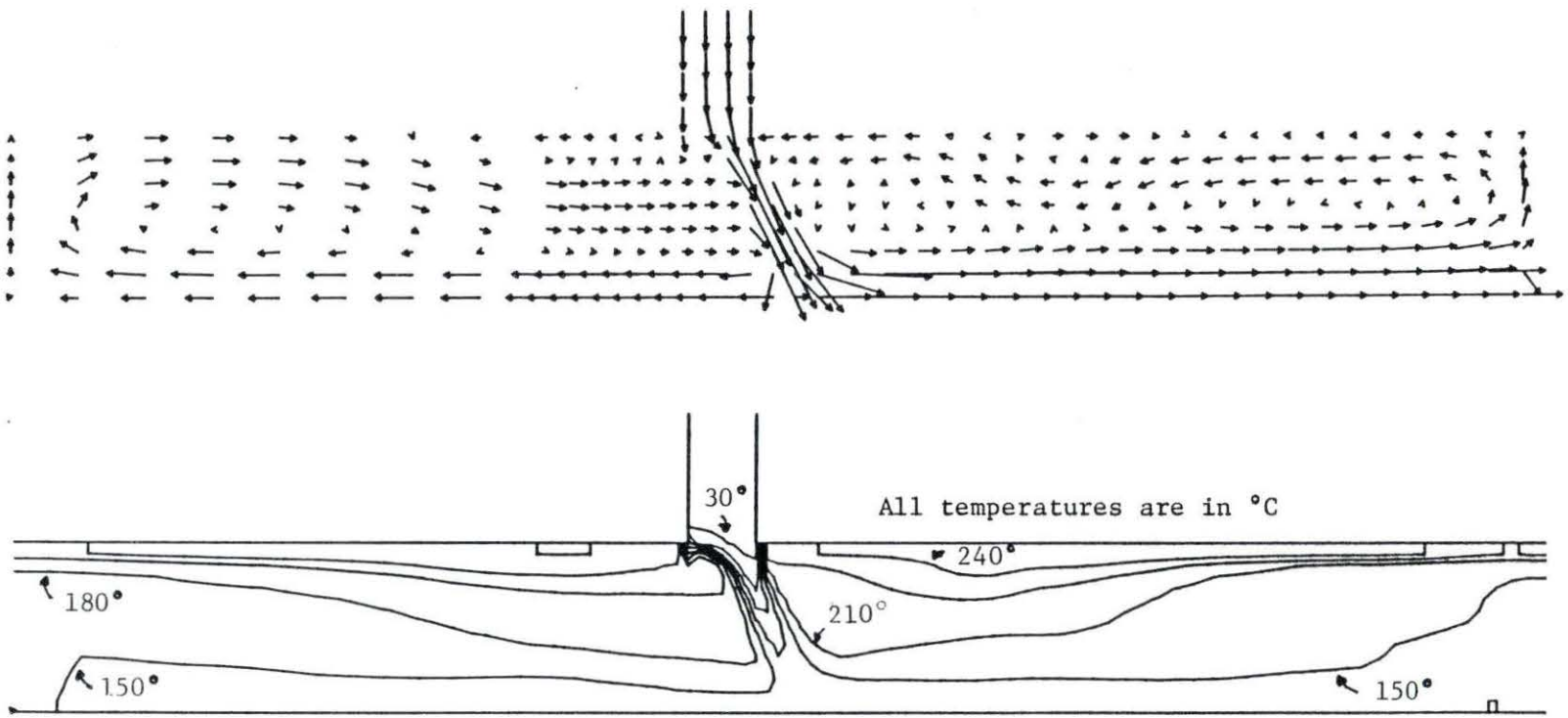

Figure 5.13 Temperature and velocity profiles at 44.2 seconds

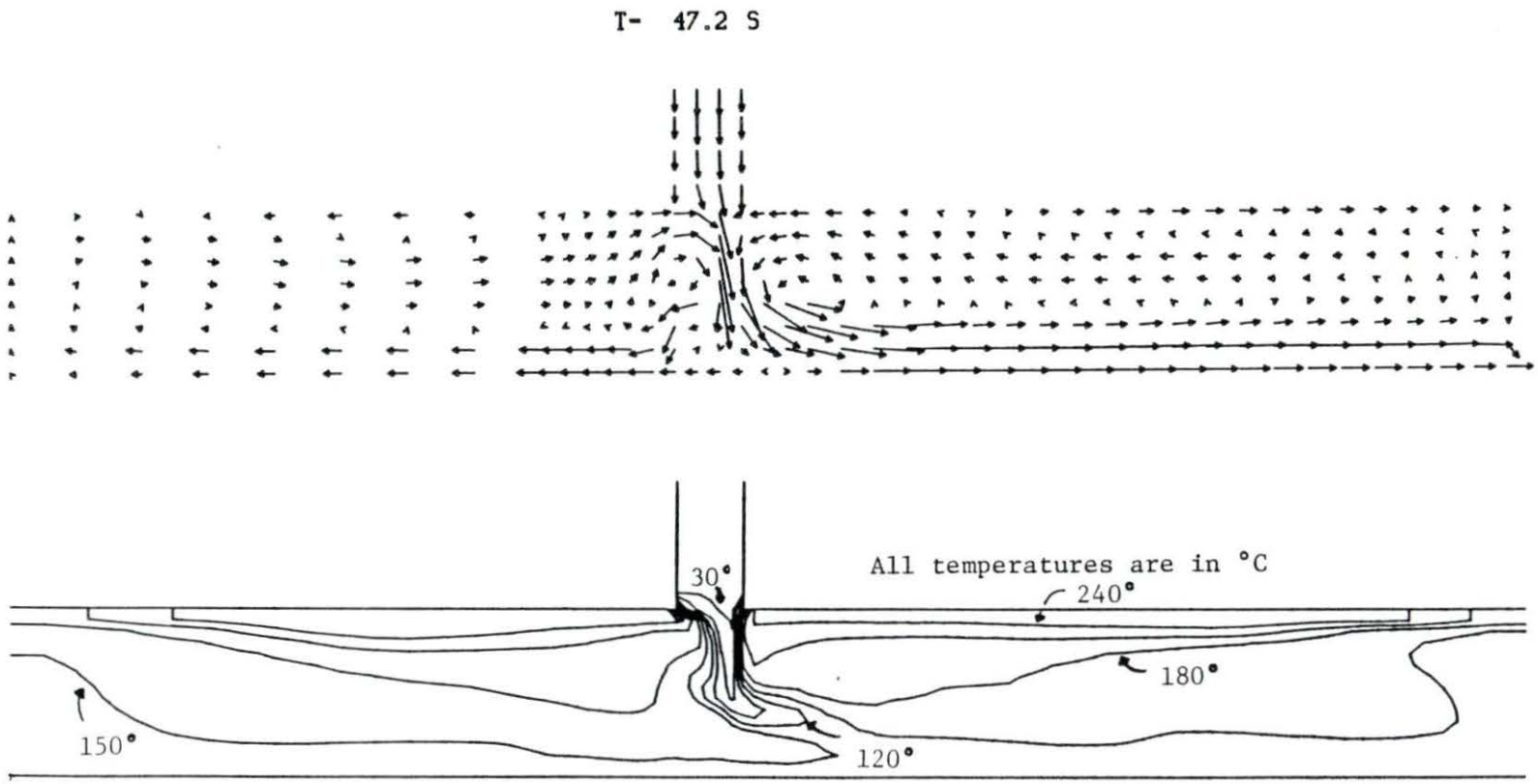

Figure 5.14 Temperature and velocity profiles at 47.2 seconds

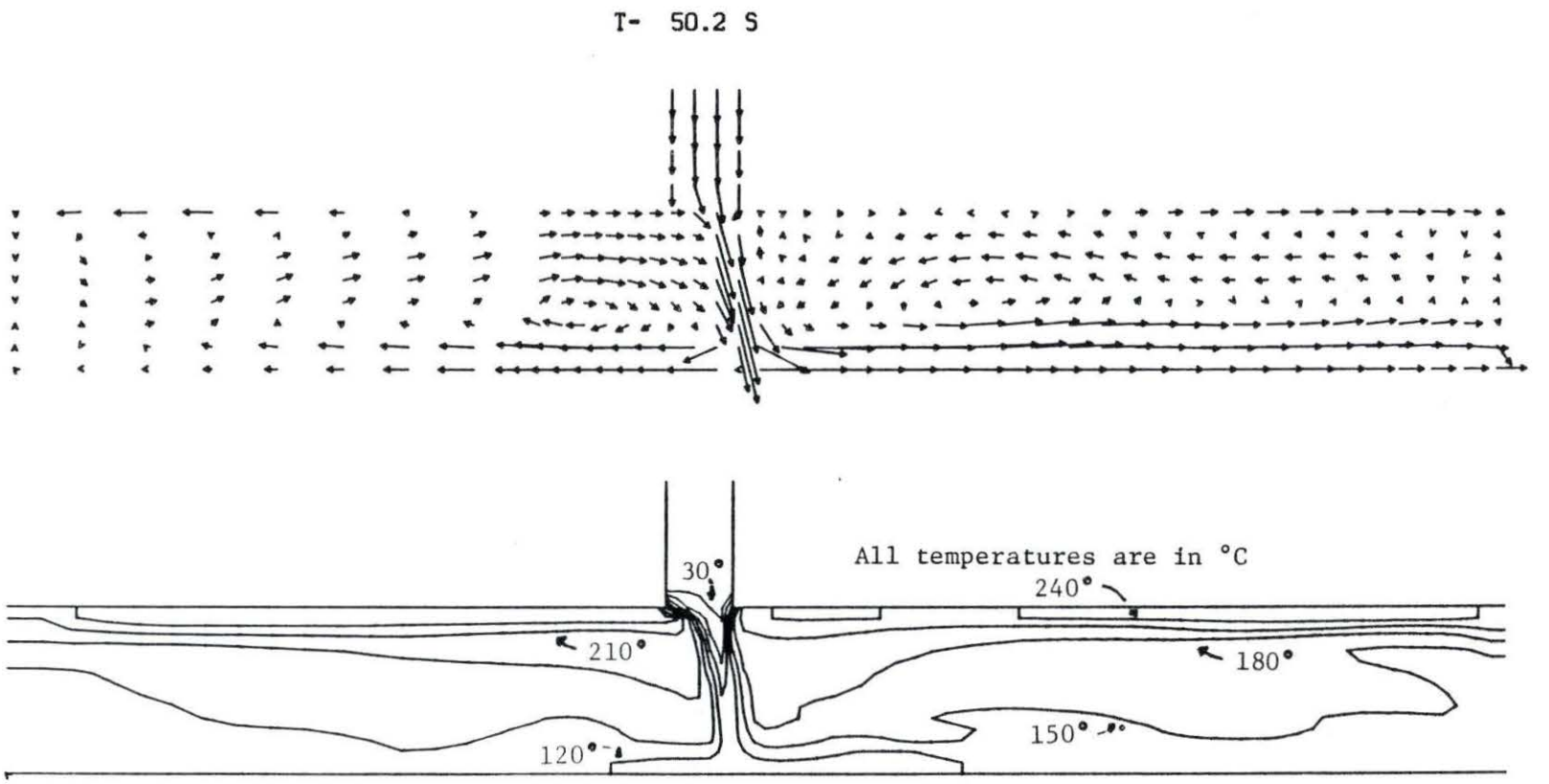

Figure 5.15 Temperature and velocity profiles at 50.2 seconds

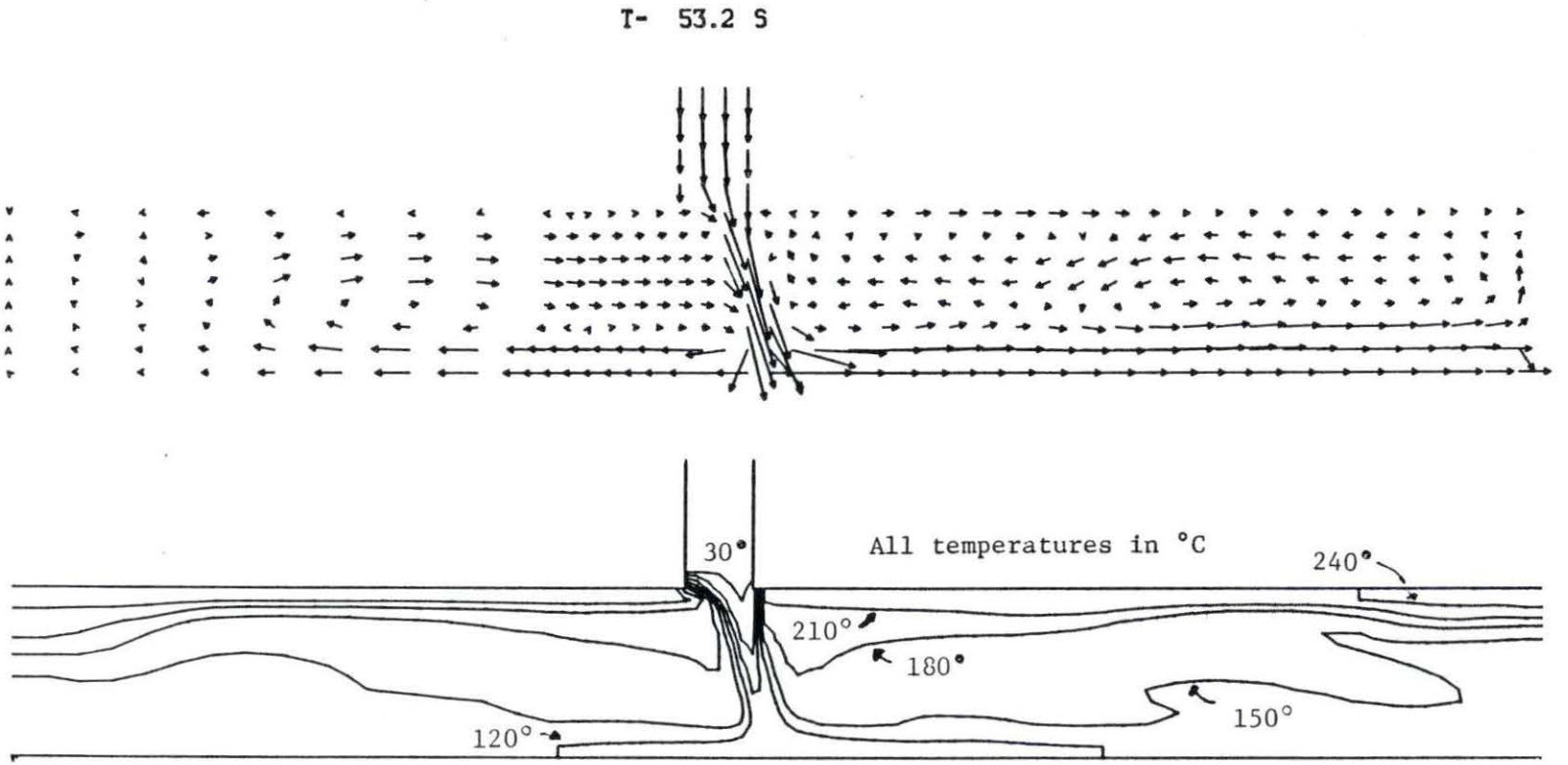

Figure 5.16 Temperature and velocity profiles at 53.2 seconds

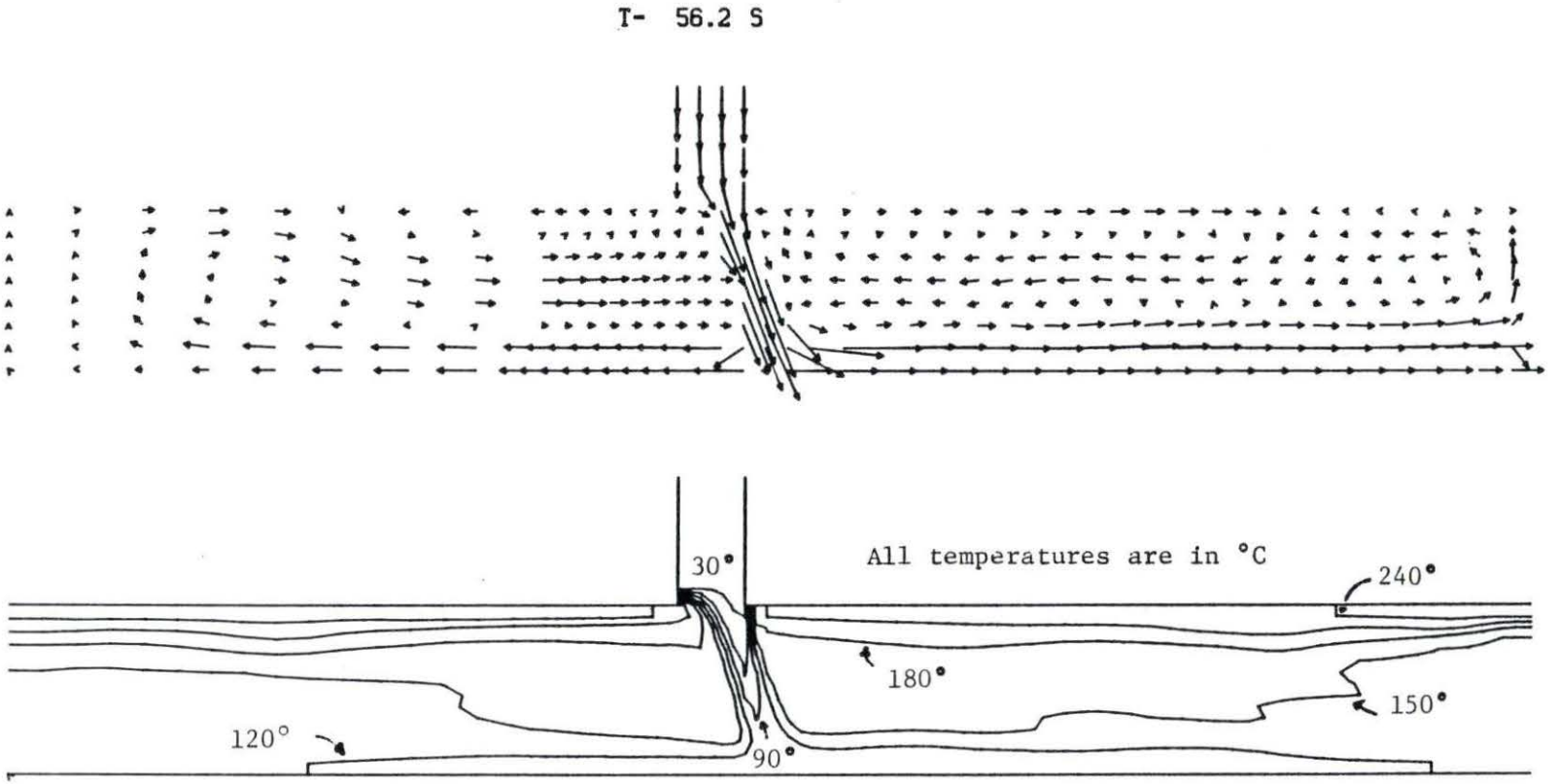

Figure 5.17 Temperature and velocity profiles at 56.2 seconds

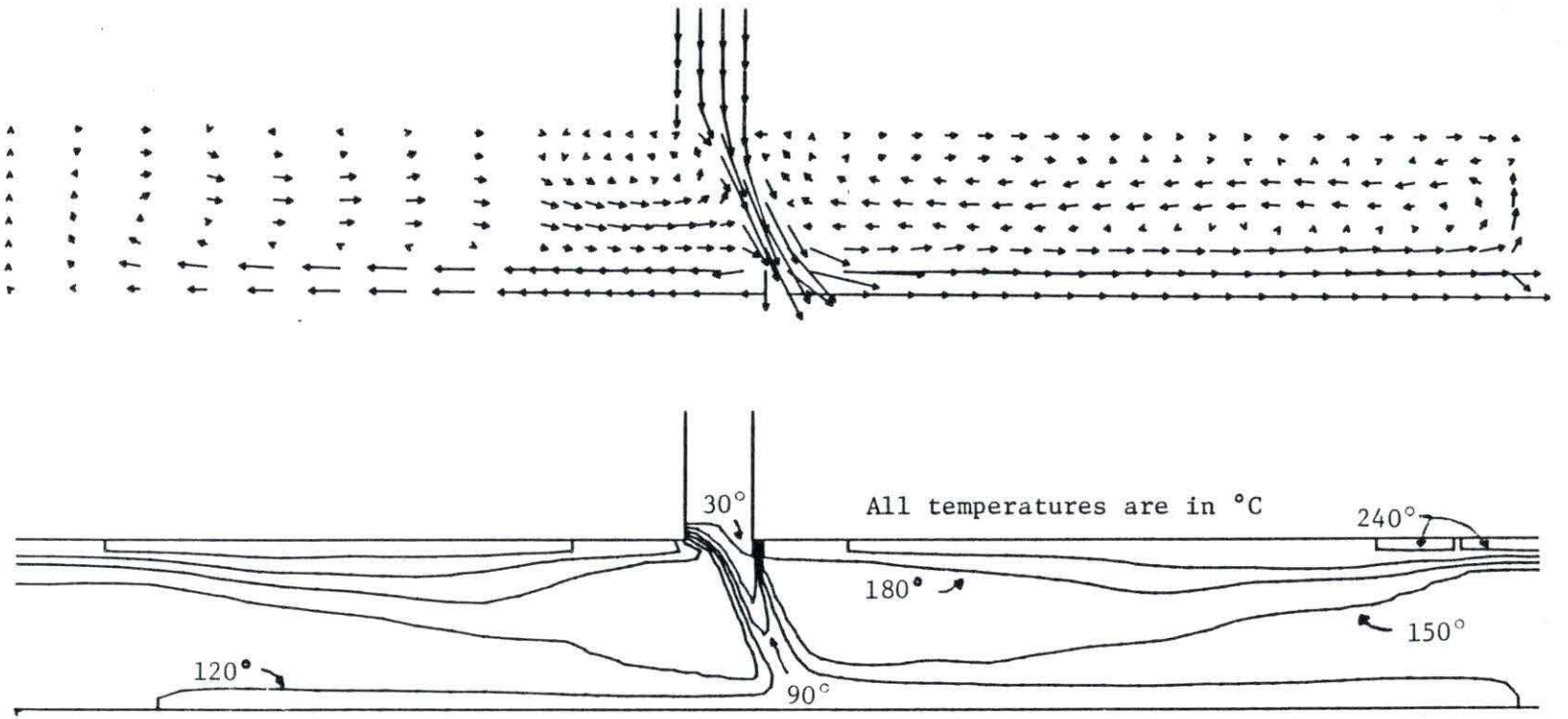

Figure 5.18 Temperature and velocity profiles at 59.2 seconds

5.2. A Quantitative Discussion of the Results

There have been many quantitative investigations of buoyancy and stratification in fluids other then the Creare experiments, such as those described in references 10, 15, 29, and 33. Unfortunately, the results derived in other buoyant flow situations such as thermal discharge from a power plant into an ocean or lake, are not directly applicable because the results are very sensitive to geometric details. However, all of the results cited above show a strong dependence on Froude number. This dependence on Froude number for the HPSI case can be proven in the following way.

Much of the existing literature on buoyancy and stratification uses the concept of an entrainment coefficient. This entrainment coefficient, E, is a measure of the increase in mass flux in the turbulent layer and can be directly related to the bulk fluid temperature. It is defined as:

$$\frac{\text{(the rate of mass entrained by the jet)}}{\text{(the initial jet mass flow rate)}}$$

The parameter, E, does not give any information about the temperature of the fluid at the fluid-wall interface. This represents a serious drawback since it is the temperature of the fluid at the wall which is of prime significance in the case under investigation. This temperature forms the boundary condition for the thermal analysis of the reactor vessel wall.

In other words, an equation of the form:

$$\rho_w C_{\rho w} \frac{\partial T_w}{\partial t} = \frac{1}{r} \frac{\partial}{\partial r} \left(Kr \frac{\partial T_w}{\partial r}\right)$$

needs to be solved with the following boundary condition for surface heat flux:

$$q = h \left(T_{fluid}\Big|_I - T_w\Big|_I\right)$$

where the subscript w represents the properties of the reactor vessel wall and the subscript I represents the interface.

The more typical convection boundary condition, which involves T_{Bulk} of the fluid, cannot be used in the conduction problem of the reactor vessel wall because of the complex nature of the buoyancy-driven stratification. Since the relationship between T_{Bulk} and $T_{surface}$ can not be generally derived for complex flow situations; typically, in cases where the entrainment coefficient method is used, E is used to find T_{Bulk} which is then related to $T_{surface}$ by an experimentally determined non-dimensional temperature profile. Such non-dimensional profiles have been developed for many turbulent jet situations [1,15] but none would be applicable in this case because of the differences in geometry. The experimental data which are available are not sufficient to deduce a temperature profile since only 3 radial temperatures were measured at any one axial distance. The code-predicted temperature profiles for 2 locations, one midway between the injection point and the open-end of the cold leg and one at the open end of the cold leg (both at T=59.2 sec.) are presented in Figures 5.19 and 5.20.

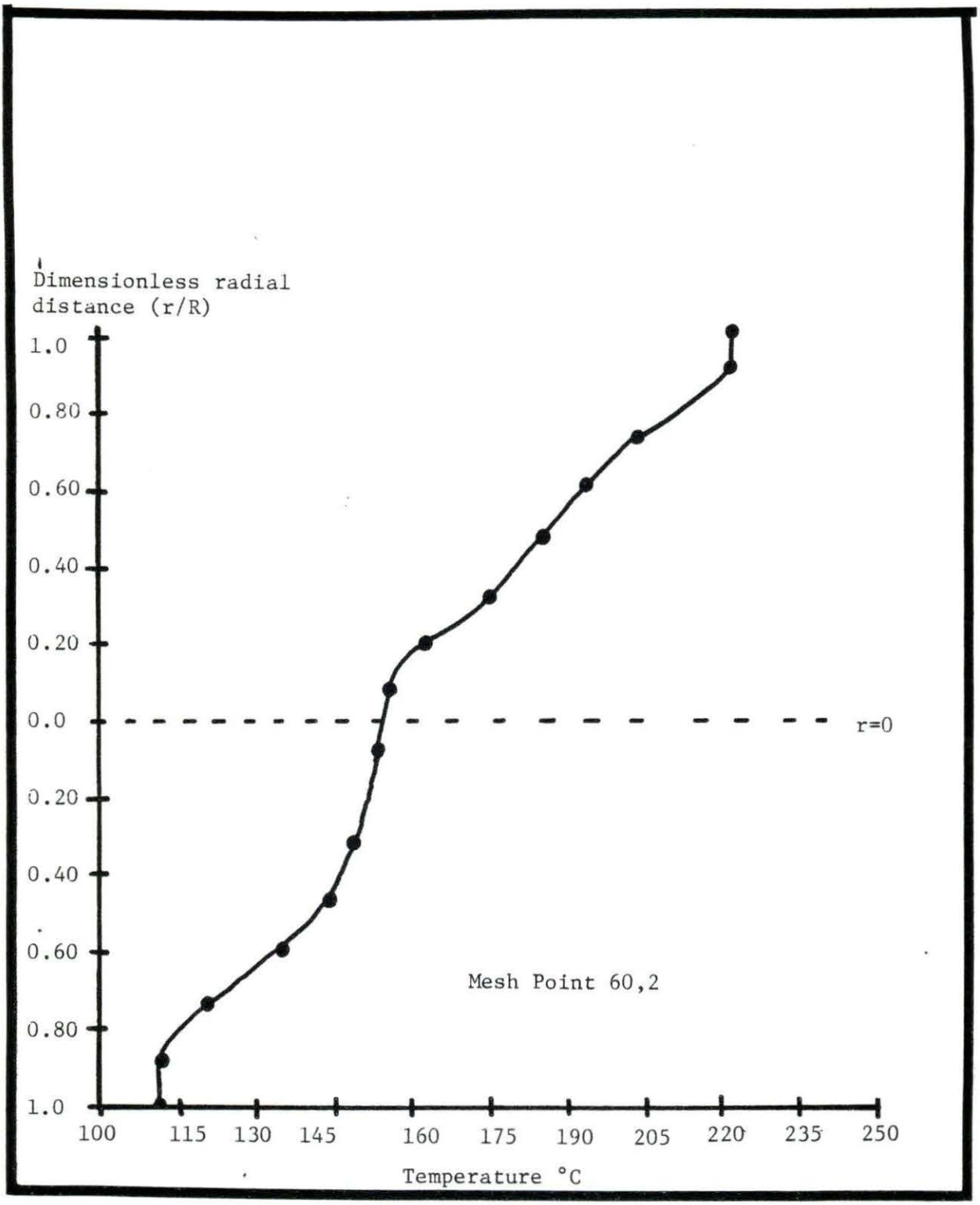

Figure 5.19 Temperature profile at distance 1.83 m from HPSI and time equal to 59.2 seconds

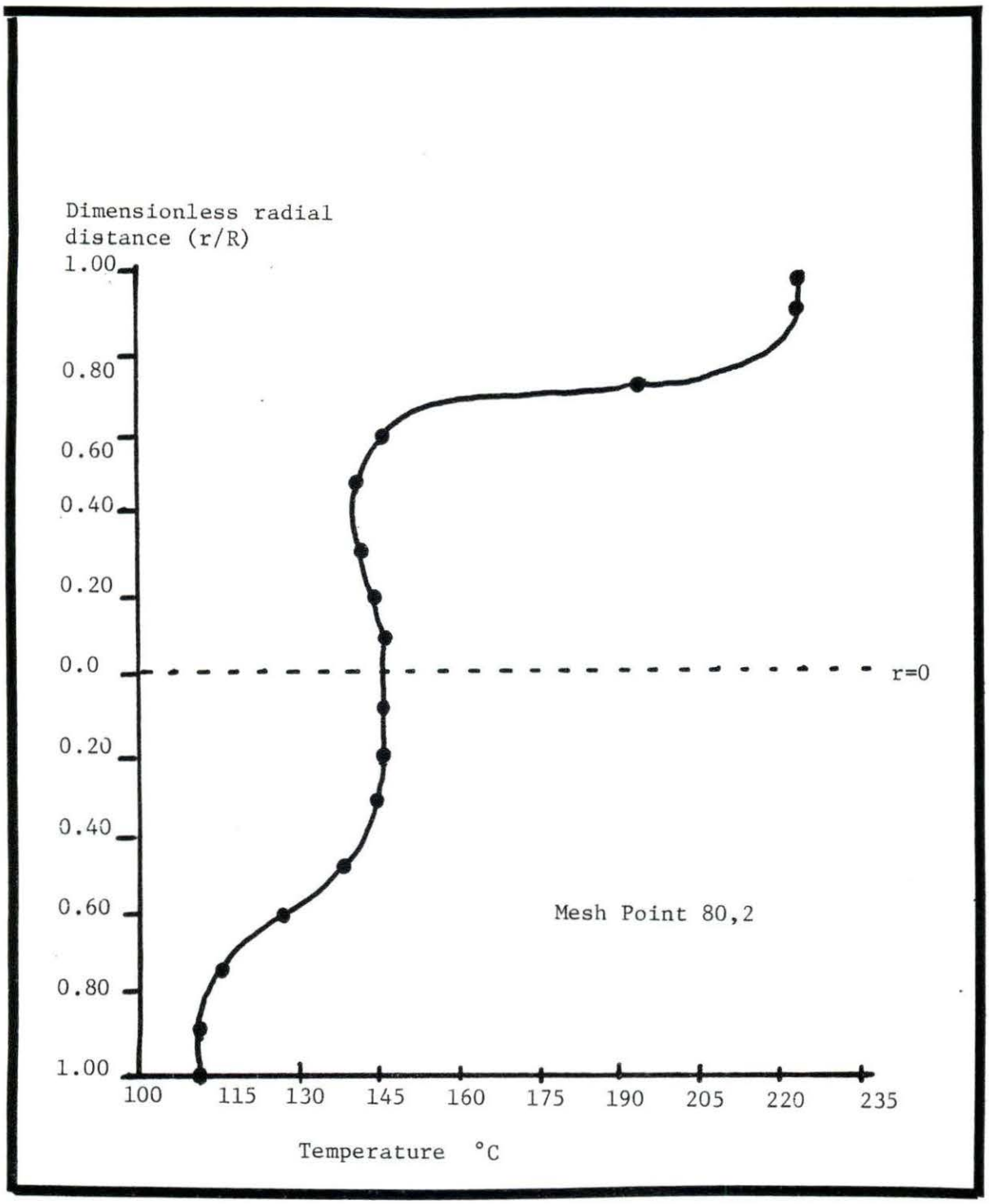

Figure 5.20 Temperature profile at distance 3.51m from HPSI and time equal to 59.2 seconds

An additional problem with the entrainment coefficient concept is that since the problem under investigation is a transient problem where bulk fluid temperature decreases with time, the entrainment coefficient itself must be a function of time. The published correlations are for steady-state problems where the entrainment coefficient is constant.

Nevertheless, it is instructive to compare the entrainment coefficient as derived from the experiment and the analysis. For both the experiment and the analysis, E can be crudely calculated by applying a mass and energy balance to the volume shown in Figure 5.21.

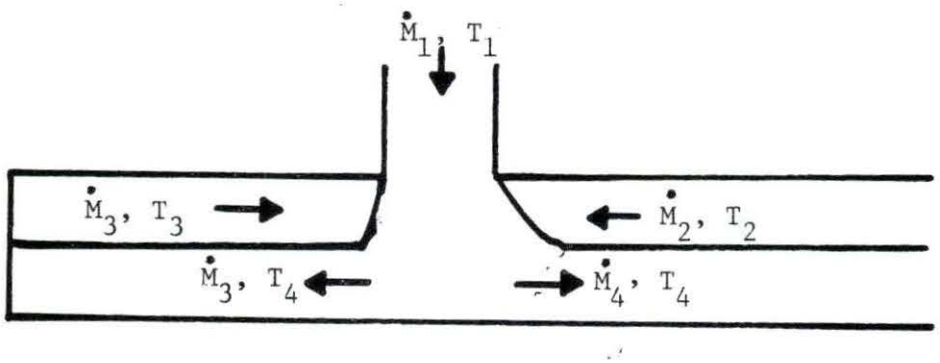

Figure 5.21 Sketch for the derivation of E

One can write that:

$$C_{p1}\dot{M}_1T_1 + C_{p2}\dot{M}_2T_2 + C_{p3}\dot{M}_3T_2 = C_{p3}\dot{M}_3T_4 + C_{p4}\dot{M}_4T_4 \qquad (5.1)$$

This also assumes that T_3 equals T_2. This assumption was experimentally determined to be reasonable. Additionally:

$$\dot{M}_4 = \dot{M}_1 + \dot{M}_2 \tag{5.2}$$

By definition:

$$E = \frac{\dot{M}_2 + \dot{M}_3}{\dot{M}_1} = \frac{\text{(Mass flowrate entrained)}}{\text{(Initial jet mass flowrate)}}$$

By manipulating equations 5.1 and 5.2, it is found that:

$$E = \frac{C_{\rho 4}T_4 - C_{\rho 1}T_1}{C_{\rho 2}T_2 - C_{\rho 4}T_4} \tag{5.3}$$

To arrive at an entrainment coefficient for the computer model, T_4 was taken to be the temperature of grid point 60, 7 while T_2 was taken to be the temperature grid point 60, 11 at time equal to 60 seconds. T_1 is, of course, 26.67°C. This leads to:

$$E = 6.08 \text{ (at Fr = .032)}$$

which represents an average entrainment coefficient over the first 60 seconds of the transient.

Experimentally, T_4 was taken to be the average of thermocouples 51 and 55 while T_2 was taken to be the average of thermocouples 54 and 55 also at time equals 60 seconds. The results of the entrainment coefficients for three different Froude numbers are presented in Table 5.1.

Table 5.1 Experimentally determined entrainment coefficient for various Froude numbers

Froude Number	.017	.025	.051
Creare Test Number (Reference 9)	103	105	100
E	11.20	8.56	2.83

In references 10, 15, 29 and 33, the entrainment coefficient varied either directly or inversely with the Froude number depending on the geometry and flow conditions investigated. For the HPSI case, by examining Table 5.1 which is plotted in Figure 5.22, it is seen that the entrainment coefficient correlates quite closely with the inverse Froude number. In addition, it can be seen that the overall entrainment coefficient derived from the analysis shows reasonable agreement with the experimentally derived curve. This agreement lends confidence to the comparison of the analytical and experimental results.

While the entrainment coefficient concept does prove the functional dependence of the thermal mixing on the densimetric Froude number, this concept is not particularly useful in this problem because it provides only a "bulk" fluid temperature. As discussed previously, it is the temperature at the fluid wall interface which is required.

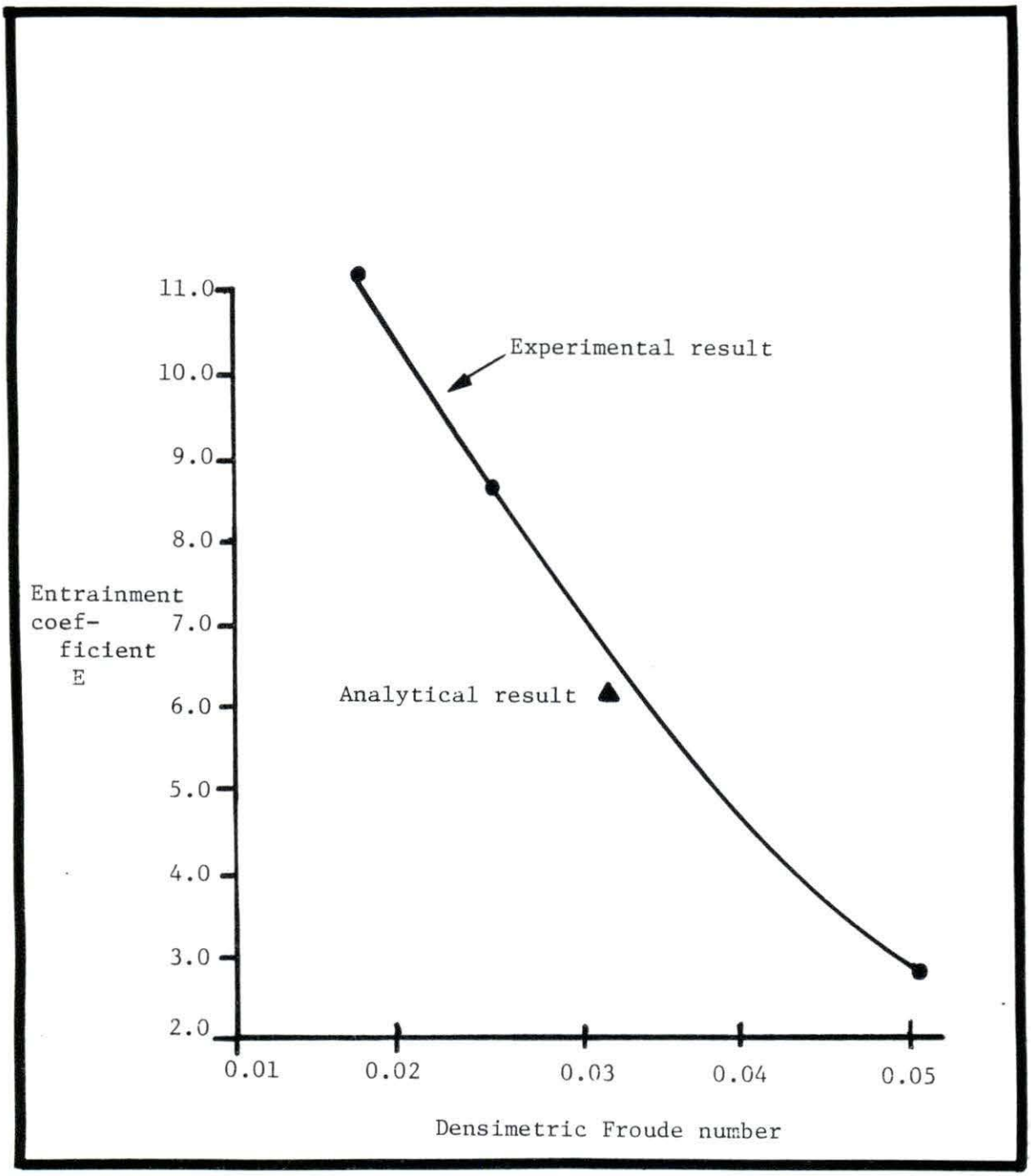

Figure 5.22 Entrainment coefficient versus Froude number

Therefore, it was desired to compare the experiment with the analysis on the basis of a particular point of interest. However, there are several problems which arise when an attempt is made to compare the analytical and experimental results quantitatively. The greatest problem is the difference in modeled geometries. The analysis modeled only the cold leg and a portion of the HPSI pipe, whereas the experiment included such components as the stalled pump, the loop seal, downcomer and lower plenum (see Figure 1.1). Another problem arises because the analysis was done using the high temperatures and pressures typical of reactor condition. Due to the difficulties of working at these conditions, the experiment used much lower temperatures and pressures. The Froude numbers of the experiments were kept prototypical of reactor Froude numbers by using both lower flow rates and salt-induced density differences. The tests were run at Froude numbers of .017, .025 and .051, whereas the conditions used for the analysis led to Fr = .032. However, since it is desirable to compare the two sets of results quantitatively some method of scaling must be found. Because of the significant differences between the experiments and the analysis, this comparison was not performed with the expectation that experimental results would in any way validate the computer model or with the belief that a direct comparison could be made. Rather, the comparison was undertaken in order to compare the trends which the two types of data showed.

In a first attempt to compensate for the differences between the analysis and the experiment a dimensionless temperature of the form:

$$\theta(t) = \frac{T(t) - T_H}{T_H - T_L}$$

was plotted versus time at various points for both the analysis and the Creare results at various Froude numbers. An example of this type of plot is presented in Figure 5.23 for mesh point 60, 2 in the analysis and experimental thermocouple 51. Both of these are located midway between the HPSI point and the open end of the cold leg at the bottom of the cold leg piping. The basic exponential nature of both of the experimental data at three Froude numbers and the analytical results is apparent. Had the experiment been performed in exactly the same geometry as was modeled, the analytical data would be expected to fall between the two experimental curves, Fr. = .025 and Fr. = .051.

As an attempt to remove the geometry effects, θ was plotted against a dimensionless time. The dimensionless time accounted for several discrepancies. First, the Creare experiments took the time, t(o), to occur when the HPSI fluid first enetered the cold leg, while the analytical t(o) occurred when the HPSI fluid entered the HPSI piping. Therefore, the dimensionless time, ϕ(o), was chosen to occur when the HPSI jet first impacts the bottom of the cold leg piping. This occurred at time equal to 3.2 seconds in the analysis,

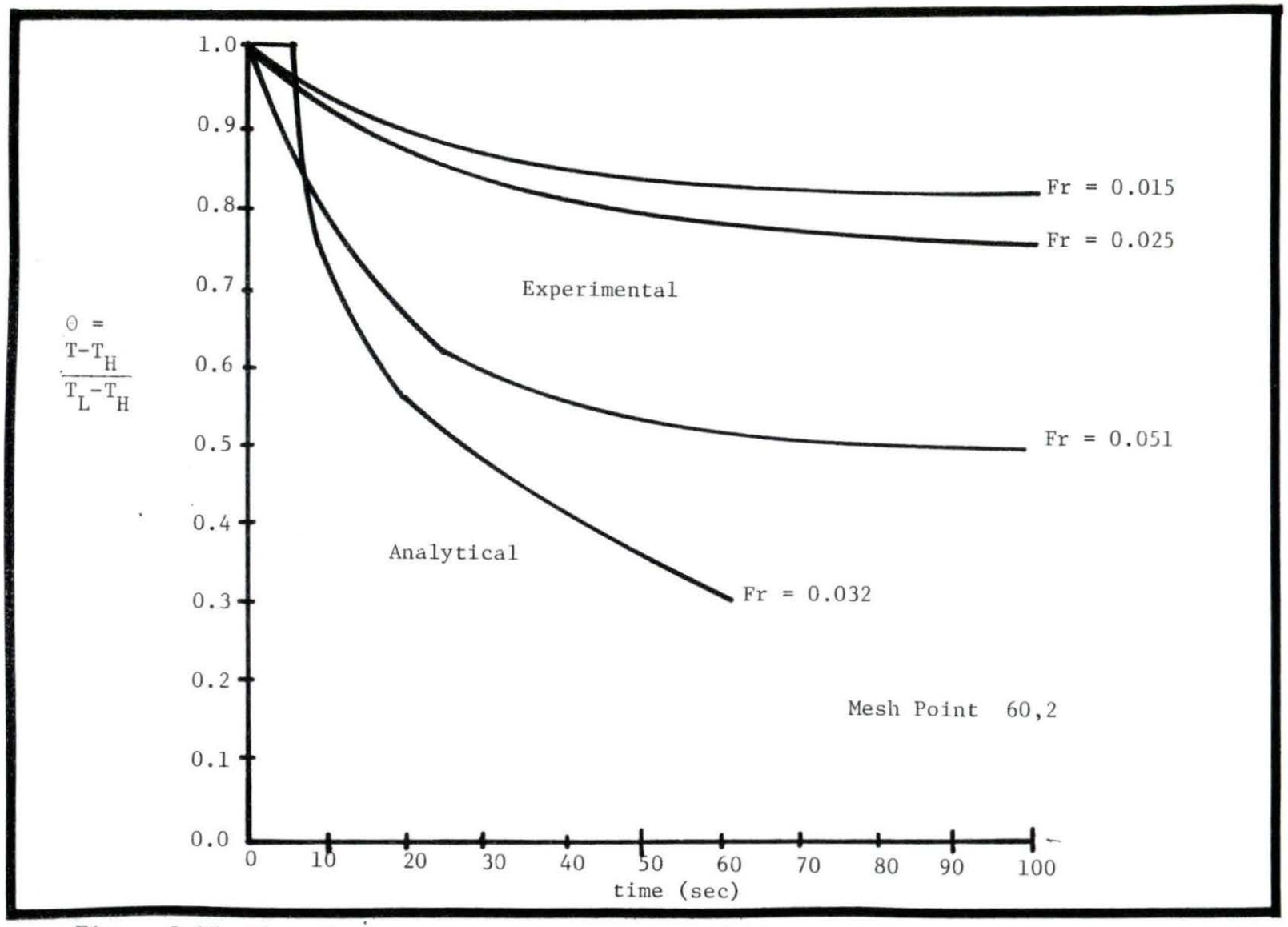

Figure 5.23 Dimensionless temperature versus real time

time equal to 1.52 in the Creare experiment where Froude number equaled .025 and time equal to .76 seconds when Froude number equaled .051. These variables times will be designated transit times, t_{tran} (see Figure 5.24). Additionally, ϕ was chosen to eliminate the effect of different lengths of piping since the Froude number accounts for the diameter effects, but not length effects.

To accomplish these goals, ϕ was chosen such that

$$\phi = \frac{t - t_{tran}}{L/V}$$

where L was the distance from the point of injection to the point of interest and V was the velocity.

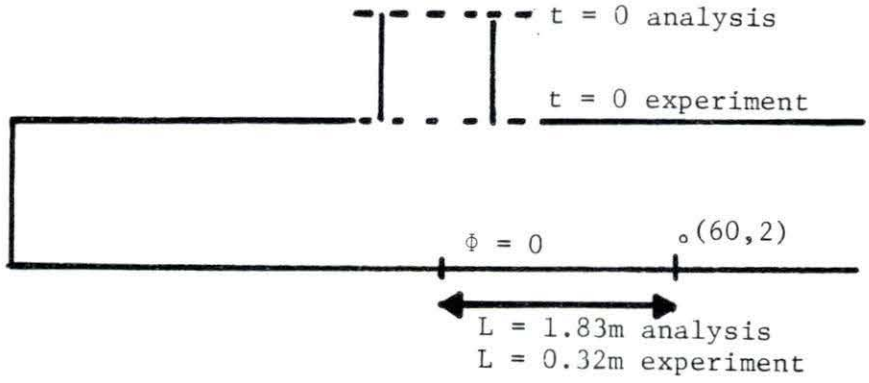

Figure 5.24 Sketch for ϕ - dimensionless time

A sample of these results are shown in Figure 5.25. Again, the basic exponential nature is shown, but a large descrepancy still exists. This shows that the dimensionless time was not sufficient to remove all of the geometry effects due to the large additional volumes of the pump, loop seal, downcomer and lower plenum. Therefore, a different method of scaling the data was investigated.

Creare reported that the general temperature behavior for any point in the system could be described by [9]:

$$T = T_H + (T_L - T_H)\exp(-t/\tau) \tag{5.4}$$

where

T_H - HPSI fluid temperature

T_L - Initial loop temperature

t - Time in seconds since onset of transient

τ - Characteristic mixing coefficient which depends on location of the point, modeled volume and Froude number

Since this can be rewritten as:

$$\frac{T(t) - T_H}{T_L - T_H} = \exp(-t/\tau) \quad \text{or} \quad \theta = \exp(-\phi)$$

which is what Figure 5.23 and 5.25 show, this equation seems valid.

If the validity of this equation is accepted, one could scale the data from a particular experiment with a given T_H and T_L to any other T_H and T_L by finding τ from the experimental data, then substituting

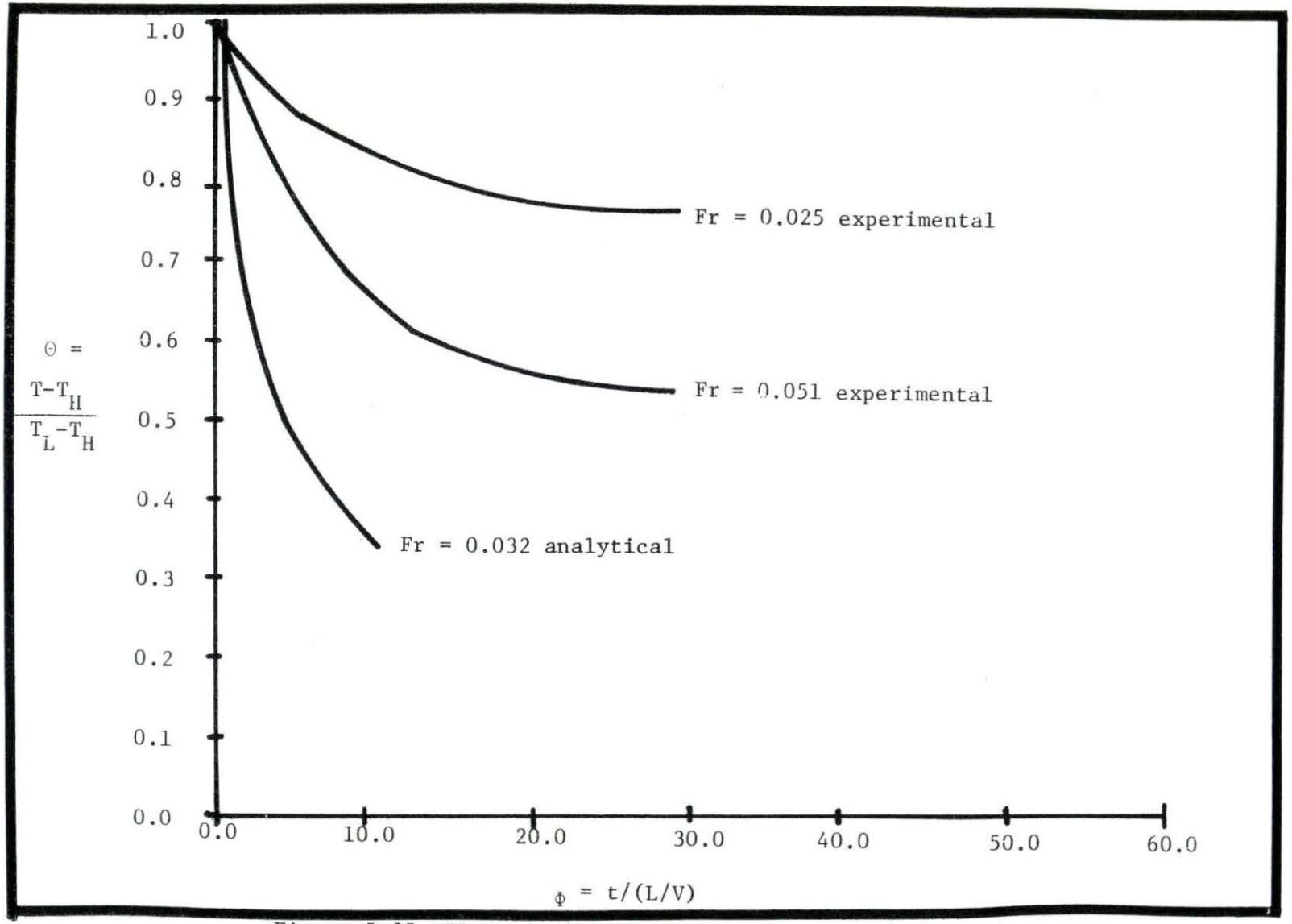

Figure 5.25 Dimensionless temperature versus dimensionless time

these τ's and the desired temperatures into equation 5.1, again assuming the same Froude number and modeled volume. This is done in Figure 5.26 for mesh point 33, 2. For the moment, the difference between the Froude number of the experiment (0.025) and the Froude number of the analysis (0.032) is ignored. Point 33, 2 represents a point on the cold leg wall directly opposite the point of HPSI fluid injection. Because of this location, this is the point which one would expect to have the most severe transient. Point 60 referred to in Figure 5.26 is the number of the thermocouple in the experiment which most closely corresponds to mesh point 33, 2. Figure 5.26 is generated by substituting the experimental temperatures of T_H = 13.9°C and T_L = 66.7°C into equation 5.1 along with experimental temperatures as a function of time in order to find τ, which varies approximately linearly with time. These same values of τ were substituted back into equation 5.4 with the analytical T_H of 26.7°C and T_L of 282°C.

In examining this figure, it is seen that the basic exponential nature of the decay is predicted by the model but the characteristic mixing coefficients are quite different. This is to be expected since τ is a function of both volume and Froude number. The effect of Froude number on decay can be seen in Figure 5.27 where the results from three experiments with different Froude numbers are plotted for mesh point 60, 2 which represents a point midway between the HPS injection point and the open end of the cold leg. The dashed lines represents an estimate of where Fr = .032 might fall. The estimate of where Fr = .032 might lie was performed by graphing τ at 60 seconds

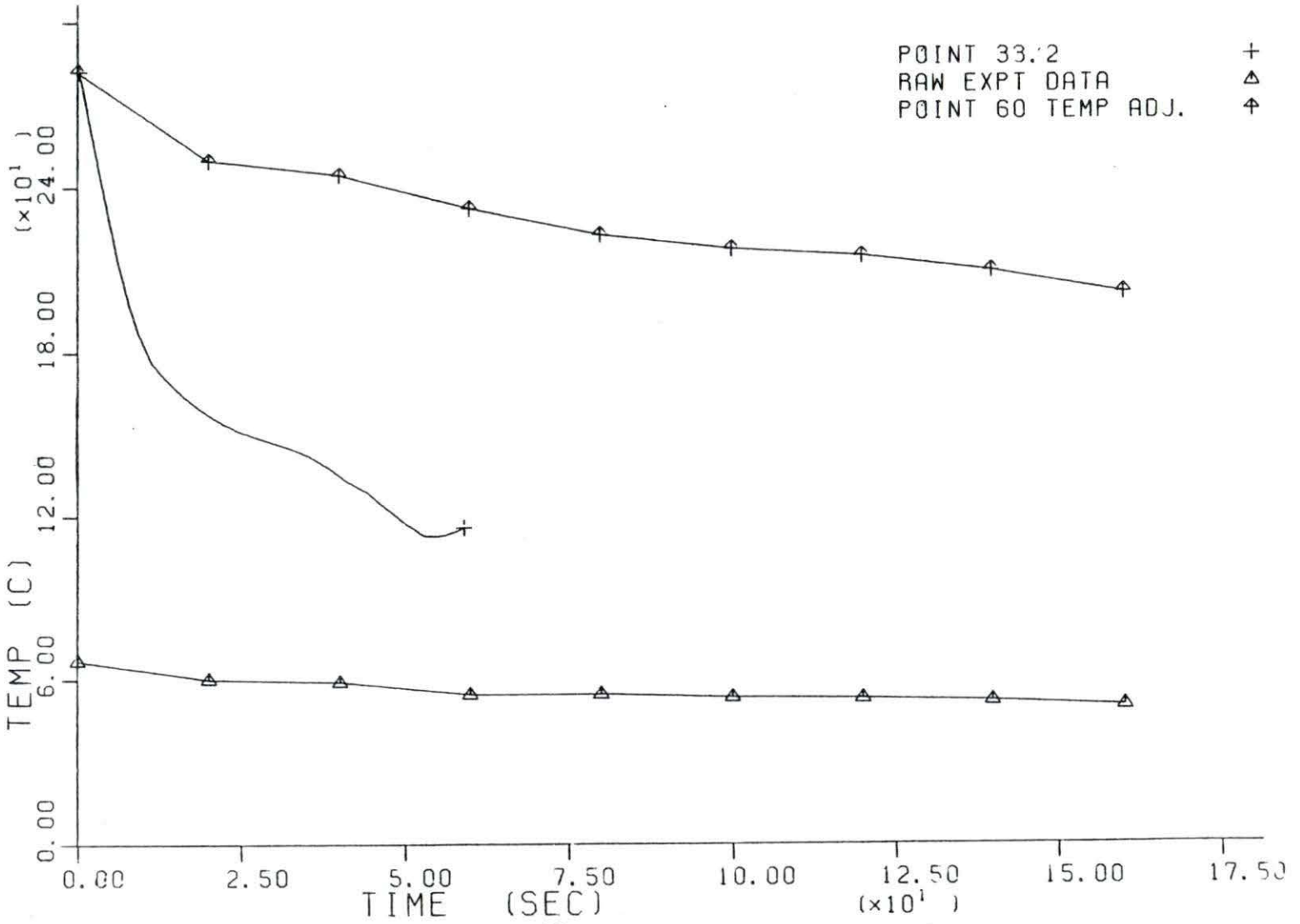

Figure 5.26 Analytical results for mesh point 33,2 versus experimental results at thermocouple 60

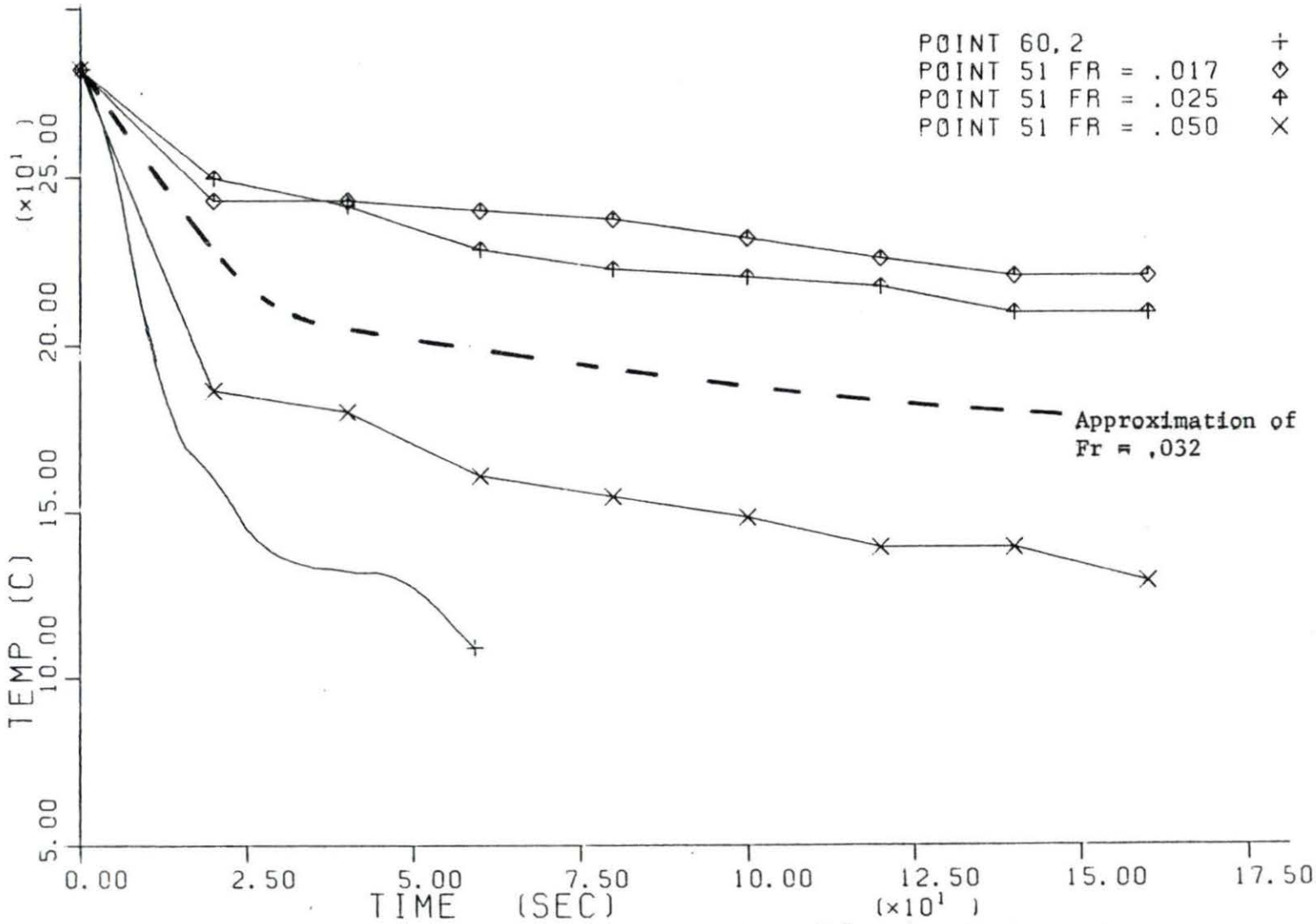

Figure 5.27 Analytical results for mesh point 60,2 versus experimental results at various Froude numbers

versus Froude number as shown in Figure 5.28. τ varies non-linearly with Froude number. The τ for Fr = .032 was interpolated from the graph for point 60, 2 and used to calculate T(t) for the dashed line in Figures 5.27.

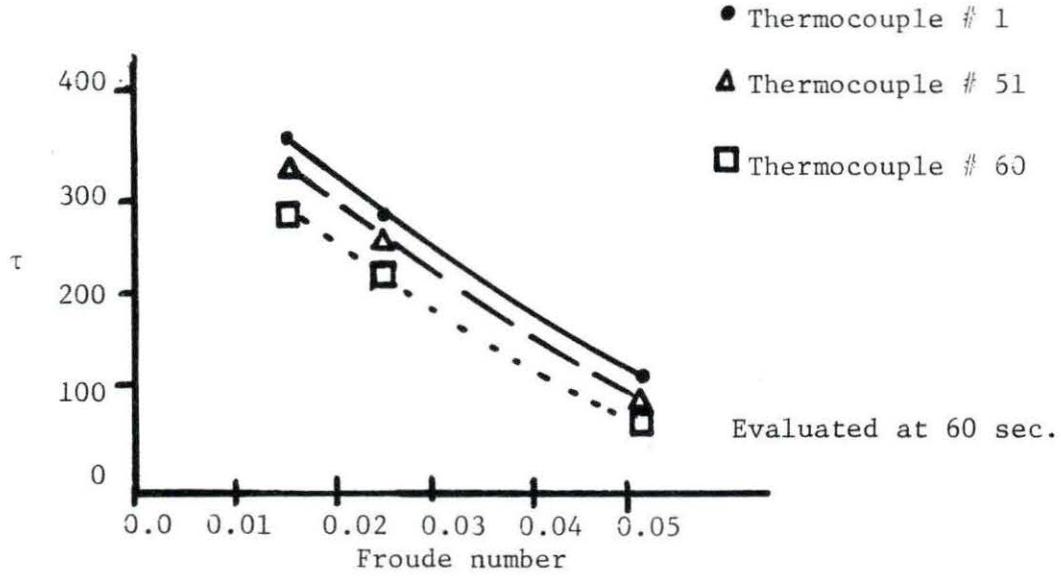

Figure 5.28 Examples of how τ varies with Froude number at various experimental points

The effect of increased Froude number is to increase the severity of the transient. Figures 5.29 and 5.30 also demonstrate this effect.

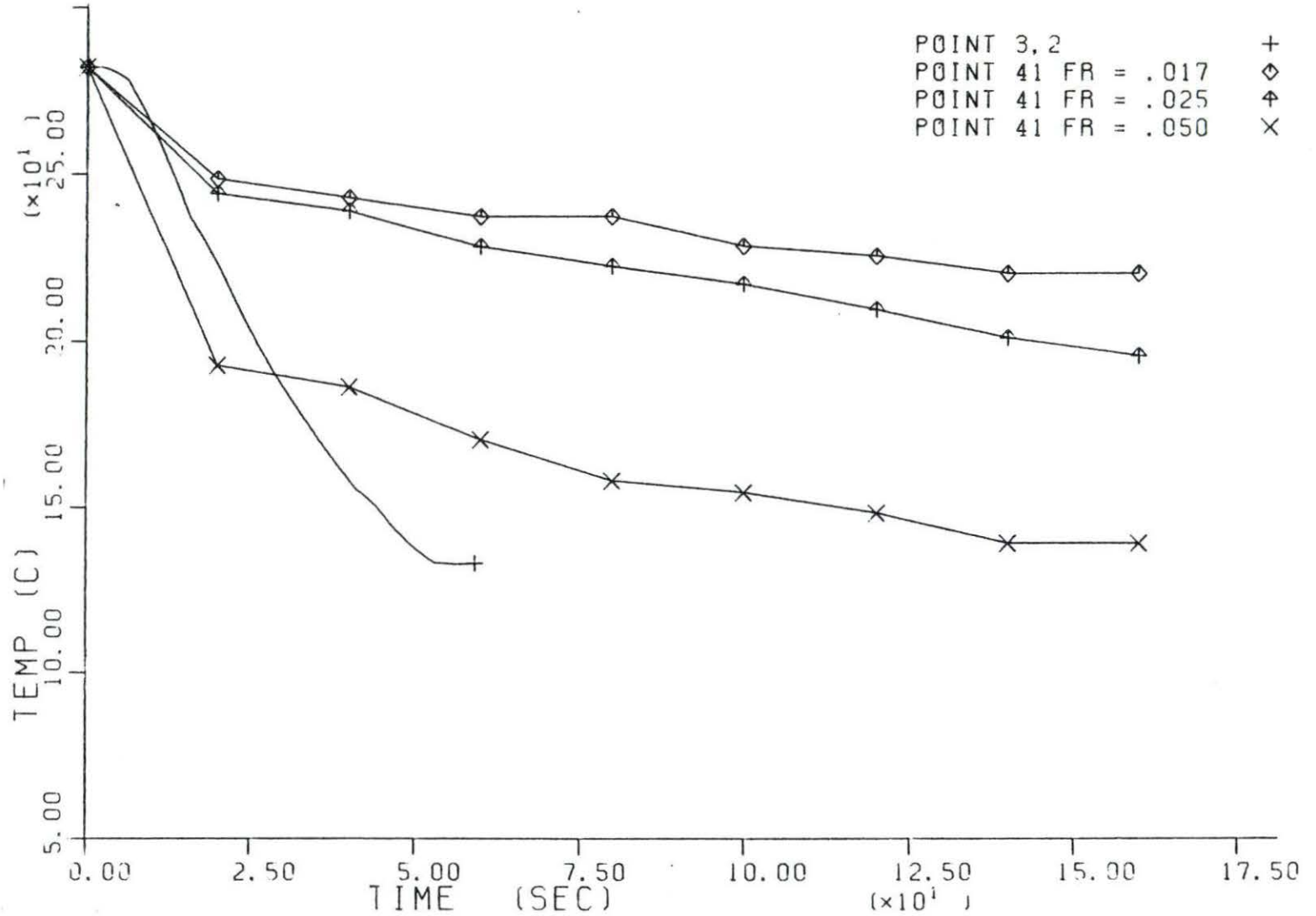

Figure 5.29 Analytical results for point 3,2 versus experimental results at various Froude numbers

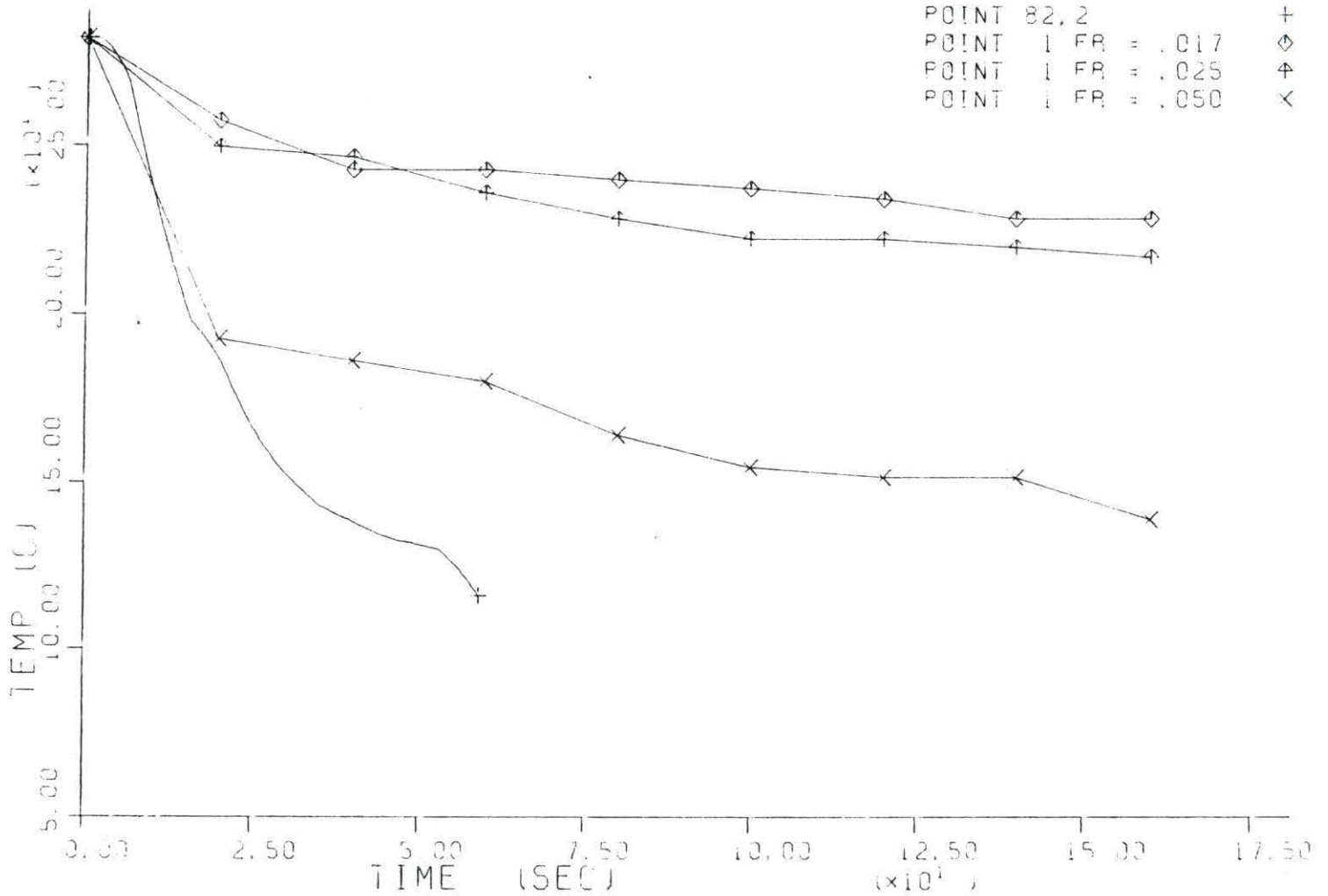

Figure 5.30 Analytical results for point 82,2 versus experimental results at various Froude numbers

The temperatures will decrease more quickly at higher Froude number because as shown in Figure 5.22 proportionately less hot water is entrained by the increased HPSI flow. It is obvious that this does not completely account for the difference between the experimental and analytical results because an additional fact - the different modeled volumes - also has an effect.

It is difficult to account for different volumes in the two sets of data because the volume factor is not the same as the actual facility volume. The volume of each component has differing effectiveness in showing the temperature decay. For example, during experimentation [9] it was found that the 57% increase in volume due to the addition of the lower plenum to the test geometry led to only a 17% increase in mixing time, while the 25% increase in volume due to the pump and loop seal led to a 43% increase in mixing time. Therefore, the pump and loop seal are more effective in slowing the transient than the lower plenum. The experimental data suggest that the addition of the loop seal, pump and lower plenum to the model would have the effect of increasing τ by 67%. Figure 5.31 is a graph which shows the experimental transient with the effect of less volume taken into account for mesh point 60, 2. By comparing Figure 5.27 and Figure 5.31, it can be seen that the experimental and analytical data agree more closely after this adjustment but a discrepancy is still apparent. One of the most probable reasons for this remaining discrepancy arises from the fact

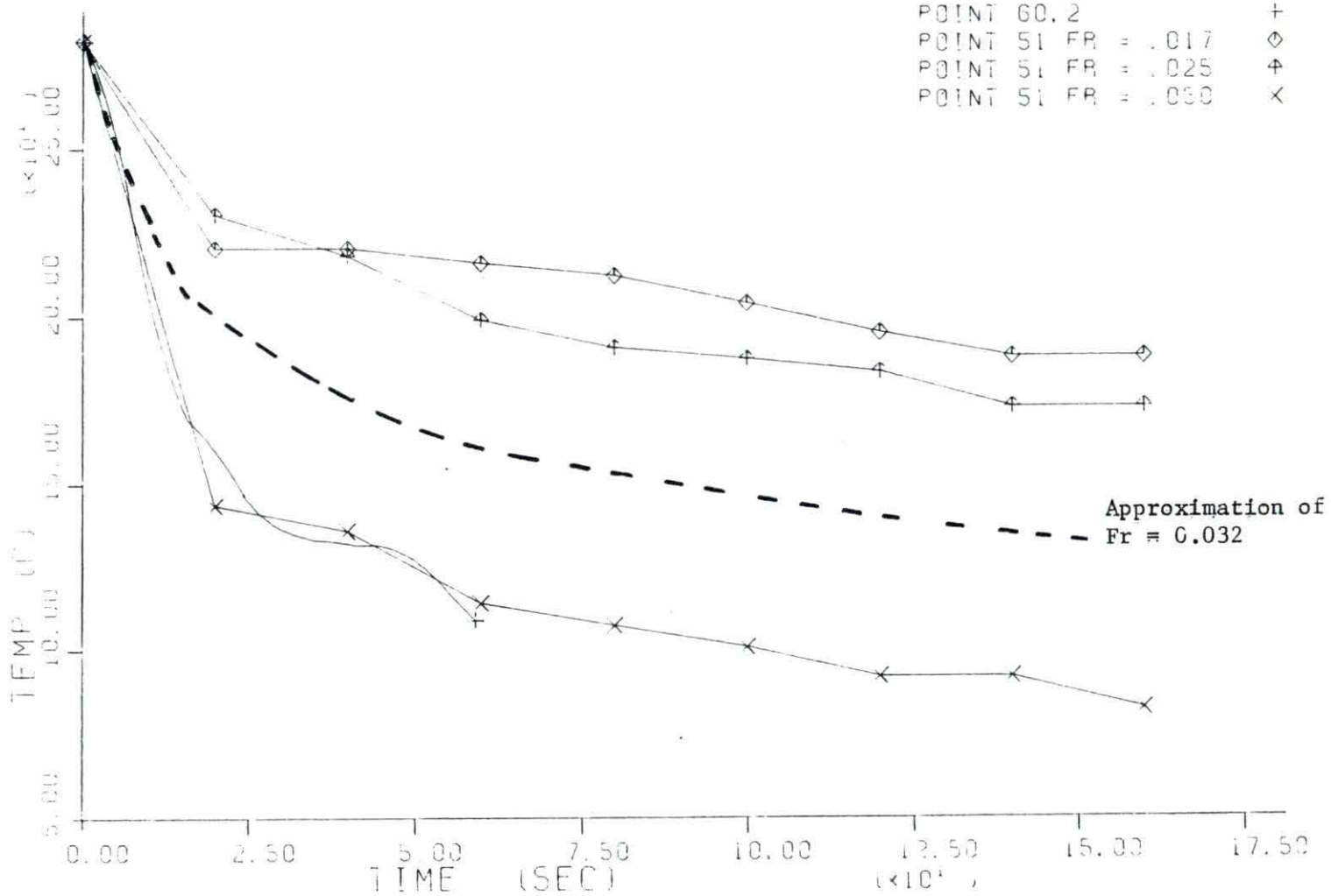

Figure 5.31 Analytical results for point 60,2 versus experimental results compensated for additional volume

that the experimental data still include the slowing effect of the downcomer where as the analytical data does not. A comparison of Figure 5.29 with Figure 5.32 and Figure 5.30 and 5.33 shows the same trends.

No experimental data exist on the quantitative effect of the downcomer on the characteristic mixing time. The downcomer represents an addition of 160% to the total modeled volume. If the addition of this volume were to have the effect of increasing τ approximately 60% than the extrapolated experimental results at Fr = .032 would match the analytical results quite closely. If this were the case, then the downcomer effectiveness factor:

$$\text{Eff} = \frac{\%\text{ increase in characteristic mixing time}}{\%\text{ increase in volume}}$$

would equal .38. Since this lies between the experimentally determined .30 effectiveness factor of the lower plenum and the 1.7 effectiveness factor of the loop seal and stalled pump, it seems plausible.

It is important to note that the assumption that a 2-D Cartesian geometry can accurately model a 3-D cylindrical geometry could also account for part of the discrepancy. In the 2-D geometry, a fluid particle can not leave the plane of the paper. Perhaps the 2-D geometry forces the particle to flow past a point in the cold leg more quickly that the 3-D geometry would. In a 3-D geometry a

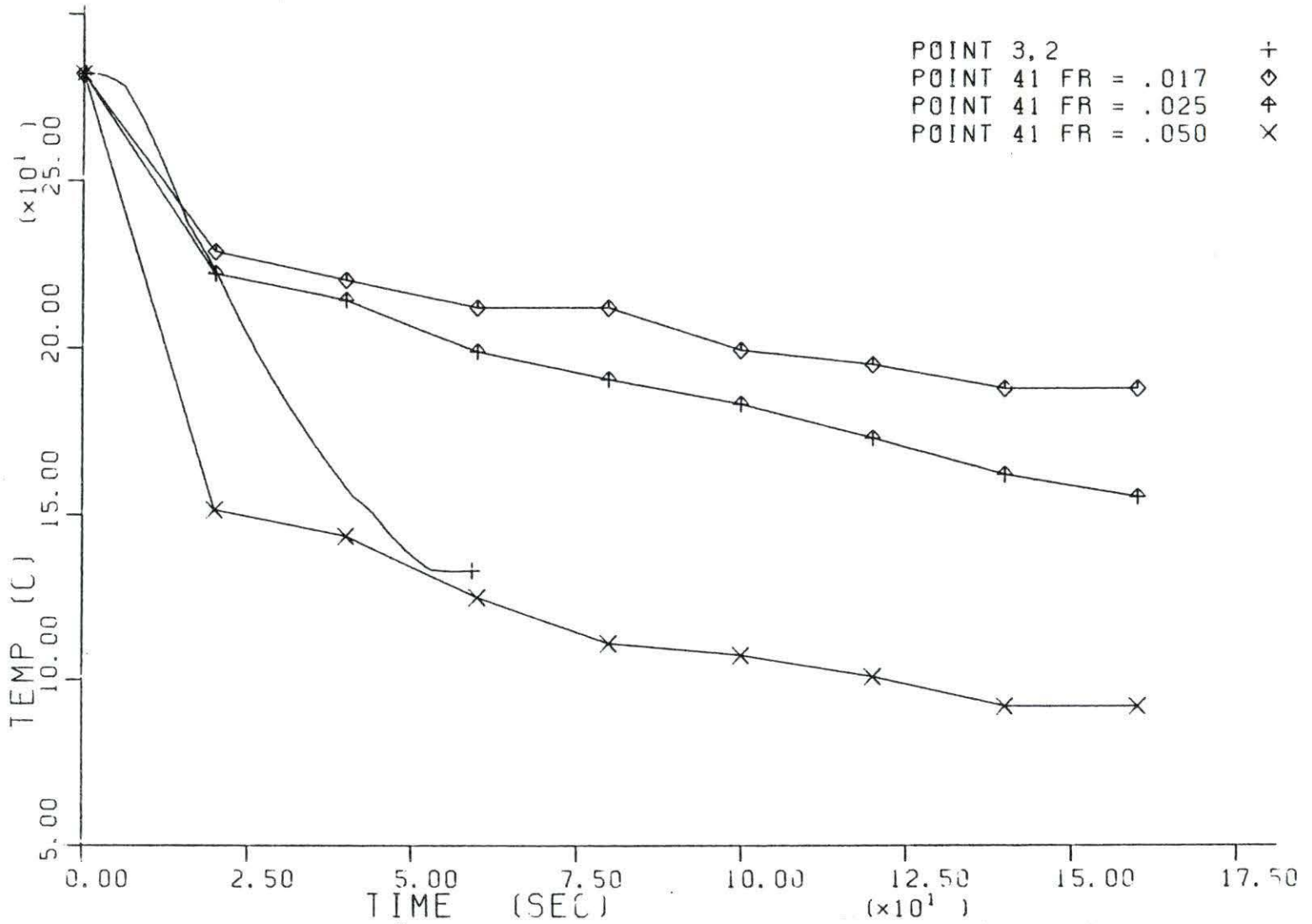

Figure 5.32 Analytical results for point 3,2 versus experimental results compensated for additional volume

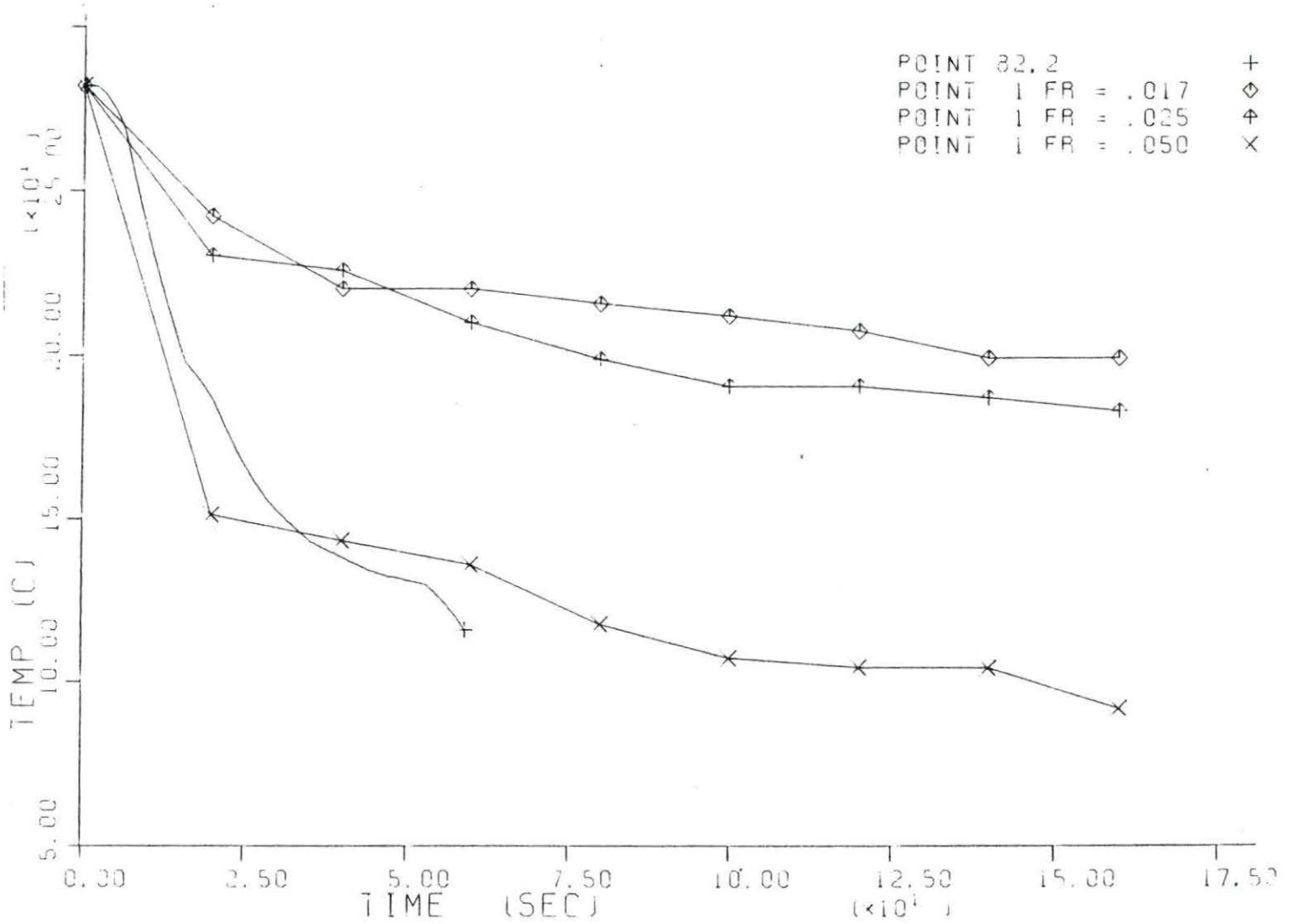

Figure 5.33 Analytical results for point 82,2 versus experimental results compensated for volume

particle can move out of the plane of the paper. This additional freedom of movement has the effect of volume which would result in a slower transient just as Figures 5.31 through 5.33 show. Therefore, at least part of the discrepancy between the experimental and analytical results could be due to the use of 2-D Cartesian geometry. The turbulence model, itself, with all its implicit assumptions would also lead to a discrepancy between the experimental and analytical results. However, it is impossible to predict whether this discrepancy would result in a faster analytical transient.

For the convenience of the reader, several other figures are included, all of which show the same trends discussed above:

- Figure 5.34 which graphs experimental data, which has been adjusted for the different volumes, at various Froude numbers for mesh point 15, 2 which represents a point at the bottom of the cold leg midway between injection point and the closed end of the cold leg.

- Figure 5.35 which shows the results of the comparison for point 60, 9 which is a point lying on the centerline of the pipe midway between the injection point and open end of the chosen leg.

- Figure 5.36 which shows the Creare results for Fr = .025 at t=60 seconds. It compares these to the analytical results which were adjusted to account for the differing test temperatures. This was done by assuming the analytical results follow the same basic form:

$$T = T_M + (T_L - T_M) \exp(-t/\tau)$$

τ was calculated by using the results from the ULYSSE code, then a T_H of 13.90°C and T_L of 66.7°C were substituted

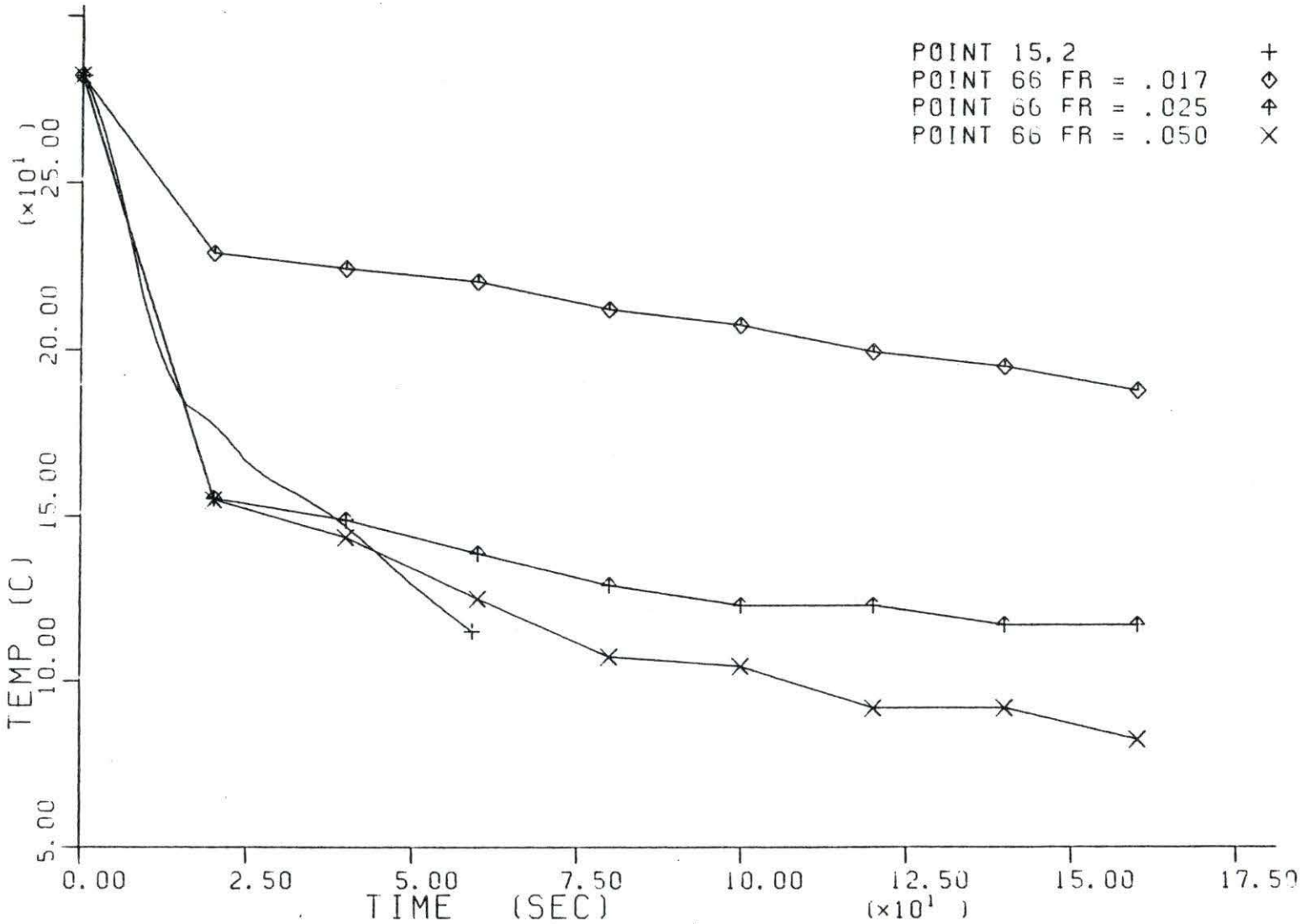

Figure 5.34 Analytical results for point 15,2 versus experimental results at various Froude numbers

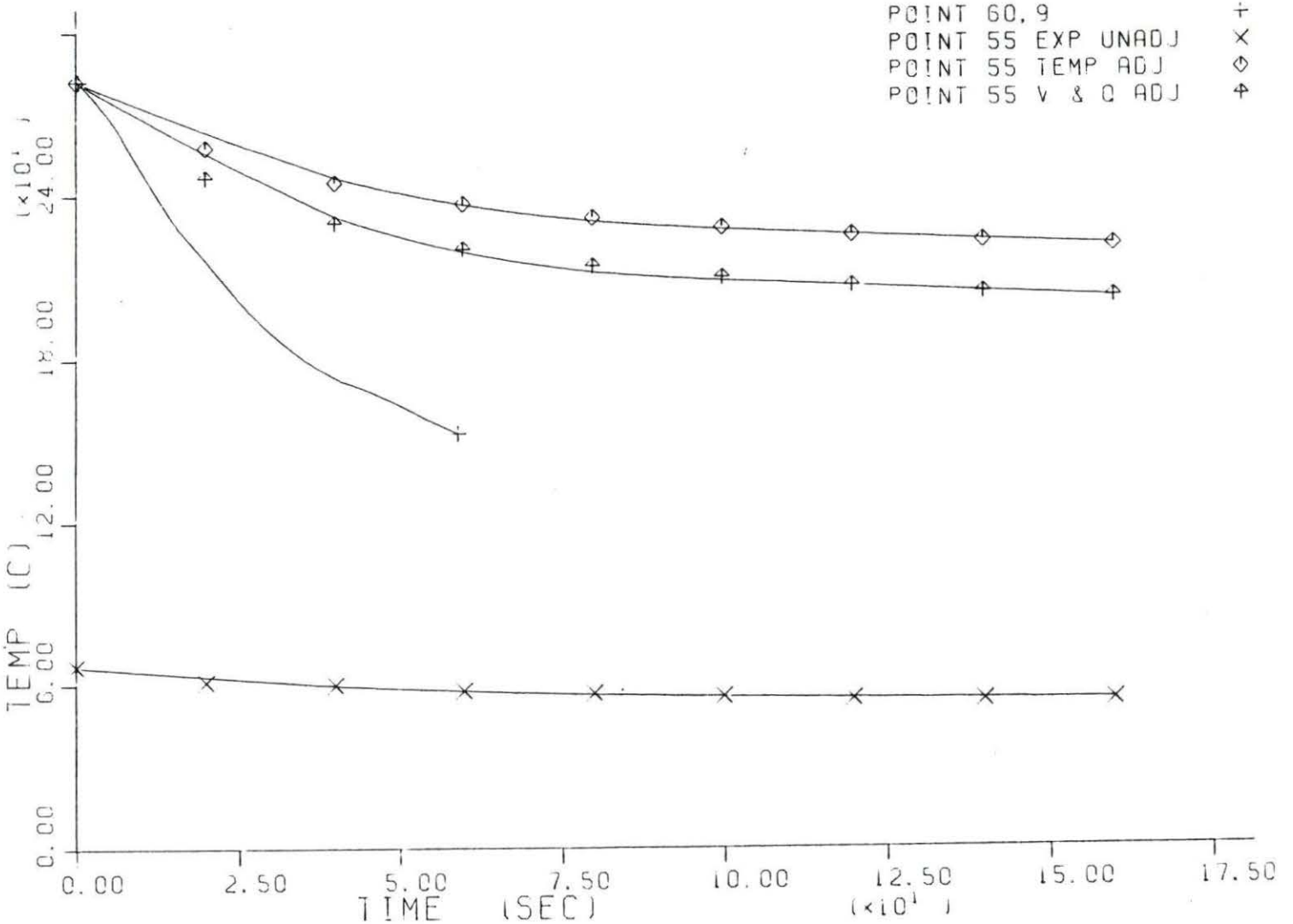

Figure 5.35 Analytical results for point 60,9 versus experimental results at FR = .025

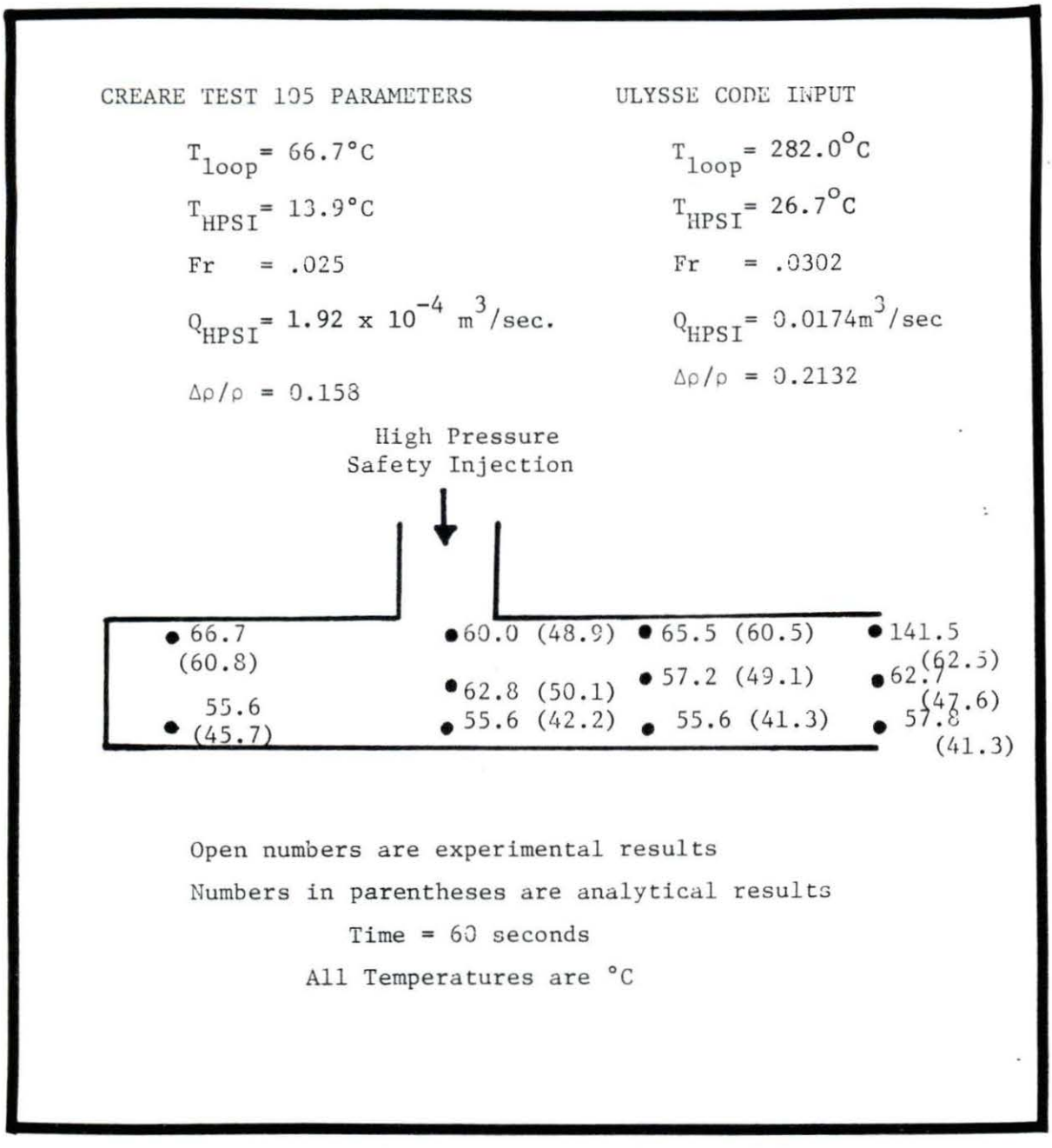

Figure 5.36 Experimental results versus collapsed analytical results

to find the value of the temperature at different points. This allows a comparison of the total flow field. The code predicted temperatures are always conservative, since they represent a faster transient.

For the purpose of PTS analysis, which is the reason this situation was investigated, one would like to have a simple equation which could be used for the boundary condition for the reactor vessel wall analysis. It was believed that the desired equation could be derived by assuming that the analytical results followed the equation:

$$T = T_H + (T_L - T_H) \exp(-t/\tau) \qquad (5.4)$$

τ was calculated for point 82,2 which represents the junction of the cold leg and downcomer, since the transient it experiences would conservatively represent the transient experienced by the reactor vessel wall. τ is plotted as a function of time in Figure 5.37. It is obviously not a simple function of time, though it seems to vary randomly about a curve which increases with time. Other τ's derived from analytical results for other points in the grid showed similar behavior. It must be concluded that equation does not apply to the analytical data and that there is no simple equation which can adequately describe this complex flow situation.

As a result of these investigations, the major sources of discrepancy between the experimental and analytical results arise from:

- the inability to exactly match a computational grid point with a thermocouple location.

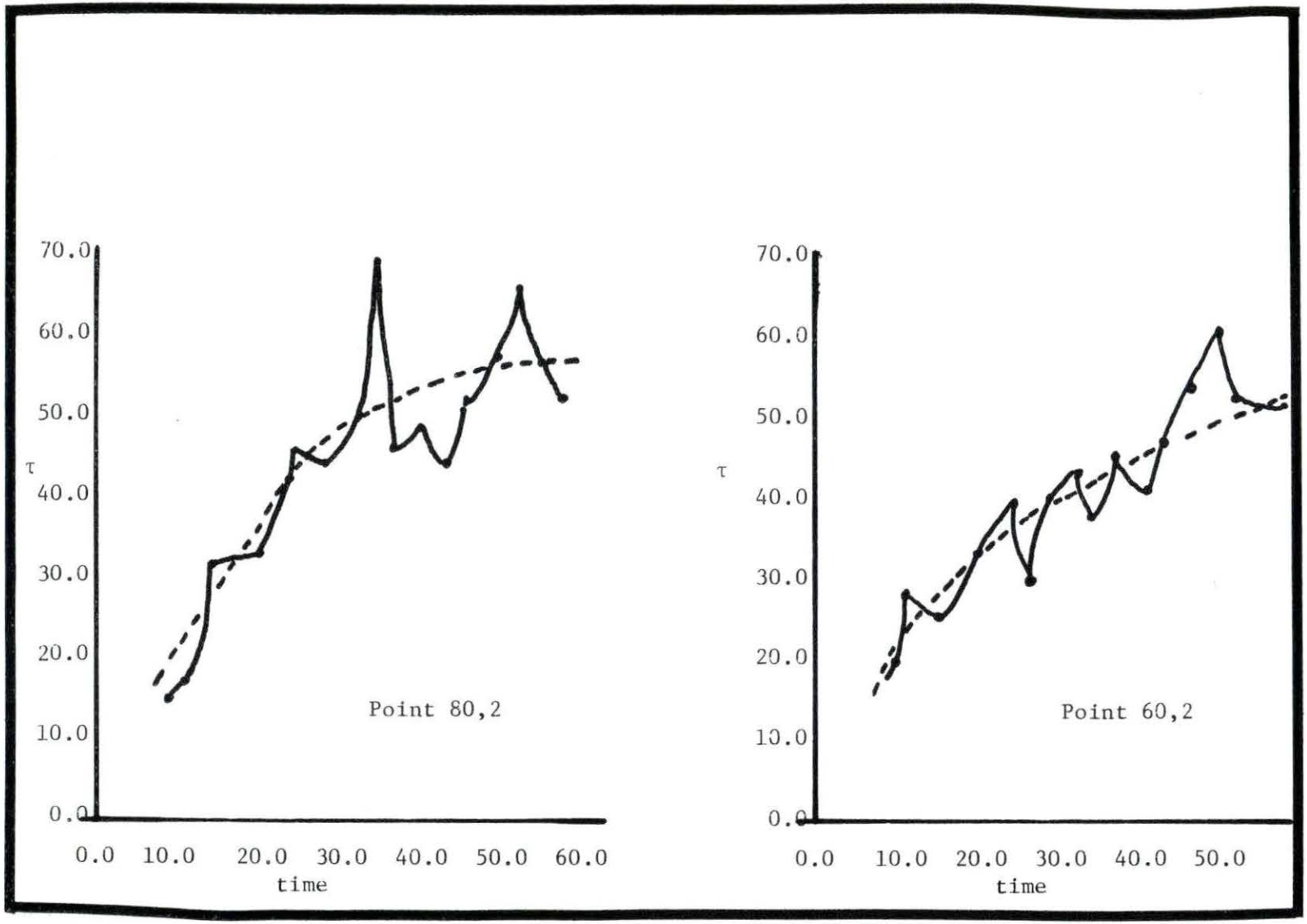

Figure 5.37 τ - Characteristic mixing time versus real time

- the HPSI fluid was injected exactly perpendicular to the pipe in both the analysis and the experiment where Fr = .025. The fluid was injected 30^{o} off the perpendicular in the tests where Fr = .017 and Fr = .051. This causes a difference in the flow patterns and temperatures.

- prototypical Froude numbers were preserved by using salt-induced density differences to simulate the temperature induced differences. Reference 29 discussed this effect. Experimental results show large differences between the data from salt and heat in the same range of density differences. These discrepancies can only be explained by invoking the different molecular diffusivities. Therefore, a second dimensionless number, the Peclet number, must enter the problem. However, its functional relationship is unknown.

- the transport properties of the fluid vary from point to point and time to time within the grid because they are all functions of temperature. However, all properties are considered constant except the density which is approximated by a linear relationship. This is an obvious idealization of such temperature dependent properties as C_{ρ}, μ, k and ρ.

and, most importantly,

- the difference in volumes modeled. Experimental results included the volume of the downcomer while the analytical results did not. There is no satisfactory way to account for the difference in these volumes since the "effectiveness" of the downcomer has not been studied. However, in light of the fact that the greater the volume, the slower the transient, the results presented in Figures 5.19 to 5.36 are to be expected.

Because of these significant differences, it is not easy to discern whether or not the initial assumption that a three dimensional cylindrical problem can be modeled by a two dimensional Cartesian geometry is correct nor can the adequacy of the $k-\varepsilon$ turbulence model be definitively determined. Nonetheless, when one considers the factors listed above along with the inaccuracies associated with the experiment itself and the fluctuating, random nature of turbulence,

the similarity between the analysis and the experimental results leads to basic confidence in the model. Additionally, since all the results show that the model predicts a more severe transient than that actually observed during experimentation, the model is certainly conservative if the temperatures it generates are used to predict thermal stresses in the reactor vessel.

6. SUMMARY, CONCLUSIONS AND RECOMMENDATIONS FOR FURTHER WORK

The goal of this work was to investigate the use of a two-dimensional nodal solution to the Navier-Stokes equations to solve the problem of thermal mixing of the HPSI fluid with the stagnant fluid in the cold leg during certain Small Break LOCA scenarios. The result of interest was the temperature at the reactor vessel wall as a function of time. The results generated by the computer model were compared both quantitatively and qualitatively with experimental results generated by Creare and reported in references 7-9. The computer model successfully predicted all qualitative aspects of the observed flow phenomena including:

- buoyancy induced stratification
- recirculation in the closed end of the cold leg
- counter current flow into the open end of the cold leg.

However, quantitatively the computer code did not match the experimental results well. There are several major differences between the model and the experimental system which may account for the lack of agreement including the following:

- different modeled geometry
- different angles of injection for the tests with Froude numbers equal to .017 and .051.
- the use of salt-induced density differences to preserve prototypical Froude numbers rather than the strictly temperature-induced density differences found in the reactor.

- the difficulty of exactly matching a computational mesh point with an experimental thermocouple.

Considering these differences and the fact that stratification is known to add a number of complicated phenomena to sheer flow such as energy radiation, strong anisotropy and steplike density profiles [7], none of which are accounted for in the present mathematical model, the agreement between the theoretical and experimental results is certainly reasonable.

Because of these differences between experiment and analysis, one can not conclude whether the two dimensional computational solution with averaged transport properties and a constant k-ε model of turbulence accurately predicts a three dimensional geometry. However, it can be concluded that the model was conservative and, therefore, adequate for use with a thermal analysis of the reactor vessel wall. Unfortunately, the calculations require a great deal of computational time (e.g. the results presented herein required one hour of C.P.U. time). Nonetheless, since "prediction" by means of an experiment is usually even more expensive, calculational methods are in great demand. While the computational scheme has been validated in a number of buoyant flow situations [30,3132], none were quite as complex as the one investigated in this work. The results should be used with caution.

Therefore, it seems as though future efforts should be concentrated in the experimental investigation of the following three areas:

- the exact effect of salt versus thermally induced density differences

- the exact functional relationship to the Froude number
and
- the exact geometry effects of specific reactor components.

7. REFERENCES

1. G. N. Abramovich, The Theory of Turbulent Jets (The M.I.T. Press, Cambridge, Mass., 1963).

2. J. L. Anderson, F. L. Parker, and B. A. Benidict, Negatively Bouyant Jets in a Cross-Flow, American Society of Civil Engineers International Symposium on Stratified Flows, Novosibirsk, 1972.

3. J. P. Benque, G. Labadie, and J. Ronat, A Finite Element Method for Navier-Stokes Equations Coupled with a Temperature Equation, Proceedings of the Symposium on Refined Modelling of Flows, Sept. 1982.

4. R. B. Bird, W. E. Stewart, and E. N. Lightfoot, Transport Phenomena, (John Wiley & Sons, New York, New York, 1960).

5. A. J. Chorin, The Numerical Solution of the Navier-Stokes Equations for an Incompressible Fluid, Bulletin of the American Mathematical Society, 73, 928 (1967).

6. Combustion Engineering, Inc., Evaluation of Pressurized Thermal Shock Effects due to Small LOCA's with Loss of Feedwater for the Combustion Engineering NSSS, CEN-189, 1981.

7. Creare R&D Inc., Fluid and Thermal Mixing in a Model Cold Leg and Downcomer with Loop Flow, EPRI NP-2312, 1982.

8. Creare R&D Inc., Fluid and Thermal Mixing in a Model Cold Leg and Downcomer with Loop Flow, EPRI NP-2312, 1982.

9. Creare R&D Inc., Transient Cooldown in a Model Cold Leg and Downcomer, EPRI-NP3118, 1983.

10. D. A. Ervine, E. McKeogh, and E. M. Elsawy, Effect of Turbulence Intensity on the Rate of Air Entrainment on Falling Jets, Proceedings of the Institute of Civil Engineers, Part 2, 69, 425 (1980).

11. F. W. Frost and T. H. Moulden, Handbook of Turbulence, Volume I, (Plenum Press, New York, 1977).

12. J. Goussebaile, Notice d'Utilisation de'Odysse, Edf-LNH Report No. He/41/82.13 (1982).

13. M. Hino, N. S. Hung, and K. Nakamura, Entrainment and Friction at the Interface of a Salt Wedge, Second International Symposium on Stratified Flows, Trondheim, 1980.

14. J. O. Hinze, Turbulence (McGraw-Hill, New York, 1975).

15. E. G. Hopfinger, Development of Stratified Turbulent Sheer Flow, American Society of Civil Engineers International Symposium on Stratified Flows, Novosibirsk, 1972.

16. W. M. Kays and M. Crawford, Convective Heat and Mass Transfer (McGraw-Hill, New York, New York, 1982).

17. D. W. Knight, et al., The Measurement of Vertical Turbulent Exchange in Tidal Flows, Second International Symposium on Stratified Flows, Trondheim, 1980.

18. J. H. Lee, Stability and Mixing of a Round Buoyant Discharge in Shallow Water, Second International Symposium of Stratified Flows, Trondheim, 1980.

19. R. R. Long, Some Properties of Turbulence in a Stratified Sheering Flow, American Society of Civil Engineers International Symposium on Stratified Flows, Novasibinsh, 1972.

20. J. L. Lumley, A Model for the Computation of Stratified, Turbulent Flow, American Society of Civil Engineers International Symposium on Stratified Flows, Novosibirsk, 1972.

21. Macagno, A., Interactions between Circulation and Density Stratification, American Society of Civil Engineers International Symposium on Stratified Flows, Novosibirsk, 1972.

22. A. S. Monin, Turbulence and Diffusion in Stratified Flows, American Society of Civil Engineers International Symposium on Stratified Flows, Novosibirsk, 1972.

23. W. Rodi, The Modeling of Turbulent Flows Using Transport Equations, Proceedings from the Symposium on Refined Modeling of Flows, Paris, 1982.

24. W. Rodi, Turbulence Models and Their Application in Hydraulics, International Association for Hydraulic Research, Delft, 1980.

25. A. Sesonske and S. Glasstone, Nuclear Reactor Engineering (Van Nostrand, Reinhold Co., New York, 1981).

26. L. M. Shotkin and N. Zuber, Downcomer Mixing for PTS, Nuclear Regulatory Commission, Memo to O. E. Basset, August 19, 1982.

27. U. Svensson, On the Numerical Prediction of Vertical Turbulent Exchange in Stratified Flows, Second International Symposium on Stratified Flows, Trondheim, 1980.

28. A. A. Townsend, The Structure of Turbulent Sheer Flow (Cambridge University Press, Cambridge, 1976).

29. J. S. Turner, Buoyancy Effects in Fluids (Cambridge University Press, Cambridge, 1973).

30. P. L. Viollet and J. Goussebaile, On the Modeling of Turbulent Flows Under Strong Buoyancy Effects in Cavities With Curved Boundaries, EDF-LNH Report No. He41/82/10 (1982).

31. P. L. Viollet, J. P. Benque, and A. M. Bisch, Plane Modeling of Unsteady Non-Isothermal Incompressible Flows, Proceedings of the International Topical Meeting on Advances in Mathematical Methods for the Solution of Nuclear Engineering Problems, Munich, 1981.

32. P. L. Viollet, J. P. Benque, and J. Goussebaile, Two-Dimensional Numerical Modeling of Non-Isothermal Flows for Unsteady Thermal Hydraulic Analysis, EDF-LNH Report No. He44/82/10 (1982).

33. I. R. Wood and G. Webby, The Effects of Boundaries Near Turbulent Jets, Second International Symposium on Stratified Flows, Trondheim, 1980.

8. ACKNOWLEDGEMENTS

Any engineer is more comfortable with equations then with words. Words seem so inadequate at times. Nevertheless, since there are no equations for "thank you" as yet, I shall try to convey in words my appreciation to everyone who has helped me as I wrote this thesis.

Special thanks are due to:

- Dr. Richard A. Danofsky, always fondly referred to as "Dr. Dan", for his helpfulness, patience and good humor while he advised me in this work. He'll always have my vote as "Major Professor of the Year."
- Electricite de France for allowing me to use their ULYSSE code for the calculations herein.
- Electricite de France, the Chicago Section of the American Nuclear Society and the Power Affiliates Program for financial support.
- Sally, Tim, Masoud, John and Jordi for putting up with me during this time. (Yes, I know I was unbearable.)

and especially,

- My mother, father and Bill, each of whom gave me the most valuable thing of all, love.